



**NANYANG
TECHNOLOGICAL
UNIVERSITY**

Scalar & Homoskedastic Models For SAR & POLSAR Data

Thanh-Hai Le

School of Computer Engineering

A thesis submitted to the Nanyang Technological University in partial
fulfillment of the requirement for the degree of

Doctor of Philosophy (PhD)

Aug 2013

Abstract

SAR and POLSAR stochastic data are multiplicative and heteroskedastic in their natural domain. It is hence desirable to establish additive and homoskedastic models, such that the benefits of homoskedastic statistical estimation framework can be demonstrated and realized for practical applications such as speckle filtering. In addition, the processing of multi-dimensional POLSAR data requires the establishment of discrimination observables which are to be scalar and statistically consistent. Moreover, these same scalar observable quantities also need to be naturally representative for the multidimensional POLSAR data.

In this thesis, the effects of homoskedasticity on SAR and POLSAR speckle filtering within the framework of computational and statistical estimation are extensively studied. Concurrently, the statistical behaviour of the determinant of POLSAR covariance matrix is also explored, where it is shown to be the representative scalar observable for the multidimensional POLSAR, similar to the role of the intensity in SAR.

As a result of these studies, several scalar statistical models based on the determinant of POLSAR covariance matrix are proposed and validated. These generic models for POLSAR are also shown to be both multiplicative and heteroskedastic, similar to the models for SAR intensity. Subsequently, logarithmic transformation is applied onto both SAR and POLSAR models to convert them into additive and homoskedastic models. From these models, the benefits of homoskedastic statistical estimation framework are then further explored.

There are several beneficial implications of the theory proposed in this thesis. Since the scalar and representative models for POLSAR extend the

traditional models for SAR's intensity, its main benefit is that it enables the adaptation of many existing SAR data processing techniques for POL-SAR data. Similarly, the homoskedastic model carries additional benefits. For inexperienced researchers (such as this author when he began this research), who attempt to process either SAR or POLSAR data using existing computation algorithms which most of the time expect an additive and homoskedastic input, this thesis proposes alternative and more familiar additive and homoskedastic models. For more experienced researchers, besides the unified scalar statistical theory for both SAR and POLSAR, this thesis also proposes several ways that homoskedastic data processing can be used to neutralize certain existing negative impacts of heteroskedasticity on the statistical estimation framework for (POL)SAR.

To those in need,

With love and hard work.

Acknowledgement

“Not many appreciate the ultimate power and potential usefulness of basic knowledge accumulated by obscure, unseen investigators who, in a lifetime of intensive study, may never see any practical use for their findings but who go on seeking answers to the unknown without thought of financial or practical gain.”

EUGENIE CLARK

Before anything, I would like to express my gratitude towards my family, specifically my wife, my parents and my kids, whose constant love and unconditional support I have greatly relied upon. Their immeasurable sacrifices together with their continuous encouragement have always been the motivation for me to follow this academic pursuit. They are the first and foremost people that this work is dedicated upon.

This thesis would also not have been possible without the patient and helpful guidance of Professor Ian McLoughlin and Associate Professor Nicholas Vun Chan Hua, under whose supervision I am gratefully under. The supervisors have provided firm support, as well as spot-on guidance. During all the stages of my research work, be it conceptualization or result analysis, be it writing, presentation or publishing .. their kind attention and wise advice command my utmost respect and admiration.

Special thanks go to my friends and colleagues, whose friendship and companionship have made the journey a truly enjoyable one. They include but are not limited to: Brian Nguyen Quang Huy, Erwin Anggadjaja and Hamid Reza Sharifzadeh ...

Last but not least I would like to give my appreciation to all NTU staff in PDCC, SCE and GSO whose quiet but continuous supporting efforts played a very important role in any measure of success this dissertation may be associated with.

“The roots of education are bitter, but the fruit is sweet.”
– Aristotle

Contents

Content Tables	i
List of Symbols	v
List of Equations	ix
List of Figures	xi
List of Tables	xii
List of Source Code	xiii
1 Introduction	1
1.1 Research Motivation	2
1.2 Research Objective	4
1.3 Research Methodology	4
1.3.1 Statistical Estimation Framework for (POL)SAR data	5
1.3.2 Data Collection	7
1.3.3 Result Interpretation and Evaluation	8
1.4 Research Contributions	9
1.5 Organisation of the Thesis	11
2 Current Methods in Processing SAR and POLSAR Data	13
2.1 The Stochastic and Multivariate Nature of (POL)SAR data	13
2.1.1 The Stochastic Nature of SAR data	13
2.1.2 The Multivariate Nature of POLSAR data	15
2.1.2.1 The polarization property of Electro-Magnetic waves .	15
2.1.2.2 Full Polarimetry and the Polarimetric Signatures	19
2.1.2.3 Partial Polarimetry and the Stokes Vector	22
2.1.2.4 The Polarization Basis Transformation	25
2.2 Current methods in SAR and POLSAR Data Processing	27
2.2.1 Current Statistical Models for SAR and POLSAR data	27
2.2.2 Existing Discrimination Measures for (POL)SAR data	30

2.2.3	Current Methods for SAR speckle filtering	32
2.2.4	Current Methods for POLSAR speckle filtering	36
2.2.5	Current Techniques to Evaluate SAR Speckle Filters	39
2.3	Summary	41
3	Homoskedastic Models for Heteroskedastic SAR Data	43
3.1	Original Heteroskedastic Model of SAR data	43
3.2	The Effects of Heteroskedasticity in SAR Processing	44
3.3	The Homoskedastic Effect of Logarithmic Transformation	46
3.4	Consistent Measures of Distance in the Log-Transformed Domain	48
3.4.1	Sampling distribution of Variance in Log-Transformed domain .	52
3.4.2	Sample variance as a statistical measure of homogeneity	53
4	Scalar Models for the Multidimensional POLSAR data	56
4.1	POLSAR statistical analysis	56
4.2	Heteroskedastic POLSAR data and the Homoskedastic Log-Transformation	58
4.3	Consistent Measures of Distance for POLSAR data	61
4.4	SAR as the Special Case of Polarimetric SAR	62
4.5	Validating the models against real-life data	65
4.5.1	Explaining practical data with the given Number-of-Looks	65
4.5.2	Comparing Theoretical Assumptions and Practical Implementations	70
4.5.3	Estimating the Effect Number-of-Looks (ENL)	71
4.5.4	Using the estimated ENL to better explain practical data	72
5	Applications of The Proposed Models	76
5.1	Clustering SAR images using the consistent measures	76
5.1.1	Developing k-MLE clustering Algorithm	77
5.1.1.1	Homogeneous Maximum Likelihood Estimation	77
5.1.1.2	Heterogeneous k-MLE Clustering	78
5.1.1.3	Determining number of clusters	80
5.1.2	Evaluating the k-MLE algorithm	81
5.1.2.1	Using the k-MLE clustering algorithm for speckle filtering	81
5.1.2.2	Evaluation of the kMLE speckle filter on simulated targets	83
5.1.2.3	Evaluation of the k-MLE speckle filter on Real Images .	84
5.2	SAR Speckle filtering using the consistent measures	85
5.2.1	The f-MLE SAR Speckle Filters	87

5.2.1.1	f-MLE Estimation	88
5.2.1.2	Preservation of Log-Distance Histogram Consistency	89
5.2.1.3	Recursively Applying The f-MLE Filters	89
5.2.2	Evaluating the f-MLE SAR speckle filters	91
5.2.2.1	Qualitative Evaluation on Real Images	91
5.2.2.2	Evaluating Speckle Suppression Effects	94
5.2.2.3	Evaluating Target Detection Performance	94
5.2.2.4	Summary	98
5.3	Evaluating SAR Speckle Filters using the consistent measures of distance	99
5.3.1	Speckle Filtering Process And The Homoskedastic Log-transformed Domain	100
5.3.2	Evaluating SAR Speckle Filters Over Homogeneous Areas	103
5.3.2.1	Estimating ENL from the log-variance index in homogeneous areas	103
5.3.2.2	Using MSE criteria to evaluate speckle filters	105
5.3.3	Evaluating SAR Speckle Filters over Heterogeneous Scenes	108
5.3.4	Using MSE to find the most suitable speckle filter for practical SAR images	114
5.3.5	Discussion and Summary	118
5.3.5.1	Discussion	118
5.3.5.2	Summary	120
5.4	Evaluating POLSAR Speckle Filters using the consistent measures of distance	121
5.4.1	POLSAR ENL Estimation using the Homoskedastic Property	121
5.4.2	Evaluating POLSAR Speckle Filters over Homogeneous Areas	123
5.4.3	Evaluating POLSAR Speckle Filters over Heterogeneous Areas	125
6	Conclusions	128
6.1	Contributions of the Thesis	128
6.2	Discussion of the proposed models	130
6.2.1	Beneficial implications of the proposed models	131
6.2.2	Limitations of the proposed models	133
6.3	Possible Future Work	133
A	Log-Chi-Square Distribution	136

A.1	Averages and Variances of POLSAR Covariance Matrix Determinant and Log-Determinant	139
A.2	Deriving the Characteristic Functions for the Consistent Measures of Distance	140
A.3	SAR intensity as a special case of POLSAR covariance matrix determinant	142
A.4	Original Domain: SAR Intensity and its ratio	144
A.5	Log-transformed domain: SAR log-intensity and the log-distance	145
A.6	Deriving the PDF for SAR dispersion and contrast	148
	References	150

List of Symbols

1. Glossary

Polarimetric Synthetic Aperture

Radar: the extension of single-channel SAR imaging solution to multiple-channel imagery using polarimetric properties.

POLSAR: Polarimetric Synthetic Aperture Radar

SAR: Synthetic Aperture Radar

Synthetic Aperture Radar: an active side-looking-radar remote sensing solution based on doppler-effect

2. Nomenclatures

C_v : denotes the **polarimetric covariance matrix**

C_h : denotes the **polarimetric coherency matrix**

M^{*T} : denotes the **complex conjugate transpose** of matrix M

$pdf(x; k)$: denotes the **probability density function** of the **random variable** x , given the known and **constant** k

$cdf(x; k)$: denotes the **cumulative distribution function** of the **random variable** x , given the known and **constant** k

$cf(x; k)$: denotes the **characteristic function** of the **random variable** x , given the known and **constant** k

$X \sim Y$: denotes the observable values X , which behaves as a single or a combination of random process(es) Y .

$|M|$: denotes the **determinant** of the matrix M , also denoted as $\det|M|$

Z : denotes the **scaled polarimetric covariance matrix**, $Z = LC_v$ (see: C_v)

$\Gamma(x)$: denotes the **Gamma function**.

$tr(M)$: denotes the **trace** of matrix M .

$\chi^2(2L)$: denotes the **Chi-Square distribution** with $2L$ degrees of freedom.

$\Lambda(2L)$: denotes the **Log-Chi-Square distribution** with $2L$ degrees of freedom.

List of Equations

2.1	SAR Real and Imaginary Components PDF	14
2.2	SAR Amplitude PDF	14
2.3	SAR Intensity PDF	14
2.8	Covariance Target Vector of Full Polarimetric SAR	20
2.9	Coherence Target Vector of Full Polarimetric SAR	20
2.10	Covariance Matrix of Full Polarimetric SAR	20
2.11	Coherence Matrix of Full Polarimetric SAR	20
2.12	Polarization Synthesis Process of Full-Pol data	21
2.13	Complex Wishart Distribution Likelihood Test Statistics	31
2.14	Complex Wishart Distribution Likelihood Test Statistics (Log Domain) .	31
2.15	Weighted Least-Square Error	32
3.1	SAR Unit Amplitude PDF	43
3.2	SAR Unit Intensity PDF	43
3.3	SAR Unit Log Amplitude Observable	47
3.4	SAR Log Amplitude Observable	47
3.5	SAR Unit Log Intensity Observable	47
3.6	SAR Log Intensity Observable	47
3.7	SAR Unit Log Amplitude PDF	47
3.8	SAR Log Amplitude PDF	47
3.9	SAR Unit Log Intensity PDF	47
3.10	SAR Log Intensity PDF	47
3.11	SAR Amplitude Distance Observable	49
3.12	SAR Intensity Distance Observable	49
3.13	SAR Log Amplitude Distance Observable	49
3.14	SAR Log Intensity Distance Observable	50
3.15	SAR Amplitude Distance PDF	50
3.16	SAR Intensity Distance PDF	50
3.17	SAR Log Amplitude Distance PDF	50

3.18	SAR Log Intensity Distance PDF	50
3.19	SAR Amplitude Contrast Observable	50
3.20	SAR Intensity Contrast Observable	50
3.21	SAR Log Amplitude Contrast Observable	50
3.22	SAR Log Intensity Contrast Observable	50
3.23	SAR Log Amplitude Contrast PDF	51
3.24	SAR Log Intensity Contrast PDF	51
3.25	SAR Two Samples Log Intensity Variance PDF	52
3.26	SAR Two Samples Log Amplitude Variance PDF	52
4.1	POLSAR Target Vector: Complex Gaussian Distribution PDF	57
4.2	POLSAR Covariance Matrix: Complex Wishart Distribution PDF	57
4.3	Determinant Ratio and the Product of Chi-Squared Distributions	58
4.4	Logarithm of Determinant Ratio and the Sum of Log-Chi-Squared Distributions	58
4.5	POLSAR Covariance Matrix Determinant Distribution PDF	58
4.6	POLSAR Covariance Matrix Log-Determinant Distribution PDF	58
4.7	Chi-Squared Distribution PDF	59
4.8	Log-Chi-Squared Distribution PDF	59
4.9	Log-Chi-Squared Distribution: Characteristic Function	59
4.10	Log-Chi-Squared Distribution: Characteristic Function	59
4.11	POLSAR Determinant is not biased	60
4.12	Variance of POLSAR Determinant is Heteroskedastic	60
4.13	POLSAR Log-Determinant is biased	60
4.14	The Variance of POLSAR Log-Determinant is homoskedastic	60
4.15	POLSAR Determinant-Ratio Observable	61
4.16	POLSAR Log-Distance Observable	61
4.18	POLSAR Dispersion Observable	61
4.19	POLSAR Contrast Observable	61
4.20	POLSAR Determinant Ratio Distribution PDF	61
4.21	POLSAR Log-Distance Distribution PDF	61
4.22	POLSAR Dispersion Distribution PDF	61
4.23	POLSAR Contrast Distribution PDF	61
4.24	ENL Estimation Formula for POLSAR data	72
5.1	Conditional Probability of SAR Pixel Intensity	77
5.2	MLE Estimation in the Log-Transformed Domain	78
5.3	Boxcar Speckle Filter Estimation	87

5.4	k-MLE Speckle Filter Estimation	87
5.5	f-MLE Estimation (Inclusive Version)	88
5.6	f-MLE Estimation (Exclusive Version)	88
5.7	MSE Evaluation Metrics for SAR	101
5.8	Approximation of Homoskedastic Log-Variance from given SAR ENL . . .	104
5.9	Estimation of SAR ENL from Variance in Log-Transformed Domain . . .	104
5.10	Estimate ENL from log-variance of POLSAR homogeneous areas	121

List of Figures

3.1	Observed histogram of a homogenous area and modelled PDF response	49
3.2	Observed and modelled PDF of dispersion and contrast in homogeneous log-transformed intensity images.	51
3.3	Sample Variance: Observable and Modelled CDF Response	53
4.1	Multi-Look SAR dispersion and contrast showing that the modelled response matches very well with the histograms from real-life captured data.	65
4.2	Validating the dispersion and contrast models against both partial and full polarimetric AIRSAR Flevoland data.	67
4.3	Validating determinant-ratio and log-distance models with $ \Sigma_v $ is computed using $\text{avg}(\ln \mathcal{C}_v)$	68
4.4	Validating determinant and log-determinant models with $\Sigma_v = \text{avg}(\mathcal{C}_v)$	69
4.5	The relationships between ENL and the sample variance of log-determinant and log-intensity	73
4.6	9-look processed Radarsat2 data does not exactly exhibit 9-look data characteristics. An homoskedastic model in the log-transformed domain can be used to successfully estimate the effective ENL and thus offer a better model of the data.	74
4.7	AIRSAR Flevoland also exhibits the over-sampling phenomena, though to a much smaller extent than the RADARSAT 2 data.	74
5.1	Speckle filtering effects by various threshold-value	83
5.2	Blur effects of larger window size	84
5.3	Improving Homogeneous error with iterative k-MLE filter	84
5.4	Qualitative evaluation on point targets	85
5.5	Qualitative evaluation on urban and agricultural areas	86
5.6	Consistent Distance Property and the f-MLE Estimations	89
5.7	Consistent Distance Property and the f-MLE Estimations	90

5.8	Iteratively Improving in Distance Histograms	91
5.9	Qualitative Evaluation of f-MLE filter on Real Life Scene of Natural Surface	92
5.10	Qualitative Evaluation of f-MLE filter on Real Life Scene of Urban Landscape	93
5.11	MSE in the log-transformed domain is related to the ENL index	94
5.12	Homogeneous Area: MSE criteria and speckle suppression power of f-MLE filters	95
5.13	Histogram discriminability and the ROC Curve	96
5.14	Invariant ROC Curve	97
5.15	Heterogeneous Patterns: MSE criteria and f-MLE performance	97
5.16	SAR simulation, processing and filtering schema	100
5.17	Visualising Removed “Noise”: Ratio images in the original domain vs. Residual images in the log-transformed domain	102
5.18	The Inconsistency evident in the original SAR domain and the Emerged Consistency demonstrated in the log-transformed domain	106
5.19	Filtered results: consistency in log-transformed domain	107
5.20	Example windows of ground truth patterns, each 32×32 pixels in size.	109
5.21	Target and Clutter Separability: Histograms and resulting ROC Curve visualisation	110
5.22	Bias Error Investigation: Image and Histogram Visualisation	111
5.23	Ground Truth Images for simulation	114
5.24	Filtering Simulated Real Images: Qualitative Validation	116
5.25	Filtering Real Images: Smaller $MSE_{benchmark}$ suggests visually better images	117
5.26	Checking the preservation of the consistency property for POLSAR speckle filters	123
5.27	POLSAR 3×3 boxcar filter preserves the consistency property. Consistency means: as long as the area is homogeneous, regardless of the underlying signal Σ_v the shapes of the histograms should be the same.	124
5.28	Visually Evaluating POLSAR Boxcar 3×3 vs. 5×5 Speckle Filters on AIRSA Flevoland part-pol data (HH-HV) with expected $MSE=1.0312$ at $ENL=4$	126
6.1	Observable convolution of PSF	134

List of Tables

1.1	Collected imagery data	8
3.1	Mean and Variance of Original SAR data	44
3.2	Mean and Variance of Log Transformed values: here the variance is no longer dependent on σ	48
3.3	The properties of observable SAR random variables	48
3.4	Cut off values	54
5.1	Speckle Suppression Power: ENL and Variance	105
5.2	Performance of various filters over homogeneous areas	108
5.3	Lower MSE suggest better feature detection, measured by the AUC index	113
5.4	The correlation between MSE and AUC evaluation criteria (inside the brackets are corresponding p-values)	113
5.5	If the best filters are the ones with smallest true MSE, then their observable noise-MSE are also the ones closest to the MSE of inherent noise	115
5.6	Our Conjecture: Most Suitable Speckle Filter For The Scene Can Be Chosen Using The Residual MSE.	115

List of Source Code

5.1	k-MLE Clustering Algorithm Template	78
5.2	Iteratively find better cluster centers	79
5.3	Homogeneous partitions number growing	80

Chapter 1

Introduction

Synthetic Aperture Radar (SAR) is a technology with many advantages. Compared to optical remote sensors - which are passive, SAR uses active sensors to provide weather independent and night-inclusive operational capabilities. Compared to other radar based active sensors, for example Real Aperture Radar (RAR), SAR provides state-of-the-art resolution and coverage. In the past decades, the exponential growth in computational power has made the once overly excessive computationally demanding SAR technology to become a feasible and preferred earth observation solution [1]. Thus SAR has now become the preferred choice for continuous and autonomous large-scale remote surveillance solutions.

As state-of-the-art technology, the SAR technique has been extended in a few directions, one of which is Polarimetric SAR (POLsar). POLsar is the natural extension of SAR, exploiting the natural polarization property of Electromagnetic (EM) waves. It extends the SAR acquisition information from the traditional single SAR channel to multi-channel POLsar data, corresponding to a different combination of transmitted and received polarizations. Similar to the extension from black-and-white images to colour photography, the polarimetric extension brought about multi-channel POLsar data as compared to the traditional one-channel SAR data.

With both SAR and POLsar data becoming cheaper and more readily available, the recent research emphasis is on understanding and developing applications using these data. However, both SAR and POLsar suffer from speckle phenomena, which hampers the human capabilities to understand SAR images. Speckle arises due to the random

interference of many de-phased but coherent backscattered waves. Thus both SAR and POLSAR data are stochastic by nature.

1.1 Research Motivation

The big picture, as introduced above, is that POLSAR data is multi-dimensional, stochastic, multiplicative and heteroskedastic. Under this condition, it is very important to understand the statistical models for its data. It is these models that form the foundation for different (POL)SAR data processing techniques, for example speckle filtering, target detection, image segmentation, and other clustering, classification techniques. In fact, due to the random nature of speckle, all of these techniques are essentially based on statistical estimation theory, which comprises statistical modelling and validation, estimator design and development as well as evaluation of different estimators' accuracy. And central to this statistical estimation theory is the need for statistically consistent discrimination measures which are commonly derived from the statistical models.

That is, while different statistical models have been developed for different POLSAR observables, for a statistical model to be useful, scalar discrimination measures need to be derived from it. At the same time, the extension from SAR to POLSAR brings about a representation difficulty in that: there exists not one, like the intensity in SAR, but many observable quantities in POLSAR. Thus, on the one hand, practical applications for POLSAR data processing require measures which are scalar, consistent and preferably homoskedastic. On the other hand, the observable quantity being modelled needs to be naturally representative of the high dimensional POLSAR data.

In addition, most of these data processing techniques are traditionally designed for additive and homoskedastic data. In fact, unless proven otherwise, it is both convenient and acceptable to assume that the additive white noise model is appropriate for any given set of data samples. This is due to a number of reasons, for example the prevalence of the normal distribution which results from the central limit theorem, or the prevalence of the additive noise model which probably arises due to the linear and additive nature of digital data. It should be noted that even for the case of SAR data which is digital and not additive, the above statement is still true as SAR actually has two components, the real and imaginary parts, both of which follow the standard Additive White Gaussian Noise model.

Both SAR and POLSAR data however are multiplicative and heteroskedastic by nature. While there is no doubt that a number of data processing techniques have been proposed to handle certain aspects of the data, the breadth and depth of these studies trails in comparison to that of the more familiar additive and homoskedastic model. This leads to the fact that a lot of times, existing statistical or computational techniques initially designed for additive and homoskedastic models are applied on multiplicative and heteroskedastic data, in ignorance of the incompatibility. An example is the use of mean, variance and squared error criteria, which are linear by nature and work excellently on additive and homoskedastic models, being applied on multiplicative and heteroskedastic distribution such as the gamma distribution. Such use, however, is known to be not very robust for these so-called heavy tailed distributions.

Similarly speaking, heteroskedasticity poses numerous negative impacts on the usual framework of statistical estimation, which most of the time makes use of various different techniques and criteria known to work very well on the usual models. For example, in modelling, it is very common to use subtractive differences to discriminate and to make decisional inferences. However, for heteroskedastic SAR, it is known that such use should be avoided in preference to a ratio-based discrimination measure. Another example is in the normal performance evaluation stage of statistical estimators, where the Ordinary Least Square (OLS) is widely used as the best evaluation criteria which is probably due to the Gauss Markov theorem. For SAR data, however, its heteroskedasticity directly violates the homoskedastic assumption of the theorem and thus many different ways to evaluate SAR speckle filters were proposed.

Furthermore, since POLSAR can be considered as the multi-dimensional extension of traditional SAR, a common problem exists for both SAR and POLSAR data. That is: the sense of subtractive distance is seriously flawed in the original multiplicative and heteroskedastic domain of both types of data. In contrast, the digital technologies which range from image processing and display to artificial intelligence and machine learning algorithms used to process (POL)SAR data are linear and additive in nature. This linear and additive nature is manifested, for example, in a large number of algorithms in the field of computational intelligence which make use of MSE as an objective function, as well as the extensive use of variance and contrast in digital image processing. Thus it will be very useful to develop homoskedastic models for this heteroskedastic data so that the benefits of an additive and homoskedastic statistical estimation framework can be explored.

1.2 Research Objective

While the statistical model for SAR is quite well understood, the understanding of the POLSAR statistical model trails behind. The complex POLSAR data have been statistically modelled as following the complex Wishart distribution, which apparently is multi-dimensional, complex and un-intuitive. There have been a few published scalar statistical models for POLSAR, but none of them fit the dual criteria of being highly representative of the data and at the same time lead to scalar discrimination measures. There are also a few POLSAR discrimination measures proposed, but all of them are based on the likelihood test statistics, which so far have only shown to be based on an asymptotic distribution.

In another thread of study, to combat the negative impacts caused by multiplicative and heteroskedastic properties for SAR data, experienced researchers in the field have developed numerous ingenious ways to tackle these issues. For example, when the sense of subtractive distance is not consistent for SAR data, the ratio is proposed as its discrimination measure [2]. Or when the MMSE criteria is not very suitable to evaluate SAR speckle filters, other criteria like radiometric preservation and speckle suppression power evaluation are employed. Unfortunately, these counter-intuitive measures are not very popular outside the SAR community, and newcomers to the field are frequently found being trapped by these pitfalls.

Some of the problems described above have been studied using different approaches in the literature. However, they have not been presented in a systematic manner nor with a strong underlying foundational theory. Hence the **main problem statement** of this thesis arises. That is, this thesis focuses on providing a solution for the dual-problem of: 1) establishing scalar and representative statistical models for the multi-dimensional and inter-correlated POLSAR data and 2) providing consistent measures of distance for both SAR and POLSAR data which allow the benefits of the homoskedastic statistical estimation framework to be demonstrated.

1.3 Research Methodology

The overall research methodology is to first focus on the simpler one dimensional SAR domain, and then extend the obtained insights and processing techniques towards the

more complex multi dimensional POLSAR data domain. This is achieved as the theoretical models for POLSAR are shown to be the multi dimensional extensions of the one dimensional SAR model.

The development of these models are based on rigorous statistical mathematics transformations. The assumptions used are minimal and also widely acknowledged for this type of data. Then, the variable change theorem is applied to derive the statistical model for these transformed observables. The derived theoretical models are validated against real life data. The imperfect conditions found in practice (in comparison to the theoretical assumptions) are also investigated, and the models are shown to be robust, capable of handling these imperfections. The theoretical properties of these models, as well as many of their benefits, are also proven using rigorous mathematical principles.

As both the SAR and POLSAR data are stochastic in nature, many of the associated data processing techniques, such as speckle filtering has been put into the framework of statistical estimation. For such application, the research methodology is based extensively on the statistical estimation framework. The framework consists of three stages:

Stage 1: data statistical analysis. We propose a preferred data transformation and decomposition that may allow applications of existing computer science techniques.

The statistical models built after such a transformation are validated against real-life data.

Stage 2: predictor and estimator development. Various statistics-based computational intelligence and/or signal processing methods are to be applied.

Stage 3: results analysis and performance evaluation. Experiment results are evaluated both qualitatively on real images and quantitatively through simulated data.

1.3.1 Statistical Estimation Framework for (POL)SAR data

Even though the research topic seems to spread across different sub-fields, the common framework that binds them all together is the application and development of statistical estimators. For example, for speckle filtering, it is the estimation of underlying back-scattering coefficients being corrupted with stochastic noise. For the problem of target

detection or classification, it is the estimation of the likelihood that the target belongs to a certain category.

Thus a significant portion of this research effort focuses on developing a computational framework for simulation, evaluation, processing and classification of target polarimetric signatures. The benefits of such a framework are many fold. Firstly, simulation allows one to quickly carry out experiments on small synthesized and well-designed scenarios, without the need for highly expensive satellite imagery. Secondly, simulation provides ground-truth, without which quantitative evaluation of estimators would have been impossible. Last but certainly not least, such a framework allow one to apply estimators repeatedly, and results from different estimators can be statistically and reliably compared. For example, this would allow different authors to compare results quantitatively.

The objective of such framework being:

1. To build, develop and validate statistical models for different stochastic processes that are inherent within the polarimetric SAR domain.
2. To allow easy, fast and repeatable simulations and experiments of various stochastic processes in designed, focused, as well as broad-based scenarios.
3. To allow easy application of different existing estimators as well as various transformations into focused and simulated scenarios as well as into practical real measured data.
4. To allow development and calculation of good performance indices for estimators.
5. To allow visualization and analysis of the performance of different stochastic estimators.
6. Ultimately, to allow development of better and more accurate estimators, whose results can be verified: not only qualitatively on real life images, but also quantitatively through rigorous simulations.

The possible benefits of this computational framework are:

1. Practical benefits

- (a) The computational frameworks allow for faster, quicker and more focused experiments. Often, a statistical hypothesis can be observed or rejected by designing and implementing an appropriate computational experiment.
- (b) The framework allows for easier analysis, and thus more insight to be gained, on the performance of an estimator. This, in turn, allows for design and development of better estimators.

2. Academic benefits

- (a) The computational framework allows for quantitative evaluation and comparison of estimators. With fast and repeated experiments, the framework allows one to not only compute a single performance value on a single experiment, but also to analyze the whole behaviour of such performance measures over repeated stochastic simulations.
- (b) The computational framework provides significant help in deriving new performance evaluation criteria for statistical estimators.

1.3.2 Data Collection

This work has made extensive use of simulated data, which have a number of advantages listed below:

1. Once the model is validated against real-life data, simulated experiments can be carried out on more focused scenarios. This allows smaller data sets to be generated and analysis can become faster and more accurate.
2. Contrary to real-life images where underlying coefficients are to be estimated, ground truth is readily available in simulated experiments.
3. Quantitative evaluation is possible not only via a single experiment on a single real-image but via repeated stochastic runs. Thus not only single values of mean or mean-squared-error are to be evaluated. As the whole response PDF is available, statistical bias or heteroskedasticity can also be reported.

Besides simulated data, we have gathered a large amount of real-life data. Table 1.1 lists data made available to us, courtesy of EADS Innovation Works Singapore.

Radar Platform	Polarization Mode	Data Capture Time
RadarSat 2	Full Quad Pol	29 Apr 2009
RadarSat 2	Full Quad Pol	05 Apr 2009
RadarSat 2	Full Quad Pol	12 Mar 2009
RadarSat 2	Full Quad Pol	23 Jan 2009
RadarSat 2	Full Quad Pol	30 Dec 2008
RadarSat 2	Full Quad Pol	06 Dec 2008
RadarSat 2	Full Quad Pol	19 Oct 2008
RadarSat 2	Full Quad Pol	12 Nov 2008
RadarSat 2	Full Quad Pol	25 Sep 2008
TerraSar-X	Dual Pol (HH-VV)	18 Apr 2008
NASA-JPL AirSar	Full Quad Pol	2001

Table 1.1: Collected imagery data

1.3.3 Result Interpretation and Evaluation

The achievement of the research objectives stated above not only provides novel solutions to the stated problem, it also illustrates the advantages and beneficial implications of the proposed theory. Compared to existing published techniques, the advantage of the proposed theory is qualitative, which does not require direct quantitative comparisons. Instead a straightforward binary evaluation would be sufficient. For the POLSAR scalar model, its advantages are that not only does it lead to consistent discrimination measures, it also generalizes the traditional model for one dimensional SAR intensity. For the homoskedastic models, their advantage is that they enable an additive and homoskedastic statistical framework, which is not only capable of overcoming various negative impacts of heteroskedasticity, but also results in a single better evaluation criteria that can combine and represent many different existing performance criteria.

To validate the theoretical models, real-life data are used in this work. Specifically, estimated theoretical PDFs are plotted against the histogram of real data, and a good visual match indicates a good validation. In cases where theoretical PDF cannot be derived, simulated data are then generated and their histograms are matched against real-life data for validation.

To evaluate the application of these models in a statistical estimation framework, a practical point of view is adopted. Practically, all estimators would eventually need to be applied on and work for real images. Contrary to experiments on simulated data, experiments on real images can often only be compared qualitatively. This however is

critical and will always be included in our investigations. The reason is that this helps to guard against any systematic errors in the various assumptions and approximations made in developing the theoretical models. Towards that end, real-data can help to build and validate statistical models.

1.4 Research Contributions

Interestingly, the dual-problems stated above are found to have a single solution. They are the derivation of scalar, representative and homoskedastic statistical models for the multidimensional, inter-correlated and heteroskedastic POLSAR data.

These theoretical models are studied and validated in this thesis. They are based on a highly representative observable, which is the determinant of the POLSAR covariance matrix. Out of many different possible scalar projections of the multi-dimensional data, the proposed projection is highly representative. When the dimension number is collapsed to one, the special case of the proposed model matches perfectly with the commonly used statistical model for SAR intensity. Furthermore, the proposed statistical model also leads to the derivation of existing as well as the newly proposed discrimination measure: determinant-ratio which is the generalized multi dimensional version of the widely used SAR intensity ratio.

Another novelty of the contributions in this thesis comes from the systematic treatment towards the problem of statistical estimation of heteroskedastic SAR data. While many different ways to combat the negative impacts caused by multiplicative and heteroskedastic properties for SAR data have been proposed over the years, they have often been handled in a piecemeal manner. Here, a systematic homoskedastic framework of statistical estimation is developed, where not only homoskedastic statistical models are proposed, the impacts of homoskedasticity on estimator development and performance evaluation of statistical estimators is also studied. This comprehensive treatment not only explains why the original SAR data requires special treatment very different to the common practice of computational sciences, it also encourages a thorough and unique discussion, for example on evaluating different evaluation criteria for statistical estimators. And since the POLSAR data can be considered as the multi dimensional extension of traditional SAR data, these treatments are shown extensible towards POLSAR data which is definitely yet another novelty.

Specifically, the following results are to be obtained:

1. Scalar and representative statistical models for the multi-dimensional and inter-correlated POLSAR data are to be derived.
 - (a) A scalar statistical model for the POLSAR observable, being the determinant of the covariance matrix, is to be derived.
 - (b) The statistical models for different discrimination measures which are based on the observable are to be established together with its consistent property.
 - (c) The representation power of these observables is to be illustrated by showing that when the multi-channel POLSAR data is collapsed into the traditional one-channel SAR data, this determinant is transformed into the representative SAR intensity.
 - (d) The model os to be validated against practical real-life captured POLSAR data.
2. Homoskedastic statistical models for the heteroskedastic (POL)SAR data are to be derived.
 - (a) The fact that (POL)SAR data are heteroskedastic in the original domain and logarithmic transformation can convert this into a homoskedastic model are to be shown
 - (b) Homoskedastic measures of distance for the multi dimensional POLSAR as well as for the one dimensional SAR data are to be derived.
 - (c) These statistical models are to be validated against both practical SAR and POLSAR data
3. The beneficial applications of these statistical models are to be demonstrated. Specifically:
 - (a) To show how the consistent sense of variance helps break the vicious cycle in the problem of SAR speckle filtering: a new statistical test for homogeneity and a new speckle filter is derived.
 - (b) To show how the consistent sense of subtractive distance helps in the problem of evaluating (POL)SAR speckle filters: the log-MSE is proposed to combine the evaluation of radiometric preservation and speckle suppression power.

- (c) An example where an existing SAR processing technique is extensible towards POLSAR data is to be demonstrated

In summary, the first main objective is to derive a scalar and representative statistical model for POLSAR data. The second main objective is to derive homoskedastic measures of distance despite its multiplicative and heteroskedastic nature. This is first applied on the simpler case of SAR data. To combine these two seemingly disconnected threads of research, the results for SAR are extended to POLSAR, since the thesis also shows that the POLSAR models are a generic multi-dimensional superset of the traditional SAR data.

1.5 Organisation of the Thesis

The rest of this thesis is organized into five chapters as follows.

Chapter 2 will survey the related publications and the state-of-the-art techniques in modelling, processing, filtering and evaluating (POL)SAR speckle filter. It will also discuss the different measures of distance for both SAR and POLSAR data, together with their extensive applications. Through these discussions, the need for a homoskedastic and scalar model for the multivariate and heteroskedastic POLSAR is brought forward.

Chapter 3 begins by highlighting that SAR data are heteroskedastic in the original domain, whereas logarithmic transformation converts this into a homoskedastic model. It also derives consistent and homoskedastic measures of distance for the one dimensional SAR data. These models for SAR are then validated against real-life practical data. (i.e. see Research Contribution 2a to 2c)

Chapter 4 then derives several scalar statistical models for the determinant of the POLSAR covariance matrix and shows that this is heteroskedastic in the original domain as well as homoskedastic in the log-transformed domain. It also derives the heteroskedastic discrimination measures as well as several homoskedastic measures of distance for the data. Then the models for SAR are shown to be a special case of the proposed models for POLSAR and finally it validates these proposed models (i.e. see Research Contribution 1a to 1d)

The beneficial applications of these models is presented in chapter 5, where the property of a consistent sense of variance helps to break the vicious cycle in SAR speckle filtering.

It also shows how MSE can again be applicable in the additive and homoskedastic domain to evaluate SAR speckle filters. An example of extending existing techniques from SAR to POLSAR is also demonstrated in this chapter where the MSE evaluation criteria is also shown capable of evaluating POLSAR speckle filters. (i.e. see Research Contribution [3a](#) to [3c](#)) Finally, the contribution of the thesis with respect to the research objectives and research impact is discussed in the concluding chapter [6](#).

Chapter 2

Current Methods in Processing SAR and POLSAR Data

This chapter reviews the published literature for SAR and POLSAR data processing. Specifically, its first section describes the multi-dimensional and stochastic nature of the (POL)SAR data. The second section then illustrates the different approaches that have been published to address the grand challenge of modelling, processing and ultimately understanding these types of data.

2.1 The Stochastic and Multivariate Nature of (POL)SAR data

2.1.1 The Stochastic Nature of SAR data

The stochastic nature of SAR data arises due to the process of SAR image formation. Specifically, since one SAR resolution cell is very big in comparison to the radar wavelength, it normally consists of many elementary scatterers. The data point of each SAR pixel then arises from the combined interference effect of the backscattered waves from these different scatterers. This effect causes natural variation in SAR intensity image even when the underlying scene is highly homogeneous.

SAR speckle phenomena are explained as the interference of many coherent but de-

phased backscattering components; each reflecting from different and distributed elementary scatterers [3, 4]. The random nature of the SAR data arises due to the unknown and varying location, height and thus distance of each elementary scatterer; which, in turn, generates random phases in their back-scattering responses. Assuming the number of these elementary back scatterers is sufficiently large, then the Central Limit Theorem is applicable [5]. Consequently the interference of these randomly phased responses can be considered as a random walk on the 2D complex plane [6]. Specifically the real part A_r as well as the imaginary part A_i of the observed SAR signal A can be considered as random variables from uncorrelated Gaussian distributed stochastic processes with zero means and identical variances $\sigma^2/2$ [7]. Their probability density functions (PDF) are given as:

$$pdf(A_x) = \frac{1}{\sqrt{\pi}\sigma} e^{-\left(\frac{A_x^2}{\sigma^2}\right)} \quad (2.1)$$

It can then be shown that the measurable amplitude $A = \sqrt{A_r^2 + A_i^2}$ is a random variable of Rayleigh distribution. Subsequently the SAR intensity $I = A^2 = (A_r^2 + A_i^2)$ is a random variable of a negative exponentially distributed random process. The PDFs of these two properties can then be expressed as:

$$pdf(A) = \frac{2A}{\sigma^2} e^{-\left(\frac{A^2}{\sigma^2}\right)} \quad (2.2)$$

$$pdf(I) = \frac{1}{\sigma^2} e^{-\left(\frac{I}{\sigma^2}\right)} \quad (2.3)$$

As SAR speckle phenomena arises from the stochastic nature of SAR, it seriously hinders the interpretation and understanding of SAR images. Speckle noise on SAR images are hence routinely reduced through a speckle filtering process for easier human interpretation and more accurate post-processing.

2.1.2 The Multivariate Nature of POLSAR data

2.1.2.1 The polarization property of Electro-Magnetic waves

The propagation of Electro-Magnetic (EM) wave in space is governed by Maxells equations. The general solution to these equations is a linear superposition of waves, each having the form of:

$$\begin{aligned}\vec{E}(\vec{r}, t) &= g(\phi(\vec{r}, t)) = g(\omega t - \vec{k} \cdot \vec{r}) \\ \vec{B}(\vec{r}, t) &= g(\phi(\vec{r}, t)) = g(\omega t - \vec{k} \cdot \vec{r})\end{aligned}$$

where g is any well-behaved function of a dimensionless argument ϕ , ω is the angular frequency (in radians per second), and $\vec{k} = (k_x, k_y, k_z)$ is the wave vector (in radians per meter).

Because of the divergence between the electric and the magnetic fields, there will be no fields in the direction of wave propagation. Thus if we define the z direction as the travelling direction of the EM wave, then both the electric and the magnetic fields are fluctuating in the x,y plane. Furthermore, when considering wave propagation, it is conventional that only the electric field vector is described and the magnetic field is ignored since it is perpendicular to the E field and is proportional to it. Projecting this vector into x,y directions, we have:

$$\vec{E}(z, t) = \begin{pmatrix} E_x^0 \cos(wt - kz + \phi_x^0) \\ E_y^0 \cos(wt - kz + \phi_y^0) \\ 0 \end{pmatrix} = \begin{pmatrix} \xi_x(t) \\ \xi_y(t) \\ 0 \end{pmatrix}$$

where ϕ_0 is the initial phase angle, that is dependent on the choice of space-time origin.

In other words, the EM vector can oscillate in more than one orientation, and this denote the polarization property of EM wave. The exact shape traced out in a fixed projective plane by the tip of the electric vector as the plane propagate is a description of the polarization state. This shape is characterized by the formula:

$$\frac{\xi_x^2(t)}{|E_x^0|^2} + \frac{\xi_y^2(t)}{|E_y^0|^2} - 2 \frac{\xi_x \xi_y}{E_x^0 E_y^0} \cos(\Delta\phi) = \sin^2(\Delta\phi)$$

where $\Delta\phi = \phi_y^0 - \phi_x^0$. The formula characterizes what is termed as the polarization

ellipse.

The parameters that describe the polarization ellipse are:

$$\tan(\theta) = \frac{E_y^0}{E_x^0}$$

with $0 \leq \theta \leq \pi/2$. The orientation angle, which is the angle between the major semi-axis of the ellipse and the x-axis, is given by:

$$\tan(\Psi) = \tan(2\theta) \cos(\Delta\phi)$$

with $0 \leq \Psi < \pi$. The ellipticity, ϵ is the major-to-minor-axis ratio. The ellipticity angle which is defined as $\chi = \arctan(1/\epsilon)$ can be calculated as:

$$\sin(2\chi) = \sin(2\theta) \sin(\Delta\phi)$$

with $0 \leq \chi \leq \pi/2$, and $0 \leq \epsilon \leq \infty$

Ignoring the scale of the electrical fields, the elementary wave polarization can be completely described by two parameters, i.e. E_y^0/E_x^0 and $\Delta\phi = \phi_y^0 - \phi_x^0$. Similarly, ignoring the scale of the ellipse, the polarization ellipse can be completely described by two angles Ψ and χ .

Other parameters includes:

Complex polarization ratio This ratio is important in explaining polarization basis changes.

It is defined as:

$$\rho = \frac{E_y^0}{E_x^0} e^{i\Delta\phi} = \frac{\cos(2\chi) + i \sin(2\chi)}{1 - \cos(2\Psi) \cos(2\chi)} \quad (2.4)$$

Jones Vector The Jones vector is defined as

$$J = \begin{pmatrix} \xi_x(t) \\ \xi_y(t) \end{pmatrix} = \xi_x(t) \begin{pmatrix} 1 \\ \rho \end{pmatrix} \quad (2.5)$$

Thus the normalized Jones vector can be given as:

$$J = \begin{pmatrix} \cos(\theta) \cdot e^{i\phi_x^0} \\ \sin(\theta) \cdot e^{i\phi_y^0} \end{pmatrix} = \begin{pmatrix} 1 \\ \tan(\theta) \cdot e^{i\Delta\phi} \end{pmatrix} = \begin{pmatrix} \cos(\Psi) \cos(\chi) - i \sin(\Psi) \sin(\chi) \\ \sin(\Psi) \cos(\chi) + i \cos(\Psi) \sin(\chi) \end{pmatrix} \quad (2.6)$$

The two parameters in the Jones vector can completely describe the polarization state (ellipse) of any elementary wave. This same Jones vector finds extensive use in quantum mechanics, and is interpreted as quantum state vector. Its bra-ket notation formula, which is normally used in quantum computation contexts is:

$$J = |\Psi\rangle = \begin{pmatrix} \cos(\theta) \cdot e^{i\phi_x^0} \\ \sin(\theta) \cdot e^{i\phi_y^0} \end{pmatrix} \quad (2.7)$$

By definitions, the horizontal linear polarized wave is defined as: $J_h = \begin{pmatrix} 1 \\ 0 \end{pmatrix}$, similarly the vertical linear polarized wave: $J_v = \begin{pmatrix} 0 \\ 1 \end{pmatrix}$, the $\pm\pi/4$ linear polarized waves $J_{\pm} = \pm\frac{1}{\sqrt{2}} \begin{pmatrix} 1 \\ 1 \end{pmatrix}$, the left circular polarized wave: $J_l = |L\rangle = \frac{1}{\sqrt{2}} \begin{pmatrix} 1 \\ -i \end{pmatrix}$ and the right circular polarized wave: $J_r = |R\rangle = \frac{1}{\sqrt{2}} \begin{pmatrix} 1 \\ i \end{pmatrix}$

Stokes Vector Another way to look at polarization is through the coherency matrix, and equivalently the Stokes matrix. The wave coherency matrix is defined as:

$$W_c = \left\langle \begin{pmatrix} \xi_x \\ \xi_y \end{pmatrix} \begin{pmatrix} \xi_x \\ \xi_y \end{pmatrix}^\dagger \right\rangle = \left\langle \begin{pmatrix} \xi_x \xi_x^* & \xi_x \xi_y^* \\ \xi_y \xi_x^* & \xi_y \xi_y^* \end{pmatrix} \right\rangle = \left\langle \begin{pmatrix} |\xi_x|^2 & |\xi_x||\xi_y|e^{-i\Delta\phi} \\ |\xi_x||\xi_y|e^{i\Delta\phi} & |\xi_y|^2 \end{pmatrix} \right\rangle$$

The Stokes vector is then defined as:

$$S_t = \begin{pmatrix} S_0 \\ S_1 \\ S_2 \\ S_3 \end{pmatrix} = \begin{pmatrix} |\xi_x|^2 + |\xi_y|^2 \\ |\xi_x|^2 - |\xi_y|^2 \\ 2\Re(\xi_x \xi_y^*) \\ 2\Im(\xi_x \xi_y^*) \end{pmatrix}$$

In the case of elementary (or fully polarized) waves, the Stokes vector can be written as:

$$S_t = \begin{pmatrix} S_0 \\ S_0 \cos(2\Psi) \cos(2\chi) \\ S_0 \sin(2\Psi) \cos(2\chi) \\ S_0 \sin(2\chi) \end{pmatrix}$$

At this point, a distinction needs to be highlighted. In comparison to the two-element Jones vector, Stokes vectors have more data, namely four elements. The Jones vector can completely describe the polarization states of an elementary wave, whose formulation is based on the assumption that the wave is very well behaved. In practice, that is not normally the case, because reflected waves are generally combinations of multiple waves which ranged over certain areas of time and frequency. As such, the polarization of the waves are normally not fully polarized. One simple analogy is that the field ratio, i.e. ξ_x/ξ_y , or the phase difference, i.e. $\Delta\phi$, are not constant at all times.

The analysis above is especially prevalent in the remote sensing community, where the area of a single resolution cell (pixel) is very large compared with the radar's wavelength. In such cases, the wave field is very stochastic and only statistical information about the variations and correlations between polarization components can be gathered.

Degree of polarization Closely related to the Stokes vector is the concept of “Degree of polarization” p , which is a quantity used to describe the portion of an EM wave which is polarized. A perfectly polarized wave has $p = 100\%$, while a fully depolarized wave is characterized by $p = 0\%$. A wave which is partially polarized can be represented as a superposition of a polarized and another unpolarized component. Thus $0 \leq p \leq 1$.

Depolarization phenomena are explained from the fact that most sources of EM radiation contain a large number of “elementary” sources. The polarization of the electric fields produced by the emitters may not be correlated, which leads to depolarization effects. If there is partial correlation among the “elementary” sources, the light is partially polarized. One may then describe the received EM wave polarization in terms of the degree of polarization and the parameters of the polarization ellipse.

In fully polarized wave, the following equation holds:

$$S_0^2 = S_1^2 + S_2^2 + S_3^2$$

In depolarized wave, it becomes an in-equation

$$S_0^2 > S_1^2 + S_2^2 + S_3^2$$

Then the degree of polarization is defined as

$$p = \frac{\sqrt{S_1^2 + S_2^2 + S_3^2}}{S_0}$$

In such general case, the Stokes Vector is written as:

$$\begin{aligned} S_t &= \begin{pmatrix} I \\ Ip \cos(2\Psi) \cos(2\chi) \\ Ip \sin(2\Psi) \cos(2\chi) \\ Ip \sin(2\chi) \end{pmatrix} \\ &= I(1-p) \begin{pmatrix} 1 \\ 0 \\ 0 \\ 0 \end{pmatrix} + Ip \begin{pmatrix} 1 \\ \cos(2\Psi) \cos(2\chi) \\ \sin(2\Psi) \cos(2\chi) \\ \sin(2\chi) \end{pmatrix} \end{aligned}$$

Alternatively, if the Stokes vector is measured and known, then the polarization characteristics of a wave are given as: I , the total power of the measured beam is $I = S_0$, p , the degree of polarization is calculated as $p = \frac{\sqrt{S_1^2 + S_2^2 + S_3^2}}{S_0}$, $2\Psi = \tan^{-1}(S_2/S_1)$ and $2\chi = \tan^{-1}(S_3/\sqrt{S_1^2 + S_2^2})$ are the angles that characterize the wave polarization state.

2.1.2.2 Full Polarimetry and the Polarimetric Signatures

This section describes the core concept of POLSAR, i.e. the target's polarimetric signature, and illustrates why research into partial polarimetry is warranted.

POLSAR radar measures the back-scattered echo received as the result of transmitting a signal. The scattering matrix relates the received signal E^{Rx} with the transmitted

E^{Tx} signal as:

$$E^{Rx} = \frac{e^{ikr}}{r} S E^{Tx}$$

Normally, horizontal and vertical linear polarization are used for transmission, and thus the scattering matrix, i.e. S , would normally have the following expanded form:

$$\begin{pmatrix} E_h^{Rx} \\ E_v^{Rx} \end{pmatrix} = \frac{e^{ikr}}{r} \begin{pmatrix} S_{HH} & S_{HV} \\ S_{VH} & S_{VV} \end{pmatrix} \begin{pmatrix} E_h^{Tx} \\ E_v^{Tx} \end{pmatrix}$$

The scattering matrix can be called the Jones matrix (relating to the Jones vector) in the forward scattering alignment. The matrix is normally called the Sinclair matrix in SAR literature, as backward scattering alignment is normally adopted for SAR [8]. In the case of mono-static SAR, i.e. both radar transmitter and receiver can be considered as located in a single place, physical reciprocity leads to $S_{HV} = S_{VH}$ [9].

The matrix can also be “stratified” to define the target scattering vector as:

$$T_{cv} = \begin{pmatrix} S_{HH} \\ \sqrt{2}S_{HV} \\ S_{VV} \end{pmatrix} \quad (2.8)$$

or

$$T_{ch} = \frac{1}{\sqrt{2}} \begin{pmatrix} S_{HH} + S_{VV} \\ S_{HH} - S_{VV} \\ S_{HV} \end{pmatrix} \quad (2.9)$$

Similar to the reason that Stokes vectors are preferred to Jones vector in wave polarization, second order statistics of the target scattering matrix are normally preferred. The covariance matrix is defined as:

$$C_v = \langle T_{cv} T_{cv}^{*T} \rangle = \begin{pmatrix} S_{HH} S_{HH}^* & \sqrt{2} S_{HH} S_{HV}^* & S_{HH} S_{VV}^* \\ \sqrt{2} S_{HV} S_{HH}^* & 2 S_{HV} S_{HV}^* & \sqrt{2} S_{HV} S_{VV}^* \\ S_{VV} S_{HH}^* & \sqrt{2} S_{VV} S_{HV}^* & S_{VV} S_{VV}^* \end{pmatrix} \quad (2.10)$$

while the coherency matrix is defined as:

$$C_h = \langle T_{ch} T_{ch}^{*T} \rangle = \frac{1}{2} \begin{pmatrix} (S_{HH} + S_{VV})(S_{HH} + S_{VV})^* & (S_{HH} + S_{VV})(S_{HH} - S_{VV})^* & (S_{HH} + S_{VV}) S_{HV}^* \\ (S_{HH} - S_{VV})(S_{HH} + S_{VV})^* & (S_{HH} - S_{VV})(S_{HH} - S_{VV})^* & (S_{HH} - S_{VV}) S_{HV}^* \\ 2 S_{HV} (S_{HH} + S_{VV})^* & 2 S_{HV} (S_{HH} - S_{VV})^* & S_{HV} S_{HV}^* \end{pmatrix} \quad (2.11)$$

Evidently the two matrices are related:

$$C_h = NC_vN^T$$

$$\text{where } N = \frac{1}{\sqrt{2}} \begin{pmatrix} 1 & 0 & 1 \\ 1 & 0 & -1 \\ 0 & \sqrt{2} & 0 \end{pmatrix}$$

The off-diagonal values in both covariance and coherence matrices are normally complex numbers. Equivalent matrices with all real value entries which carry the same information are called the Mueller and the Kennaugh matrix, which are to be used in forward and backward scattering alignment respectively[10]. They are defined as the matrix that relates the Stokes matrix of sent and received signals.

$$S_t^{Rx} = KS_t^{Tx}$$

Since the Stokes and Jones matrices are related, the Kennaugh and Sinclair matrices are also related, and this relationship is given by:

$$K = 1/2Q^*S \otimes S^*Q^{T*}$$

$$\text{where } \otimes \text{ denotes the Kronecker product, and } Q = \begin{pmatrix} 1 & 0 & 0 & 1 \\ 1 & 0 & 0 & -1 \\ 0 & 1 & 1 & 0 \\ 0 & i & i & 0 \end{pmatrix}$$

POLSAR aims to measure the target's polarimetric response. Typically, the radar transmitter will separately send different horizontal and vertical polarized waves, and measure the response also in horizontal and vertical polarization directions. The full polarimetric data, will then have four channels, i.e. $\{S_{HH}, S_{VV}, S_{HV}, S_{VH}\}$. The four channel, or quad-pol data, is considered full polarimetric data since it allows one to synthesize the target's response for any given pair of transmitted and received polarization. Such a process is called polarization synthesis. The formula is given as:

$$I^{Rx} = \begin{pmatrix} 1 \\ \cos(2\chi^{Rx}) \cos(2\Psi^{Rx}) \\ \cos(2\chi^{Rx}) \sin(2\Psi^{Rx}) \\ \sin(2\chi^{Rx}) \end{pmatrix}^T K \begin{pmatrix} 1 \\ \cos(2\chi^{Tx}) \cos(2\Psi^{Tx}) \\ \cos(2\chi^{Tx}) \sin(2\Psi^{Tx}) \\ \sin(2\chi^{Tx}) \end{pmatrix} \quad (2.12)$$

where I^{Rx} is the intensity of the target's response in a given combination of transmitted and received polarizations.

In a full polarimetric implementation, an alternate pulsing scheme is normally used to share a single time slot for transmitting two different polarizations' pulses. In partial polarimetry modes only a single polarization is sent. Since the transmitting time-slot no longer needs to be shared in the partial polarimetry modes, higher operating frequency become possible which leads to better (almost double) resolution or coverage. Clearly in such cases, only two out of four data channels is available, i.e. either $\{S_{HH}, S_{HV}\}$ or $\{S_{VH}, S_{VV}\}$. This trade-off is based on limitations of physics, and hence is likely to be around for years to come.

2.1.2.3 Partial Polarimetry and the Stokes Vector

Early works from the radar community had focused on the theoretical introduction of the scattering matrix such as the Sinclair matrix or Mueller matrices, for full, i.e. quad, polarimetric measurements [8]. These works were continued by Boerner, and the first polarimetric images were captured by NASA JPL at Caltech in 1991 [11].

Systems were then engineered and commercial POLSAR satellites, e.g. RadarSat, TerraSAR, Alos-PalSAR were launched. However due to operational restrictions on payload, power and data-downlink, the satellites also offer dual-channel polarimetric SAR modes as a compromise between theoretical polarimetric requirements and practical limitations. Initially, to the end user, while dual-channel partial polarimetry may not provide the complete polarimetric signature of the target, the loss is compensated for by either better resolutions or higher coverage and lower cost.

Until very recently, these partial polarimetry modes were not formally taken up by scientists and academia. In his pioneer paper in 2005, Souyris[12] introduced the so-called compact polarimetry mode and suggested that it may be possible to reconstruct full polarimetric information from compact polarimetric data. Raney[13] also showed that dual-channel polarimetry is not only capable of measuring the complete polarization information of the back-scattered EM wave (via Stokes parameters), it is also capable of detecting the basic target's polarimetric characteristic, e.g. odd or even bounce phenomena.

While the dual-polarization mode sensing has been available operationally for quite

some time, partial polarimetry has only recently been investigated in the scientific community. In comparison, partial polarimetry measures dual-polarized response from incoming pulses of a single polarization channel, while full polarimetry measures the same response from two (generally orthogonal) polarisation channels. Mathematically, the process is modelled as:

$$\begin{pmatrix} E_h^{Rx} \\ E_v^{Rx} \end{pmatrix} = \frac{e^{ikr}}{r} \begin{pmatrix} S_H \\ S_V \end{pmatrix} E^{Tx}$$

[12] pioneered the field with a paper on compact polarimetry. This essentially describes a partial polarimetry mode in which the incoming pulse is of linear polarization, but is of neither fully horizontal nor vertical angle. Instead, its incoming polarization of linear polarisation has an odd angle of $\pi/4$. The partial polarimetric covariance matrix is then given as

$$J = \begin{pmatrix} |s_{HH}|^2 + |s_{HV}|^2 & s_{HH}s_{VV}^* + |s_{HV}|^2 \\ +2\Re(s_{HH}s_{HV}^*) & +s_{HH}s_{HV}^* + s_{HV}s_{VV}^* \\ s_{HH}^*s_{VV} + |s_{HV}|^2 & |s_{VV}|^2 + |s_{HV}|^2 \\ +s_{HV}s_{HH}^* + s_{VV}s_{HV}^* & +2\Re(s_{VV}s_{HV}^*) \end{pmatrix}$$

In [13], Raney demonstrated a different perspective by proposing a hybrid architecture. He argued that the dual polarisation measurements effectively capture the polarisation states of the single back-scattered signal resulting from a single incoming pulse. Thus the polarisation choice of the receiving antenna is trivial (as long as they are orthogonal). The important parameter is the choice of the polarisation to be used for the incoming pulse. His hybrid architecture is again a kind of partial polarimetry in which the incoming pulse is of circular polarisation, instead of the normally encountered linear polarisation. The partial covariance matrix then becomes:

$$J = \frac{1}{2} \begin{pmatrix} |s_{HH}|^2 + |s_{HV}|^2 & s_{HH}s_{HV}^* - s_{HV}s_{VV}^* \\ +i(s_{HH}s_{HV}^* - s_{HV}s_{VV}^*) & -i(|s_{HV}|^2 + s_{HH}s_{VV}^*) \\ s_{HH}s_{HV}^* - s_{HV}s_{VV}^* & |s_{VV}|^2 + |s_{HV}|^2 \\ +i(|s_{HV}|^2 + s_{HH}s_{VV}^*) & +i(s_{HV}s_{VV}^* - s_{VV}s_{HV}^*) \end{pmatrix}$$

The benefits of this hybrid architecture, according to Raney are that it can measure certain physical polarimetric phenomena such as the odd and even bounce phenomena. The suggestion is evidenced by calculating the response of known odd-bounce trihedral and even-bounce dihedral when the incident wave is right circular polarized.

$$\Gamma_{tri} = \begin{pmatrix} 1 & 0 \\ 0 & -1 \end{pmatrix}$$

Then the response will be reversed as it can be calculated as:

$$J_r = \begin{pmatrix} 1 & 0 \\ 0 & -1 \end{pmatrix} \cdot \begin{pmatrix} 1 \\ -i \end{pmatrix} = \begin{pmatrix} 1 \\ i \end{pmatrix}$$

with $\begin{pmatrix} 1 \\ -i \end{pmatrix}$ indicating right circular polarization transmitted, and $\begin{pmatrix} 1 \\ i \end{pmatrix}$ indicating left circular polarization received.

For a dihedral target, whose main axis is at an angle θ with respect to the horizontal direction, the Sinclair matrix is given as:

$$\Gamma_{dih} = \begin{pmatrix} \cos(2\theta) & \sin(2\theta) \\ \sin(2\theta) & \cos(2\theta) \end{pmatrix}$$

The even bounce phenomena is detectable as its polarimetric response, which is then:

$$J_r = \begin{pmatrix} \cos(2\theta) & \sin(2\theta) \\ \sin(2\theta) & \cos(2\theta) \end{pmatrix} \cdot \begin{pmatrix} 1 \\ -i \end{pmatrix} = \begin{pmatrix} 1 \\ -i \end{pmatrix}$$

In [14], Raney shows that hybrid circular modes bring many conveniences to hardware calibration. Also in a follow up study [15], he demonstrated the classification power of hybrid polarimetry. Furthermore, Lardeux [16] found that for target classification using SVM techniques, compact polarimetry mode shows comparable results to full polarimetric data. Notably, the hybrid architectural concept has been adopted and brought towards implementation by NASA's upcoming Desdynl satellite [17].

The research into partial polarimetry is convenient as its data can be simulated using polarisation basis transformations such as those described above. Hardware realisation may not be needed until the final physical prototype stages. This methodology has been demonstrated and is widely used in the community. The focus into partial polarimetry

allows analysis with a smaller matrix, while its implications can be extended not only to full polarimetry modes but also towards bi-static polarimetric scenarios. Besides that, a number of research questions in this new field are still open, relevant and exciting.

Souyris, in 2005, published a paper [12] which claimed and presented an algorithm to reconstruct full polarimetric information from the given partial compact polarimetric data. The algorithm is claimed to work on natural surfaces. In [18], Nord reviewed the reconstruction problem for various different partial polarimetry modes, and an improved algorithm is given. In [19], Ainsworth reviewed performance of target classification on different partial modes, reconstructed pseudo-full mode and full polarimetric data. Chapter 3 will review this sub-topic further and introduce our work on expanding the reconstruction to urban man-made structures and surfaces (from the original system which was relevant to natural cover only).

For the tasks of target detection and classification, we believe that partial dual polarization provides a unique proposition. Compared with single-channel systems, the dual channel provides additional and useful polarimetric information. Compared with full polarimetric data, the better spatial resolution of dual channel systems could compensate for the loss of reconstructed polarimetric information, especially for the purpose of target detection and classification.

2.1.2.4 The Polarization Basis Transformation

Assuming that the polarization states are known, the wave representation can be given in terms of ξ_x and ξ_y as:

$$\begin{pmatrix} \xi_x \\ \xi_y \end{pmatrix} = A_0 e^{-i\phi_0} \begin{pmatrix} \cos(\Psi) & -\sin(\Psi) \\ \sin(\Psi) & \cos(\Psi) \end{pmatrix} \begin{pmatrix} \cos(\chi) \\ i \sin(\chi) \end{pmatrix}$$

The representation of a wave, however, depends on the choice of orthogonal reference frame basis.

Consider two different orthogonal basis, $\{x, y\}$ and $\{h, v\}$. A given Jones vector can be measured in both basis as: $J_{xy} = \begin{pmatrix} \xi_x \\ \xi_y \end{pmatrix}$ and $J_{hv} = \begin{pmatrix} \xi_h \\ \xi_v \end{pmatrix}$. The transformation from $\{h, v\}$ to $\{x, y\}$ is governed by a unitary transformation matrix U_2 , which is given

as:

$$\begin{pmatrix} \xi_x \\ \xi_y \end{pmatrix} = U_2 \begin{pmatrix} \xi_h \\ \xi_v \end{pmatrix}$$

Boerner [20] has given U_2 as:

$$U_2 = \frac{1}{\sqrt{1+\rho\rho^*}} \begin{pmatrix} 1 & -\rho^* \\ \rho & 1 \end{pmatrix} \begin{pmatrix} e^{-i\delta} & 0 \\ 0 & e^{i\delta} \end{pmatrix}$$

where ρ is the complex polarisation ratio of the Jones vector for the first new basis, and $\delta = \tan^{-1}(\tan(\Psi)\tan(\chi)) - \phi_0$ is the phase reference for the new basis, and δ is required for the determination of the initial phase of the Jones vector in the new reference basis.

In the same vein, [21] gives

$$U_2 = \begin{pmatrix} \cos(\Psi) & -\sin(\Psi) \\ \sin(\Psi) & \cos(\Psi) \end{pmatrix} \begin{pmatrix} \cos(\chi) & i\sin(\chi) \\ i\sin(\chi) & \cos(\chi) \end{pmatrix} \begin{pmatrix} e^{-i\phi_0} & 0 \\ 0 & e^{i\phi_0} \end{pmatrix}$$

From these results, it is then possible to derive equations for the transformation of the scattering matrix. Noting that by definition, $J_{xy}^r = S_{xy}J_{xy}^t$, $J_{hv}^r = S_{hv}J_{hv}^t$ and that $J_{xy}^* = U_2 J_{hv}^*$, also that $(U_2)^{-1} = (U_2)^T$, it is then trivial to show that:

$$S_{xy} = U_2 S_{hv} U_2^T$$

Using the result above, we then have:

$$\begin{aligned} S_{xx} &= \frac{1}{1+\rho\rho^*} \left(S_{HH}e^{-2i\delta} - \rho^*(S_{HV} + S_{VH}) + (\rho^*)^2 S_{VV}e^{2i\delta} \right) \\ S_{xy} &= \frac{1}{1+\rho\rho^*} \left(\rho S_{HH}e^{-2i\delta} + S_{HV} - \rho\rho^* S_{VH} - \rho^* S_{VV}e^{2i\delta} \right) \\ S_{yx} &= \frac{1}{1+\rho\rho^*} \left(\rho S_{HH}e^{-2i\delta} - \rho\rho^* S_{HV} + S_{VH} - \rho^* S_{VV}e^{2i\delta} \right) \\ S_{yy} &= \frac{1}{1+\rho\rho^*} \left(\rho^2 S_{HH}e^{-2i\delta} + \rho(S_{HV} + S_{VH}) + S_{VV}e^{2i\delta} \right) \end{aligned}$$

In the case of mono-static POLSAR, i.e. $S_{HV} = S_{VH} = S_{XX}$ and $S_{xy} = S_{yx}$, the

equations become

$$S_{xx} = \frac{1}{1 + \rho\rho^*} \left(S_{HHe} e^{-2i\delta} - 2\rho^* S_{XX} + (\rho^*)^2 S_{VVe}^{2i\delta} \right)$$

$$S_{yx} = S_{xy} = \frac{1}{1 + \rho\rho^*} \left(\rho S_{HHe} e^{-2i\delta} + (1 - \rho\rho^*) S_{XX} - \rho^* S_{VVe}^{2i\delta} \right)$$

$$S_{yy} = \frac{1}{1 + \rho\rho^*} \left(\rho^2 S_{HHe} e^{-2i\delta} + 2\rho S_{XX} + S_{VVe}^{2i\delta} \right)$$

The results here, together with Stokes Vector's formula, can be used to prove the following identity, which can form the basis of a novel approach in POLSAR speckle filtering:

$$S_t = \begin{pmatrix} S_h S_h + S_v S_v \\ S_h S_h - S_v S_v \\ 2\Re(S_h S_v^*) \\ 2\Im(S_h S_v^*) \end{pmatrix} = \begin{pmatrix} S_h S_h + S_v S_v \\ S_h S_h - S_v S_v \\ S_+ S_+ - S_- S_- \\ S_l S_l - S_r S_r \end{pmatrix}$$

where S_t is the Stokes vector and $S_+ S_+$, $S_- S_-$, $S_r S_r$, $S_l S_l$ are the intensity of received signals in $+45^\circ$ linear, -45° linear, right circular and left circular polarization respectively.

2.2 Current methods in SAR and POLSAR Data Processing

2.2.1 Current Statistical Models for SAR and POLSAR data

Different target decomposition theorems have identified many possible scalar observables for the complex POLSAR data. In [22], the performance of different scalar POLSAR observables for classification purposes are evaluated. While many scalar observables for POLSAR were presented, their corresponding statistical models and classifiers were not available. Furthermore, at its conclusion, the paper indicated that “it is impossible to identify the best one” as these “representations ... do not show a precise trend”. Although, to be fair, these observables are identified to describe a decomposed portion of the complex POLSAR data, and thus they were not precisely defined to be used individually for the purpose of single-handedly representing POLSAR data.

Given that the joint distribution for POLSAR is known to be the multi-variate complex Wishart distribution, it is possible to derive the scalar statistical models for some univariate POLSAR observables. However, such derivations are no trivial task, as the data is much more complex and the field is much less mature than that of traditional SAR statistical modelling. Thus the strategy of the pioneering works tend to be to tackle simpler versions of polarimetry.

In the literature, POLSAR data is commonly represented by its covariance matrix. For full polarimetric SAR data (full-pol) the covariance matrix has the form of

$$C_3 = \begin{bmatrix} S_{hh}^2 & \sqrt{2}S_{hh}S_{hv}^* & S_{hh}S_{vv}^* \\ \sqrt{2}S_{hh}^*S_{hv} & 2S_{hv}^2 & \sqrt{2}S_{hv}S_{vv}^* \\ S_{hh}^*S_{vv} & \sqrt{2}S_{hv}^*S_{vv} & S_{vv}^2 \end{bmatrix}$$

For partial polarimetric SAR data (part-pol), it reduces to either of the two following equations:

$$C_{2,h} = \begin{bmatrix} S_{hh}^2 & S_{hh}S_{hv}^* \\ S_{hh}^*S_{hv} & S_{hv}^2 \end{bmatrix}; C_{2,v} = \begin{bmatrix} S_{hv}^2 & S_{hv}S_{vv}^* \\ S_{hv}^*S_{vv} & S_{vv}^2 \end{bmatrix}$$

Obviously, the statistical behaviour of C_3 can be understood by understanding the behaviour of C_{2h}, C_{2v} and

$$C_{2,c} = \begin{bmatrix} S_{hh}^2 & S_{hh}S_{vv}^* \\ S_{hh}^*S_{vv} & S_{vv}^2 \end{bmatrix}$$

While C_{2v}, C_{2h} are physically related to the Stokes parameters of EM waves, C_{2c} is an artificial term derived from the ful-pol covariance matrix. In fact, in the field of polarimetric SAR, C_{2v}, C_{2h} are called cross-pol and C_{2c} is called the co-pol covariance matrice. Their main difference lies in investigating the so-called complex correlation coefficient, defined as:

$$\rho = \frac{E(S_{pq}S_{rs}^*)}{\sqrt{E(S_{pq}^2)E(S_{rs}^2)}} = |\rho|e^{j\phi}$$

with $\phi = \arg(\rho)$ is the phase difference angle. In C_{2v} and C_{2h} that are commonly used in optical physics, $|\rho_v|, |\rho_h|$ are insignificant, and ϕ_v, ϕ_h are very random, due to little correlation existing between orthogonal polarizations in monochromatic EM waves. Their equivalent lies in the “natural surface” case of POLSAR, where it is common to assume $|\rho_v| = |\rho_h| = 0$. This is, however, not true in the general case of POLSAR (i.e.

including over built-up areas). Specifically for C_{2c} , since there is correlation between the two co-pol channels, $|\rho_c|$ is almost always significant and ϕ_c is also not entirely random.

In the field of optical physics, under the assumption of no correlation between cross-polarized channels, [23], [24] and [25] derived the statistical models for C_{2h}, C_{2v} . The observables that have been studied are:

1. the polarization ellipse parameters [23]: i.e.
 - (a) the total power $S_0 = C_{11}^2 + C_{22}^2$,
 - (b) the ratio of minor to major axis of the polarization ellipse $\epsilon = \lambda_2/\lambda_1$,
 - (c) and ψ the angle that the ellipse major axis makes with horizontal axis,
2. the Stokes parameters [24]: i.e.
 - (a) $S_0 = C_{11}^2 + C_{22}^2$
 - (b) $S_1 = C_{11}^2 - C_{22}^2$
 - (c) $S_2 = \Re(C_{12})$
 - (d) $S_3 = \Im(C_{12})$
3. and the normalized Stokes parameters $s_i = S_i/S_0, i > 0$ [25]

In the field of POLSAR, under the assumption of significant correlation between polarized channels, [26], [27] and [28] derived the statistical models for not only C_{2h}, C_{2v} but also C_{2c} . Specifically the following observables were studied:

1. cross-pol ratio $r_{HV/HH} = |S_{HV}|^2/|S_{HH}|^2$ [26],
2. co-pol ratio $r_{VV/HH} = |S_{VV}|^2/|S_{HH}|^2$ [26],
3. co-pol phase difference $\phi_{VV/HH} = \arg(S_{VV}S_{HH}^*)$ [26, 27],
4. magnitude $g = |\text{avg}(S_{pq}S_{rs}^*)|$ [27],
5. normalized magnitude $\xi = \frac{|\text{avg}(S_{pq}S_{rs}^*)|}{\sqrt{\text{avg}(|S_{pq}|^2)\text{avg}(|S_{rs}|^2)}}$ [27],
6. intensity ratio $w = \text{avg}(|S_{pq}|^2)/\text{avg}(|S_{rs}|^2)$ [27],
7. and the Stokes parameters $S_i, 0 \leq i \leq 3$ [28].

Furthermore, other studies have offered statistical model for each element of the POLSAR covariance matrix $S_{pq}S_{rs}^*$ [29] as well as the largest eigen-value of the covariance matrix λ_1 [30]. While these models undoubtedly help in understanding SAR data, individually none of them satisfy the dual criteria of 1) resulting in statistically consistent discrimination measures and 2) being an representative observable for the complex POLSAR data, which are the objectives of this thesis.

2.2.2 Existing Discrimination Measures for (POL)SAR data

The commonly used measure of distance for matrices are either the Euclidean or Manhattan distances, defined as:

$$d(C_x, C_y) = \sum_{i,j} |\mathbb{R}(C_x - C_y)_{i,j}| + \sum_{i,j} |\mathbb{I}(C_x - C_y)_{i,j}|$$

$$d(C_x, C_y) = \sqrt{\sum_{i,j} |C_x - C_y|_{i,j}^2}$$

where $C_{i,j}$ denotes the (i,j) elements of the POLSAR covariance matrix C, || denotes absolute values and \mathbb{R}, \mathbb{I} denote the real and imaginary parts respectively. However, in the context of POLSAR, these dis-similarity measures are not widely used mainly due to the multiplicative nature of the noisy data.

In the field of POLSAR, the Wishart distance is probably the most widely used, as part of the well-known Wishart classifier [31]. It is defined [32] as:

$$d(C_x, C_y) = \ln |C_y| + \text{tr}(C_x C_y^{-1})$$

where $\text{tr}(C)$ denotes the trace of the matrix C. As a measure of distance, its main disadvantage is that $d(C_y, C_y) = \ln |C_y| \neq 0$.

Recent works have suggested alternative dissimilarity measures including the symmetric and asymmetric refined Wishart distance [33],

$$d(C_x, C_y) = \frac{1}{2} \text{tr}(C_x^{-1} C_y + C_y^{-1} C_x) - d$$

$$d(C_x, C_y) = \ln |C_x| - \ln |C_y| + \text{tr}(C_x C_y^{-1}) - d$$

the Bartlett distance [34],

$$d(C_x, C_y) = 2 \ln |C_{x+y}| - \ln |C_x| - \ln |C_y| - 2d \ln 2$$

the Bhattacharyya distance [35],

$$r(C_x, C_y) = \frac{|C_x|^{1/2} |C_y|^{1/2}}{|(C_x + C_y)/2|}$$

and the Wishart Statistical test distance [36]

$$d(C_x, C_y) = (L_x + L_y) \ln |C| - L_x \ln |C_x| - L_y \ln |C_y|$$

Closer investigation of these dis-similarity measures reveals that most are related in some ways. The Bhattacharyya distance is easily shown to be related to the Barlett distance. At the same time the Barlett distance can be considered a special case of the Wishart Statistical Test distance, when the two data sets have the same number of looks, i.e. $L_x = L_y$. The close relation among the measures is further supported by the fact that all of their proposing papers referred the same statistical model developed in [37] as a foundation. In [37], to determine if the two scaled multi-look POLSAR covariance matrix Z_x and Z_y , which have L_x and L_y as the corresponding number of looks, come from the same underlying stochastic process, the likelihood ratio statistics for POLSAR covariance matrix is considered:

$$Q = \frac{(L_x + L_y)^{d \cdot (L_x + L_y)}}{L_x^{d \cdot L_x} L_y^{d \cdot L_y}} \frac{|Z_x|^{L_x} |Z_y|^{L_y}}{|Z_x + Z_y|^{(L_x + L_y)}}$$

Taking the log-transformation of the above equation, and note that $C_{vx} = Z_x/L_x$, $C_{vy} = Z_y/L_y$ and $C_{vxy} = (Z_x + Z_y)/(L_x + L_y)$ then:

$$Q = \frac{|C_{vx}|^{L_x} \cdot |C_{vy}|^{L_y}}{|C_{vxy}|^{L_x + L_y}} \quad (2.13)$$

$$\ln Q = L_x \ln |C_{vx}| + L_y \ln |C_{vy}| - (L_x + L_y) \ln |C_{vxy}| \quad (2.14)$$

To detect changes, a test statistic is developed based on this measure of distance. This means a distribution is to be derived for the dissimilarity measure. However, in the

original work [37], only an asymptotic distribution has been proposed.

2.2.3 Current Methods for SAR speckle filtering

Although speckle has been extensively studied for decades, speckle reduction remains one of the major issue in SAR imaging process. Many reconstruction filters have been proposed, and they can be classified into two main categories: Weighted Least-Square Error de-speckling using the speckle model; and maximum a posteriori (MAP) de-speckling using the product model. In this section, various different approaches to SAR speckle filtering are reviewed.

In the first category the speckle random process is assumed to be stationary over the whole image. Then speckle models are proposed, such as the multiplicative speckle model is first approximated by a linear model. A class of speckle reduction filters is formulated as follows:

$$\hat{R}(t) = I(t) \cdot W(t) + \bar{I}(t) \cdot (1 - W(t)) \quad (2.15)$$

where $\hat{R}(t)$ is the filter response, $I(t)$ is the intensity at the centre of the moving window, $\bar{I}(t)$ is the averaged intensity for the whole processing window, $W(t)$ is a weight function,

For the Lee filter [38], the weight function is proposed to be:

$$W(t) = 1 - \frac{C_u^2}{C_I^2}$$

where C_u is the variational coefficient of noise, i.e. $C_u = std(u)/avg(u)$, and C_I is the variational coefficient of the true image, i.e. $C_I = std(I)/avg(I)$.

In the approach of the Kuan filter [39], the multiplicative speckle model is first transformed into a single-dependent additive noise model, and then the MMSE criterion is applied. The speckle filter thus has the same form as the Lee filter but with a different weighting function

$$W(t) = \frac{1 - \frac{C_u^2}{C_I^2}}{1 + C_u^2}$$

The Kuan filter takes into account the dependency of noise on the signal. In the special case of noise being independent of the underlying signal, the Kuan filter would

be exactly the same as the Lee filter. From this point of view, it can be considered to be superior to the Lee filter.

The Frost filter [40] is different from the Lee and Kuan filters, where the scene reflectivity is estimated by convolving the observed image with the impulse response of the SAR system. The impulse response of the SAR system is obtained by minimizing the mean square error between the observed image and the scene reflectivity model which is assumed to be an autoregressive process. The filter impulse response can, after some simplification, be written as:

$$H(t) = K_1 e^{-K_2 C_I^2(t)}$$

where K_1 is some normalizing coefficient to allow preservation of signal mean values, and K_2 is a user-selected filter parameter.

As can be seen from these three most recognised algorithms in this field, they share similar principles. When the variation coefficient C_I is small, the filter behaves like a low pass filter smoothing out the speckles. When C_I is large, it has a tendency to preserve the original observed image. The choice of functions relating speckle suppression power to local variations may be different, the weighted average as well as the weighted least square principles are apparently common.

As will be discussed at length in Chapter 4, SAR data is heteroskedastic. Our literature search yielded only a single article [41] tackling SAR data's heteroskedastic feature, suggesting a lack of appropriate attention within the research community about such characteristic and its effects. Under such conditions, Ordinary Least Square methods may not provide optimal results [42]. In fact, as is shown by Eqn. 2.15), weighted average formulae were being used. This is consistent with the knowledge that, when variance of heteroskedastic data is available, weighted least squares is an optimal estimator. However, in SAR data, this variance is not available directly and can only be estimated. Since heteroskedasticity means that this variance is dependent on the under-lying signal, thus estimating this variance is evidently as hard as estimating the un-speckled signal itself.

In the MAP approach, the filters assume that speckle is not stationary globally but is only stationary locally within the moving processing window. Such filters operate based on the MAP principle, which is given as:

$$f(x|z) = \frac{f(z|x)f(x)}{f(z)}$$

where x is the underlying signal that needs to be estimated, and z is the observed signal. The underlying signal is found by

$$x = \operatorname{argmax}\{\log(f(z|x)) + \log(f(x))\}$$

As evidenced, these classes of filter require the knowledge of the *a-priori* PDF $f(x)$. As such, various PDFs for the underlying back-scattering coefficient have been assumed.

If a normal distribution is assumed [43], then:

$$f(x) = \frac{1}{\sigma_x \sqrt{2\pi}} e^{\frac{1}{2} \left(\frac{x-\mu}{\sigma_x} \right)^2}$$

and the underlying signal is found by solving the equation

$$x^4 \Gamma^2(N) - x^3 \Gamma^2(N) \mu_x + x^2 \Gamma^2(N) 2N \sigma_x^2 - 2\sigma_x^2 z^2 \Gamma^2(N + 1/2) = 0$$

If a Gamma distribution is assumed [44], then:

$$f(x) = \frac{\sigma_x}{\Gamma(\lambda)} (x \sigma_x)^{\lambda-1} e^{-x \sigma_x}$$

For $\lambda = 1$, the Gamma distribution is identical to the exponential distribution. For $\lambda = n/2$ and $\sigma = 1/2$ the Gamma distribution is equivalent to the chi-square distribution. The underlying signal is found by solving the equation:

$$x^3 \Gamma^2(N) \sigma_x + x^2 \Gamma^2(N) (2N - \lambda + 1) - 2z^2 \Gamma^2(N + 1/2) = 0$$

If an exponential distribution is assumed, then:

$$f(x) = \sigma_x e^{-x \sigma_x}$$

and the underlying signal is found by solving the equations

$$x^3 \Gamma^2(N) \sigma_x + x^2 \Gamma^2(N) 2N - 2z^2 \Gamma^2(N + 1/2) = 0$$

If a Chi squared distribution is assumed, then:

$$f(x) = \frac{1}{2^{n/2}\Gamma(n/2)}x^{n/2-1}e^{(-x/2)}$$

and the true signal is found by solving the equation

$$x^3\Gamma^2(N) + x^2\Gamma^2(N)(4N - n + 2) - 4z^2\Gamma^2(N + 1/2) = 0$$

If a log-normal distribution is assumed [45], then:

$$f(x) = \frac{1}{\sigma_x\sqrt{2\pi}}x^{-1}e^{\frac{-1}{2\sigma_x^2}(\ln(x)-\mu_x)^2}$$

and

$$x^2\Gamma^2(N)(-2N\sigma_x^2 - \sigma_x^2 - \log(x) + \mu_x) + 2z^2\Gamma^2(N + 1/2) = 0$$

Other distributions that have been proposed include the heavy tailed Rayleigh distribution [46], Weibull distribution [47], beta distribution [47], Rician distribution [48] ... Evidently, the performance of these filters are dependent on the underlying distribution of the back-scattering coefficient on the particular surface being imaged. In this context, the community appears to focus on using Bayesian inference to choose the most suitable distributions [49]. One of the additive and homoskedastic SAR model's benefits is the possible hypothesis that the underlying distribution of the back scattering coefficient is estimable discussed in subsequent chapters.

Other approaches that have recently been actively pursued in the research community and in published literature include:

- wavelets [50, 51, 52, 53, 54, 55, 56, 57],
- curvelets [58, 59, 60],
- contourlets [61],
- ridgelets [62],
- fuzzy logic [63],
- anisotropic kernels [64],
- and autoregressive conditional heteroskedasticity [65].

Central to wavelet techniques is the discovery of a consistent and optimal choice for the wavelet coefficients. Similarly, the development of kernel methods depends strongly on the discovery of consistent predictive kernels. Evidently the choice of such coefficients are dependent on the underlying statistical characteristics of SAR signals. This variety of approaches further emphasises the importance of investigating consistent statistical properties of SAR signals. Not only is statistical analysis important in speckle filtering, the technique is also important for information extraction [66], target detection [67] and classification [68].

2.2.4 Current Methods for POLSAR speckle filtering

Compared to SAR technologies, most POLSAR techniques are relatively recent. Published literatures on POLSAR speckle filtering indicate that filtering the covariance matrix off-diagonal elements is still an open problem. The problem can be traced back to the lack of a statistical model for the covariance matrix in polarimetry.

In the first systems that captured POLSAR data, multi-look processing was used as a method of choice for speckle filtering, at the cost of spatial resolution. Novak [69] pioneered the concept of speckle reduction, and proposed the polarimetric whitening filter (PWF) to produce a single speckle reduced intensity image. The main disadvantages of the PWF filter is that polarimetric information is not well-preserved. Multi-look processing polarimetric results also exhibit bias and distortion [70].

Lee [71] proposed a new filtering algorithm which does suppress speckle for the diagonal elements, however the off-diagonal elements remain un-filtered. Later, Touzi et. al. [72] drew out the principles of speckle filtering of POLSAR data, which they summarised as:

1. Speckle can be filtered if ALL elements of the covariance matrix are filtered.
2. Single-channel SAR speckle filtering is only applicable to diagonal elements of the covariance matrix.
3. Speckle filtering needs also to be performed on off-diagonal elements, as correlation among the elements needs to be exploited, and the elements do not exist independently.

In 1999, Lee [31] extended his refined-Lee filters to POLSAR data, and argued that

all covariance matrix elements should be filtered by the same amount to preserve polarimetric properties. He then proposed to apply the weighted averaging on the full covariance matrix instead of single-channel intensities values:

$$C_{out} = C_{avg} + w(C_{curr} - C_{avg})$$

where C_{out} is the filtered covariance matrix output, C_{avg} is the average covariance matrix using an edge-aligned window, and C_{curr} is the covariance matrix of the current processing pixel. The weight w is computed within the edge aligned window from the total power image y as:

$$w = \frac{\sigma_y^2 - \mu_y^2 \sigma_v^2}{\sigma_y^2 - \sigma_n^2 \sigma_v^2}$$

where σ_y^2 and μ_y are the variance and mean computed within the edge aligned window, respectively, σ_n^2 is the user specified noise variance.

Further attempts have been made towards statistically modelling the off-diagonal elements but the application of these results for speckle suppression of off-diagonal element have not been conclusive. For instance Martinez et. al.[73] proposed a model based polarimetric filter. They first proposed to model $S_h S_v^*$ as having both additive and multiplicative components:

$$S_p S_q^* = \psi |\rho| e^{i\theta} + \psi \bar{z}_n N_c (1 - n_m) e^{i\theta} + \psi (n_{ar} + i n_{ai})$$

where $\psi = \sqrt{E(|S_p|^2) E(|S_q|^2)}$ represents the average joint power in the two channels, $\rho = |\rho| e^{i\theta} = \frac{E(S_p S_q^*)}{\sqrt{E(|S_p|^2) E(|S_q|^2)}}$ is the complex correlation coefficient that characterises the correlation among the channels, $N_c = \frac{\pi}{4} |\rho| F_{1,2}(1/2, 1/2, 2, |\rho|^2)$ basically contains the same information as the complex correlation coefficient. $F_{1,2}(a, b, c, d)$ is the Gauss hyper-geometric function, n_m is the first speckle noise component that is multiplicative with $E(n_m) = 1$ and $\text{var}(n_m) = 1$, $n_{ar} + i n_{ai}$ is the second additive speckle noise component with $E(n_{ar}) = E(n_{ai}) = 0$ and $\text{var}(n_{ar}) = \text{var}(n_{ai}) = \frac{1}{2}(1 - |\rho|^2)^{1.32}$.

The model is overly complicated and to do speckle filtering, various approximations have to be used.

Another different approach is proposed bu Lee [7] to model $S_h S_v^*$. In this method, the phase difference is defined as:

$$\phi = \arg(S_p S_q^*)$$

and the PDF for the phase difference as:

$$pdf(\phi) = \frac{\Gamma(3/2)(1 - |\rho|^2)\beta}{2\sqrt{\pi}\Gamma(1)(1 - \beta^2)} + \frac{(1 - |\rho|^2)}{2\pi} F_{1,2}(1, 1, 1/2, \beta^2)$$

where $\beta = |\rho|\cos(\phi - \theta)$ and $F_{1,2}(a, b, c, d)$ is the Gauss hyper-geometric function.

The normalized magnitude, is defined as:

$$\xi = \frac{E(S_p S_q^*)}{\sqrt{E(|S_p|^2) E(|S_q|^2)}}$$

and the PDF is found to be:

$$pdf(\xi) = \frac{4\xi}{\Gamma(1)(1 - |\rho|^2)} I_0\left(\frac{2|\rho|\xi}{1 - |\rho|^2}\right) K_0\left(\frac{2\xi}{1 - |\rho|^2}\right)$$

I_0 and K_0 are modified Bessel functions.

Again the equations looks overwhelmingly complex, and as admitted by the authors themselves: this does not allow for easy speckle filtering as the model is too complex and the complex correlation coefficient ρ is not easily estimated [7]

There have been several other attempts to filter POLSAR data. Vasile, proposed a region growing adaptive neighbourhood approach in 2006, where averaging is performed on an adaptive homogenous neighbour. The main drawback of the approach is that only the intensity was used to determine homogeneity and a primitive averaging filter is performed on off-diagonal elements [74]. In [75], J.S. Lee proposed to group homogeneous pixels based on their underlying scattering model. While the work is interesting, it is believed that pixels having similar underlying models, for example volume scattering, can still be of a very different nature. Similar to Lee's previous work, a simple weighted average filtering is applied on both diagonal and off-diagonal elements. Vasile, in 2010, published a complicated spherically invariant random vector estimation scheme to estimate the underlying target POLSAR signature [76]. While polarimetric information is estimated independently from the power span, its output results no longer follow established Wishart distribution.

In summary, while off-diagonal elements, which carry phase information, are known to be important in interpreting POLSAR data [77], their estimation and filtering is under-developed in the current research literature.

2.2.5 Current Techniques to Evaluate SAR Speckle Filters

Because of the variaties of speckle filtering available, it is hence crucial to have a framework for (a) modelling and simulation, which provide the ground-truth data in different scenarios of underlying distribution, and (b) analysing the interdependency between noise and the underlying signal, as well as the dependence of each filter's performance on the different underlying distribution scenarios and (c) establishing consistent criteria to evaluate speckle suppression power as well as the adaptive capabilities in reconstructing the underlying signal.

This section reviews the published literature for the different techniques used to evaluate SAR speckle filters. The overall requirement of speckle filtering can be broken down into two smaller requirements. On the one hand, speckle filters should preserve the underlying radiometric signal (namely the radiometric preservation requirement). On the other hand, they should reduce the variation of the additive noise (i.e. speckle suppression power). One metric that can be used to detect radiometric distortion is the ratio between the estimated and the original value $r = X_{est}/X_{org}$ [78, 45]. A somewhat similar metric is used in [79] as $r_w = (X_{est} - X_{org})/X_{org}$. Several metrics have also been developed to evaluate speckle suppression power. The most common measure is the Equivalent Number of Looks (ENL) index $ENL = avg(I)^2/var(I)$ that was proposed by Lee [80]. Another very similar metric is the ratio of mean to standard deviation, $R = avg(I)/std(I)$ [50]

It is customary to divide the performance evaluation of speckle filters into two distinct classes of homogeneous and heterogeneous region evaluation. Across homogeneous areas, speckle filters are expected to be estimated with negligible radiometric bias. As such, evaluating speckle filters over homogeneous areas has traditionally focused on evaluating the variation of the estimators' output (a.k.a the speckle suppression power).

Real-life and practical images, however, are not homogeneous. Thus there are a number of associated difficulties in evaluating speckle filters over heterogeneous scenes. The first difficulty in evaluating speckle filters for heterogeneous scenes is to select the basis for comparison. It is trivially easy to estimate the underlying radiometric coefficient if an area is known to be homogeneous. However, without simulation or access to solid ground-truth, it is practically impossible to do so for real-life images. And hence, the need for speckle filter estimation is warranted.

Without ground truth, one way to evaluate radiometric preservation of filters is to compute the ratio image mentioned above. Under a multiplicative model, the ratio image is expected to comprise solely of the noise being removed (i.e. it should be completely random). Being random, this should display as little “visible” structure as possible. However, when displaying such images for visual evaluation, the ratios that are smaller than unity are much harder to distinguish than those that are bigger [45].

Even with known ground-truth, evaluating metrics need to be defined for quantitative measurements. This is the second difficulty in evaluating speckle filters for heterogeneous scenes. Under the conditions of heterogeneity, the standard speckle filters still introduce radiometric loss, normally at local or regional levels. In fact, the common consensus is that a powerful speckle suppression filter (for example the boxcar filter) is likely to perform poorly in terms of preserving underlying radiometric differences (e.g. causing excessive blurring). Furthermore, we have not found many published articles combining the evaluation of these two seemingly contradicting requirements.

Overall, many different methods and metrics have been proposed to evaluate various aspects of speckle filters. However it is clearly advantageous to have a single metric that is able to judge if one filter is better than another. Wang [79] proposed using fuzzy membership to weight opinions of an expert panel. Although this provides a potential solution, we consider it to be tedious in implementation, fuzzy in concept and subjective in nature.

Another approach is to apply a universal mean squared error criteria into the context of SAR data. However since SAR data is heteroskedastic, which violates the assumptions of the Gauss-Markov theorem, the use of MSE is not straightforward. Thus Gagnon [50] suggested the use of the ratio between the expected mean of the signal and the RMSE of the removed noise. The metric is argued to be similar in interpretation to the standard signal-to-noise ratio (SNR). Others have suggested the use of normalised MSE, which is essentially the ratio between MSE and the expected mean.

In general, any metric to evaluate speckle filters should be relevant to the normal usage of such filters. Furthermore, the application of any speckle filter in a SAR processing framework should enable an improvement in the measurement, detection or classification of the underlying radiometric features. Thus, another way to evaluate speckle filters is by comparing the feature preservation characteristics of the original noised data and those of the filtered image. This can be applied not only whether or

not the ground-truth is available precisely. When there is no ground-truth given, the feature are estimated in both the original noised and the filtered images. Evaluation would then determine how closely related the two feature maps are.

Various methods may be applied to extract features; examples of those that have been used are the Hough Transform [45], Robert gradient edge detector [50] and edge map [40]. While significant effort has been spent on these evaluations, serious doubts remain concerning the precision of these methodologies. This is because feature extraction algorithms are only approximations, whose accuracy is not only dependent upon the characteristics of the original image but also heavily affected by the inherent noise. Unfortunately, speckle filters invariably alter the noise characteristics. Thus, without a clear understanding of these dependencies and no absolute ground truth, using feature extraction algorithms to evaluate speckle filters would leave serious questions on how to interpret the results, especially in terms of accuracy. As such, the problem of establishing an single evaluation criteria to evaluate the overall performance of speckle filters remains open for improvement.

2.3 Summary

This chapter has not only described the multi-dimensional and stochastic nature of the POLSAR data, but also illustrates the different published approaches to address the grand challenge of modelling, processing and understanding this type of data. Specifically it shows that while the statistical model for SAR is quite well understood, the understanding of the complex POLSAR statistical model trails behind. The complex POLSAR data have been statistically modelled as following the complex Wishart distribution, which apparently is multi-dimensional, complex and thus un-intuitive. There have been a few published scalar statistical models for POLSAR, but none of them is highly representative of the multi-dimensional data. None of them have so far led to published discrimination measures. A few POLSAR discrimination measures have also been proposed, but all of them are based on likelihood test statistics, which so far have only shown to be based on an asymptotic distribution.

The chapters also illustrated many different ways to combat the negative impact caused by multiplicative and heteroskedastic properties on the statistical estimation process, which includes statistical modelling of the data, estimator development and the estimator performance evaluation. Specifically, it showed that when the sense of subtractive

distance is not consistent for SAR data, the ratio is proposed as its discrimination measure [2]. It also showed that while the MMSE criteria is not very suitable to evaluate SAR speckle filters, other criteria such as radiometric preservation and speckle suppression power evaluation are employed. Unfortunately, these counter-intuitive measures are fragmented and thus not very popular outside the SAR community.

In the next chapter, theoretical models are developed to form the foundation required to systematically tackle these issues.

Chapter 3

Homoskedastic Models for Heteroskedastic SAR Data

This chapter highlights that SAR data are heteroskedastic in the original domain. Relying solely on statistical and mathematical principles, the log-transformed SAR data is then shown to be homoskedastic. From there, the consistent sense of variance and a few consistent measures of distance are proposed and validated against real-life practical SAR data.

3.1 Original Heteroskedastic Model of SAR data

The stochastic nature of SAR data has been illustrated earlier (see Eqns. 2.2 and 2.3). From a statistical viewpoint, the multiplicative nature of amplitude (A) and intensity (I) data can be explained as follows. Let us consider two fixed unit distributions which are independent to σ given below:

$$pdf(A_1) = 2A_1 e^{(A_1^2)} \quad (3.1)$$

$$pdf(I_1) = e^{(-I_1)} \quad (3.2)$$

Using the variable change theorem, it can be shown that the SAR amplitude and

intensity are equal to a scaled version of these unit variables, specifically $A = \sigma A_1$ and $I = \sigma^2 I_1$. These relationships evidently display a mutiplicative nature. In fact, the condition has long been noted, but from different perspectives, in various proposed SAR models (e.g. [81]).

Let us now consider the population expected mean and variance of the four statistical distributions for these observables, i.e. A, A_1, I, I_1 . They are given in Table 3.1. If spatial homogeneity is defined as an imaging area having the same back-scattering coefficient σ , then over a homogeneous scene, the measured values can then be considered as samples coming from a single stochastic process. However, over heterogeneous areas where σ varies significantly, it is then evidently clear that: the amplitude as well as the intensity of SAR data suffer from heteroskedastic phenomena. This means that the conditional expected variance of SAR data is dependent on the conditional expectation of the mean. In the context of speckle filtering which aims to estimate the unknown parameter σ , Table 3.1 also clearly indicates an ambiguous circle: in the original domain, estimating variance is equal to estimating the mean, but this is as hard to estimation as the variance.

Mean	Variance
$avg(A_1) = \frac{\sqrt{\pi}}{2}$	$var(A_1) = \frac{(4-\pi)}{4}$
$avg(I_1) = 1$	$var(I_1) = 1$
$avg(A) = \frac{\sqrt{\pi}}{2} \cdot \sigma$	$var(A) = \frac{(4-\pi)}{4} \cdot \sigma^2$
$avg(I) = \sigma^2$	$var(I) = \sigma^4$

Table 3.1: Mean and Variance of Original SAR data

The formulas above are extremely well known in this research field. In fact while pioneering the estimation of the equivalent number of look (ENL) index, it was noted by Lee et.al. that the ratio of expected standard deviation to mean is a constant in both cases (i.e. $snr(A) = \sqrt{\frac{4}{\pi} - 1}$ and $snr(I) = 1$) [82].

In this thesis, a different perspective will be proposed which avoids the negative effects of heteroskedasticity in SAR data processing.

3.2 The Effects of Heteroskedasticity in SAR Processing

The nature of SAR speckle is stochastic over homogeneous areas and heteroskedastic heterogeneously. Statistical models are used to describe how the underlying back-

scattering coefficient (σ) affects the distribution of the observable SAR data. While the statistical model within individual resolution cells is well established, it is only applicable to homogeneous areas. Practical images, however, are heterogeneous. Furthermore, it is precisely this spatial variation that is often of high interest.

As such, various statistical models for heterogeneous areas have been proposed (see [83] for a detailed review). However, while most of the models highlight the multiplicative nature of sub-pixel or homogeneous original SAR data, in extending the model to heterogeneous images, virtually none have noted that spatial variation also gives rise to heteroskedasticity phenomena. Heteroskedasticity, as explained later, is defined as the dependence of conditional expected variance of original SAR data on the conditional expectation of its mean or equivalently its underlying back-scattering coefficient (σ).

Speckle filters are effectively estimators attempting to estimate the unknown coefficient σ from the observable SAR signal (A). Thus, SAR speckle-filtering can be and has been positioned within the context of estimation theory [83], where the statistical framework is used to estimate unknown statistical parameters from the observable data. The stages of this framework consist of statistical modelling, estimator development and evaluating the performance of the statistical estimators. It is also known that heteroskedasticity gives rise to serious negative impacts on various stages of speckle-filtering.

In modelling, heteroskedasticity has direct consequences in the central question of homogeneity or heterogeneity. In optical images, the contrast or variance among neighbouring pixels have been used to measure homogeneity. Unfortunately such techniques do not appear to be effective under the heteroskedastic condition of original SAR data. In SAR images, both of these measures are dependent on the underlying signal (σ). This make the problem of estimating variance equal to the problem of estimating the mean and is the same as the main problem: estimating σ . The fact give rise to the ambiguity circle in SAR speckle filtering.

A case in point can be found in a recently published improved sigma filter [84]. The technique determines outlying points as being too far away from the standard deviation. However, as is done in [84], to estimate standard deviation, an estimator of the mean is required and used. It is interesting to note that the MMSE estimator used to estimate the mean in [84], itself alone, is a rather successful speckle-filter [38].

Heteroskedasticity also poses numerous challenges in designing an efficient estimator. Heteroskedasticity directly violates Gauss-Markov theorem's homoskedastic assumption.

tion. Thus it renders the efficiency of any naive Ordinary Least Square estimator in serious doubt. If the variance is known *a priori*, it has been proven [85], that a weighted mean estimator is the best linear unbiased estimator. Interestingly, as noted by Lopes [86], most known common successful adaptive filters [38, 39, 40] do make use of weighted mean estimations. The problem, however, is that in SAR speckle filtering, variance is not known *a priori*. And even though variance can be estimated from observable values, as the ambiguity circle goes, estimating the variance is as hard as estimating the underlying coefficient σ itself.

Heteroskedasticity also affects the performance evaluation stage of the estimation framework. Statistical estimators are routinely evaluated using their bias and variance performance which, when combined, normally result in MSE evaluation. Unfortunately, under heteroskedastic conditions, Least Squared Error estimation may not be optimal. In other words, Minimum Squared Error can no longer serve as a reliable evaluation metric. A number of different evaluation metrics have been proposed for SAR speckle filters, however, none have appeared capable of taking on the MSE's previous role.

Last but certainly not least, is the bad impact of heteroskedasticity on SAR image interpretation. Most of the task to be carried out in interpreting SAR images almost invariably involve target detection, target segmentation and/or target classification. All of these tasks require good discriminant functions. Fundamental to all of those is the need for a consistent measure of distance. Unfortunately, by definition, heteroskedasticity provides inconsistent measures of distance. This inconsistent measure of distance coupled with the failure of the ordinary least square regression methods have caused a large class of artificial neural networks as well as a number of other computational intelligence methods to under-perform for SAR data.

3.3 The Homoskedastic Effect of Logarithmic Transformation

In this section, a base-2 logarithmic transformation is proposed for SAR data. The choice of base-2 is due to implementation reasons, since base-2 logarithms can be computed faster by computer than either natural or decimal logarithms, and yet the ability to transform heteroskedastic speckle into a homoskedastic relationship is still maintained.

Under base-2 log-transformation, the original variables become:

$$L_1^A = \log_2(A_1) = L_1^I/2 \quad (3.3)$$

$$L_A = \log_2(A) = L_1^A + \log_2 \sigma \quad (3.4)$$

$$L_1^I = \log_2(I_1) = 2L_1^A \quad (3.5)$$

$$L_I = \log_2(I) = L_1^I + 2 \log_2 \sigma \quad (3.6)$$

The equations above highlight the relationships among random variables in the log-transformed domain. Two interesting points are evident from these formulae. Firstly, in the log-transformed domain, working on either amplitude or intensity will tend to give identical results. Secondly, the effects of converting the multiplicative nature to an additive nature through logarithmic transformation is clearly manifested. Now, bearing in mind the relationship among the random variables, application of variable change theorem leads to:

$$pdf(L_1^A) = 2 \cdot 2^{(2L_1^A)} e^{-2^{(2L_1^A)}} \quad (3.7)$$

$$pdf(L_A) = 2 \cdot 2^{(2L_A - 2 \log_2 \sigma)} e^{-2^{(2L_A - 2 \log_2 \sigma)}} \quad (3.8)$$

$$pdf(L_1^I) = 2^{L_1^I} e^{-2^{L_1^I}} \quad (3.9)$$

$$pdf(L_I) = 2^{(L_I - 2 \log_2 \sigma)} e^{-2^{(L_I - 2 \log_2 \sigma)}} \quad (3.10)$$

Noting that these distributions belong to the Fisher-Tippet family, the population expected mean and variances are obtained and presented in Table 3.2, with $\gamma \approx 0.577$ being the Euler-Mascheroni constant. Most importantly, it can be seen that the means are biased and the variances are no longer related to σ .

Table 3.2 confirms the condition of homoskedasticity, defined as the independence of

Mean	Variance
$\text{avg}(L_{1A}) = \frac{-\gamma}{2} \cdot \frac{1}{\ln 2}$	$\text{var}(L_{1A}) = \frac{\pi^2}{24} \cdot \frac{1}{(\ln 2)^2}$
$\text{avg}(L_{1I}) = -\gamma \cdot \frac{1}{\ln 2}$	$\text{var}(L_{1I}) = \frac{\pi^2}{6} \cdot \frac{1}{(\ln 2)^2}$
$\text{avg}(L_A) = \frac{-\gamma}{2} \cdot \frac{1}{\ln 2} + \log_2 \sigma$	$\text{var}(L_A) = \frac{\pi^2}{24} \cdot \frac{1}{(\ln 2)^2}$
$\text{avg}(L_I) = -\gamma \cdot \frac{1}{\ln 2} + 2 \log_2 \sigma$	$\text{var}(L_I) = \frac{\pi^2}{6} \cdot \frac{1}{(\ln 2)^2}$

Table 3.2: Mean and Variance of Log Transformed values: here the variance is no longer dependent on σ

RV	Relationships	Variance (skedasticity)	Mean (biasness)
A	$A = \sigma A_1$	Heteroskedastic $\text{var}(A) = \frac{(4-\pi)}{4} \cdot \sigma^2$	Unbiased $\text{avg}(A) = \frac{\sqrt{\pi}}{2} \cdot \sigma$
I	$I = A^2 = \sigma^2 I_1$	Heteroskedastic $\text{var}(I) = \sigma^4$	Unbiased $\text{avg}(I) = \sigma^2$
L_A	$L_A = \ln(A) = L_{1A} + \log_2 \sigma$	Homoskedastic $\text{var}(L_A) = \frac{\pi^2}{24} \cdot \frac{1}{(\ln 2)^2}$	Biased $\text{avg}(L_A) = \frac{-\gamma}{2} \cdot \frac{1}{\ln 2} + \log_2 \sigma$
L_I	$L_I = \ln(I) = L_{1I} + 2 \log_2 \sigma$	Homoskedastic $\text{var}(L_I) = \frac{\pi^2}{6} \cdot \frac{1}{(\ln 2)^2}$	Biased $\text{avg}(L_I) = -\gamma \cdot \frac{1}{\ln 2} + 2 \log_2 \sigma$

Table 3.3: The properties of observable SAR random variables

the conditional expected variance on the conditional expectation of the mean. This result is consistent with findings in [87]. The main difference would be the use of base-2 logarithm which is preferred here for more efficient computation.

The discussion so far is further summarized in Table 3.3. It shows that while the original data, especially intensity values, should be preferred for multi-look processing, the log-transformed domain with its homoskedastic distribution offers a consistent sense of variance.

To experimentally validate this theoretical discussion, real world data is extracted from a known homogenous area (from within a RADARSAT2 image). The PDF histogram from this data is then plotted in Fig. 3.1 along with the modelled PDF response. The excellent agreement observable between the real world and modelled data tends to validate the log-transformed model.

3.4 Consistent Measures of Distance in the Log-Transformed Domain

The consistent feature is explored and illustrated in this section from two different perspectives. First, the back-scattering coefficient σ is assumed to be *known a priori*. With that, let us consider the dispersion random variable which is defined as the distance

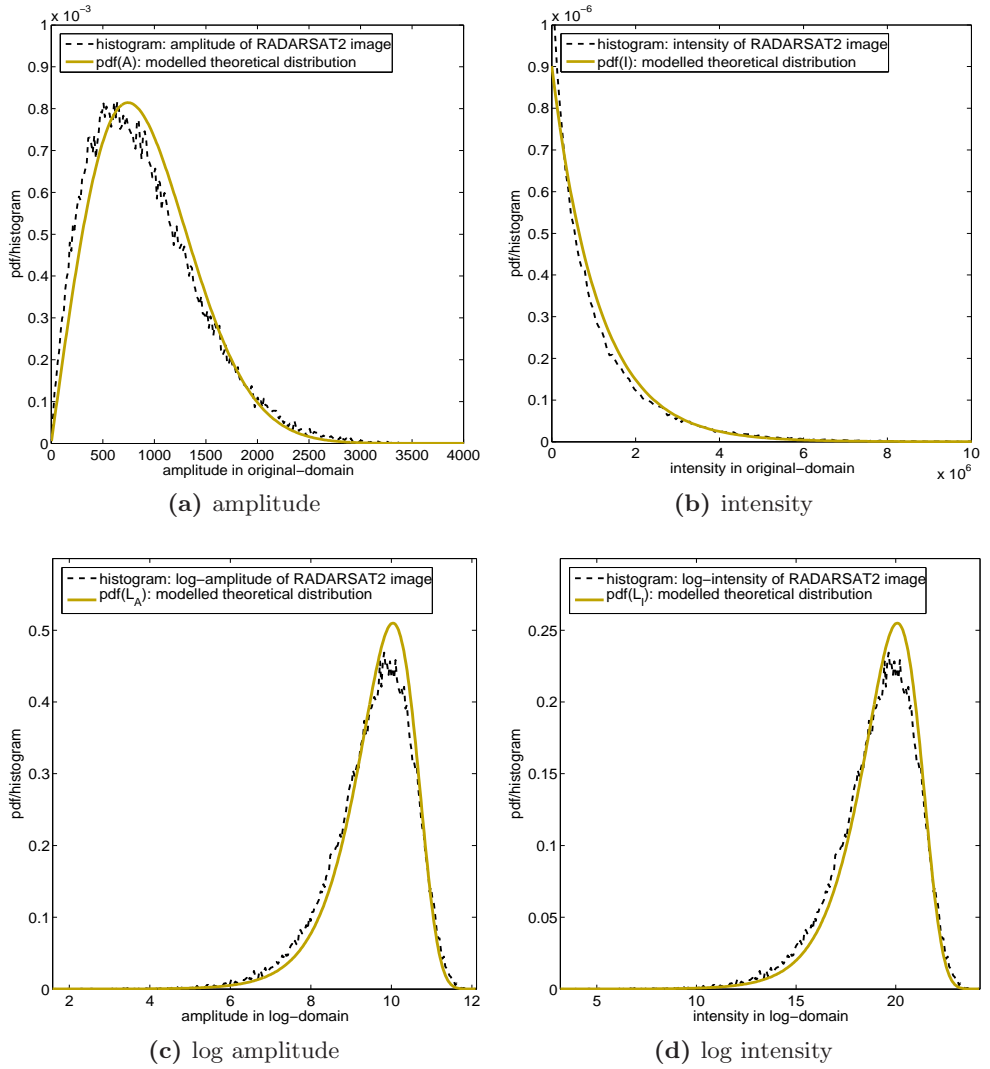


Figure 3.1: Observed histogram of a homogenous area and modelled PDF response

between an observable sample and its expected value:

$$D_A = A - avg(A) \quad (3.11)$$

$$D_I = I - avg(I) \quad (3.12)$$

$$D_{L^A} = L_A - avg(L_A) \quad (3.13)$$

$$D_{L^I} = L_I - \text{avg}(L_I) \quad (3.14)$$

Noting the results from the previous section, the PDF for these variables can be derived as follows:

$$\text{pdf}(D_A) = 2 \cdot \frac{(D_A + \sigma\sqrt{\pi}/2)}{\sigma^2} e^{-\frac{(D_A + \sigma\sqrt{\pi}/2)^2}{\sigma^2}} \quad (3.15)$$

$$\text{pdf}(D_I) = \frac{1}{\sigma^2} e^{-(D_I + \sigma^2)/\sigma^2} \quad (3.16)$$

$$\text{pdf}(D_{L^A}) = 2 \cdot 2^{(2D_{L^A} + 2\frac{\gamma}{2\ln 2})} e^{-2^{(2D_{L^A} + 2\frac{\gamma}{2\ln 2})}} \quad (3.17)$$

$$\text{pdf}(D_{L^I}) = 2^{(D_{L^I} + \frac{\gamma}{\ln 2})} e^{-2^{(D_{L^I} + \frac{\gamma}{\ln 2})}} \quad (3.18)$$

It is clear that these distributions are dependent on σ in the original domain (the upper two equations), are now independent of it when processed in the log-domain (the lower two equations).

Let us now investigate SAR data from the second perspective, where two adjacent resolution cells are known to have *an identical but unknown* back-scattering coefficient σ . Now, the contrast random variable is defined, also in the log-transformed domain, as the distance between two measured samples.

$$C_A = A_1^\sigma - A_2^\sigma \quad (3.19)$$

$$C_I = I_1^\sigma - I_2^\sigma \quad (3.20)$$

$$C_{L^A} = L_1^{A_\sigma} - L_2^{A_\sigma} = \log_2(A_1/A_2) \quad (3.21)$$

$$C_{L^I} = L_1^{I_\sigma} - L_2^{I_\sigma} = \log_2(I_1/I_2) \quad (3.22)$$

Noting that $C_x = D_1^x - D_2^x$, it should come as no surprise that the measure of contrast

is also consistent in the log-domain but inconsistent in the original domain. The PDF of the log-transformed variables can be expressed as:

$$pdf(C_{LA}) = 2 \frac{2^{(2C_{LA})}}{\left[1 + 2^{(2C_{LA})}\right]^2} \ln 2 \quad (3.23)$$

$$pdf(C_{LI}) = \frac{2^{(C_{LI})}}{\left[1 + 2^{(C_{LI})}\right]^2} \ln 2 \quad (3.24)$$

Evidently these distributions are also consistent, i.e. they are independent of σ . To illustrate this property, Fig. 3.2 is generated using the data extracted from a homogeneous area in a RADARSAT-2 image. As can be seen, it shows excellent agreement between the analytical PDF and the observable histogram of dispersion and contrast computed from an homogeneous area in the image.

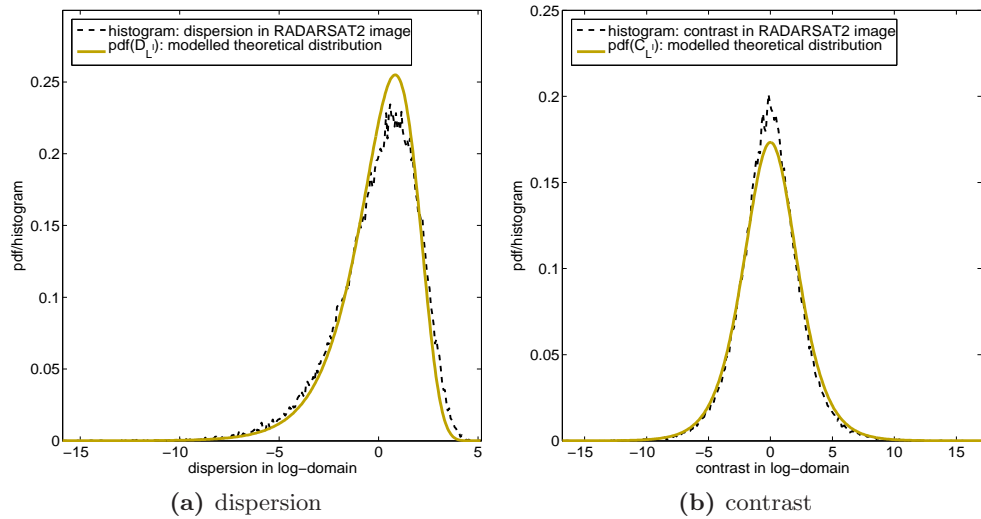


Figure 3.2: Observed and modelled PDF of dispersion and contrast in homogeneous log-transformed intensity images.

Given that real SAR images are heterogeneous and the back-scattering coefficient is unknown, it is evident that the measure of observable contrast in original SAR data differs, i.e. is inconsistent, across different homogeneous areas. On the other hand, the observable contrast in the log-transformed domain is consistently the same across different homogeneous areas. As such, one possible benefit is that should the sigma

filter [84] be designed against the $pdf(C_{L^I})$, then the scale estimator would probably no longer be required.

3.4.1 Sampling distribution of Variance in Log-Transformed domain

From the previous section result, two sample variance distribution ($V_x = C_x^2$) can be given analytically as

$$pdf(V_{L^I}) = \frac{\ln 2}{2} \frac{1}{\sqrt{V_{L^I}}} \left(\frac{2\sqrt{V_{L^I}}}{\left(1 + 2\sqrt{V_{L^I}}\right)^2} + \frac{2^{-\sqrt{V_{L^I}}}}{\left(1 + 2^{-\sqrt{V_{L^I}}}\right)^2} \right) \quad (3.25)$$

$$pdf(V_{L^A}) = \frac{\ln 2}{4} \frac{1}{\sqrt{V_{L^A}}} \left(\frac{2\sqrt{4V_{L^A}}}{\left(1 + 2\sqrt{4V_{L^A}}\right)^2} + \frac{2^{-\sqrt{4V_{L^A}}}}{\left(1 + 2^{-2\sqrt{V_{L^A}}}\right)^2} \right) \quad (3.26)$$

It could be seen that, in the log-transformed domain, not only the expected value (mean) of the observable variance is constant, its distribution is also independent of σ . The above analysis is applicable for two sample variances. For larger number of samples $n > 2$, Monte-Carlo simulation is used to visualise the distribution of sample variances. The simulation is described as follows:

1. A large number of input samples are generated ($n \cdot 10^6$ in the figure 3.3) from the PDF given in Eqn. 3.10.
2. The input samples are then divided into 10^6 independent sets, each set consisting of n samples.
3. For each input set, the sample variance is calculated.
4. For all input sets, a histogram of the calculated values is then plotted.
5. The consistent variance property is observable when the same plots are obtained, regardless of the value σ used in simulations.

Fig. 3.3 not only provides evidence for the validity of the simulation process, it also visualizes the shapes of the CDF for sample variance distribution of different look numbers.

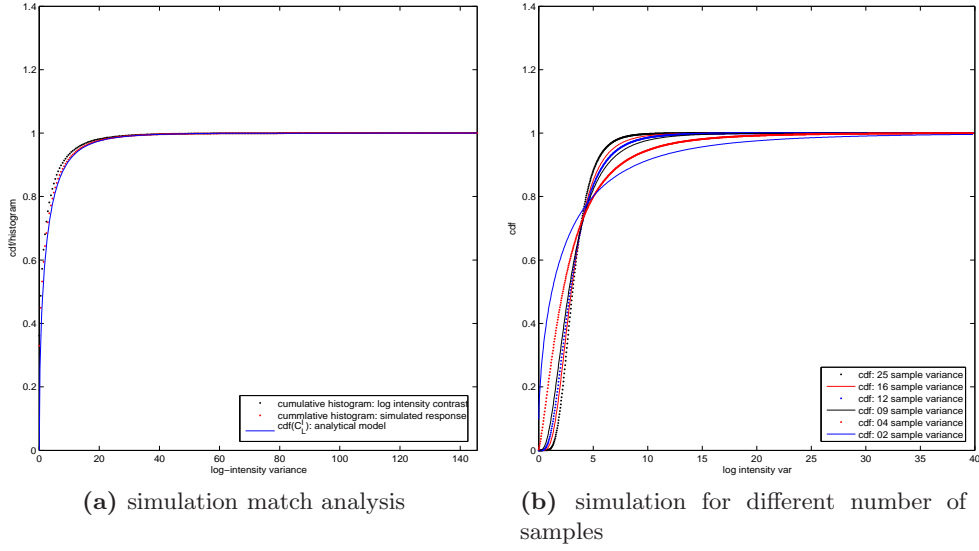


Figure 3.3: Sample Variance: Observable and Modelled CDF Response

3.4.2 Sample variance as a statistical measure of homogeneity

The discussion in the previous sub-section is based on the assumption of single stochastic processes, and thus homogeneity. In a given analysis window within real practical SAR images, such a perfect condition is unknown. The principle of SAR speckle filtering however is to group pixels into homogeneous areas, allowing stochastic components to be removed. In order to do that, a methodology is required to assert a partitioned area as being homogeneous. Fortunately the sampling distribution of log-variance provides a consistent method for testing this homo/hetero-geneity condition.

Under the null hypothesis that the given analysis area is homogeneous, the theoretical distribution of sample variance has been given earlier. The PDF, and equivalently the CDF, of this distribution can be visualized from Monte-Carlo simulations, as shown in Fig. 3.3. Thus, given a computed value of the sample variance in the log-transformed domain, the notion that a given analysis area is heterogeneous or homogeneous can be put to test. Specifically given a pre-determined threshold-value and number of samples, if the observable sample variance is higher than a cut-off value, the null hypothesis can be rejected.

The steps for finding these cut-off values are given below:

1. For each number of samples, a CDF plot is derived using the Monte-Carlo simulation described earlier.
2. Interpolating from the CDF plot, a corresponding cut-off value is derived for each threshold-level.
3. The combined results form a table, similar in structure to Table 3.4.
4. The first 3 steps are repeated a few times, and the summary statistics (i.e. mean and variance) of the cut-off values for each combination of threshold-value and look-number is reported.

Table 3.4 gives the result of one such experiment for an arbitrarily chosen set of threshold values. The table is useful in cases when an area is to be tested for homogeneity, for example in the kMLE speckle filter [88]

No	70%	75%	80%	85%	90%
2	2.9024 (0.0252)	3.7088 (0.0261)	4.7960 (0.0327)	6.3488 (0.0242)	8.7974 (0.0370)
3	3.4698 (0.0141)	4.1308 (0.0177)	4.9585 (0.0245)	6.1176 (0.0136)	7.9207 (0.0316)
4	3.6505 (0.0225)	4.2096 (0.0386)	4.9392 (0.0347)	5.9195 (0.0341)	7.4209 (0.0162)
5	3.7421 (0.0134)	4.2513 (0.0165)	4.8967 (0.0297)	5.7729 (0.0170)	7.0725 (0.0250)
6	3.7850 (0.0149)	4.2588 (0.0242)	4.8611 (0.0160)	5.6449 (0.0162)	6.8062 (0.0282)
7	3.8274 (0.0119)	4.2686 (0.0102)	4.8179 (0.0117)	5.5447 (0.0114)	6.6049 (0.0158)
8	3.8468 (0.0110)	4.2591 (0.0124)	4.7747 (0.0176)	5.4519 (0.0087)	6.4370 (0.0085)
9	3.8610 (0.0081)	4.2503 (0.0125)	4.7430 (0.0120)	5.3688 (0.0085)	6.2829 (0.0112)
10	3.8663 (0.0089)	4.2423 (0.0126)	4.6967 (0.0102)	5.3015 (0.0103)	6.1574 (0.0116)
11	3.8707 (0.0089)	4.2284 (0.0109)	4.6693 (0.0078)	5.2387 (0.0111)	6.0473 (0.0122)
12	3.8763 (0.0063)	4.2228 (0.0072)	4.6370 (0.0139)	5.1805 (0.0050)	5.9502 (0.0044)
13	3.8808 (0.0048)	4.2089 (0.0083)	4.6096 (0.0055)	5.1315 (0.0092)	5.8654 (0.0070)
14	3.8761 (0.0048)	4.1920 (0.0112)	4.5816 (0.0069)	5.0845 (0.0058)	5.7870 (0.0106)
15	3.8806 (0.0048)	4.1901 (0.0063)	4.5592 (0.0088)	5.0372 (0.0076)	5.7158 (0.0119)
16	3.8774 (0.0032)	4.1778 (0.0060)	4.5397 (0.0049)	4.9985 (0.0087)	5.6483 (0.0083)
17	3.8760 (0.0043)	4.1682 (0.0035)	4.5149 (0.0060)	4.9652 (0.0051)	5.5919 (0.0078)
18	3.8708 (0.0083)	4.1584 (0.0026)	4.4951 (0.0030)	4.9273 (0.0043)	5.5319 (0.0083)
19	3.8694 (0.0055)	4.1464 (0.0037)	4.4755 (0.0039)	4.8961 (0.0027)	5.4838 (0.0031)
20	3.8687 (0.0051)	4.1364 (0.0041)	4.4555 (0.0072)	4.8673 (0.0042)	5.4371 (0.0076)
21	3.8672 (0.0064)	4.1268 (0.0049)	4.4401 (0.0052)	4.8360 (0.0045)	5.3927 (0.0027)
22	3.8637 (0.0046)	4.1215 (0.0037)	4.4253 (0.0050)	4.8136 (0.0043)	5.3499 (0.0060)
23	3.8610 (0.0032)	4.1110 (0.0039)	4.4093 (0.0057)	4.7870 (0.0059)	5.3118 (0.0056)
24	3.8571 (0.0033)	4.1015 (0.0051)	4.3942 (0.0060)	4.7650 (0.0026)	5.2732 (0.0054)
25	3.8541 (0.0054)	4.0931 (0.0052)	4.3803 (0.0032)	4.7416 (0.0024)	5.2453 (0.0045)

Table 3.4: Cut off values

In summary, a few measurements of distance, being dispersion and contrast, are shown

to agree with the consistent sense of variance and homoskedasticity. The dispersion measurement can be used to test if a pixel belongs to a “known” class of physical scatterer. The consistent sense of contrast can be used to test if any pair of measured data points belong to the same homogeneous class. An example application of this is described in our fMLE speckle filter. The consistent sense of contrast also gives rise to consistent measures of sample variances, which for example, can be used to test if a group of pixels can form a homogeneous area. Chapter 5 presents several of these applications which further validates the models proposed herein.

Chapter 4

Scalar Models for the Multidimensional POLSAR data

This chapter derives several scalar statistical models for the determinant of the POLSAR covariance matrix and show that they are heteroskedastic in their original domain as well as homoskedastic in the log-transformed domain. It also derives a heteroskedastic discrimination measures as well as several homoskedastic measures of distance for the data. Subsequently the statistical models for SAR are shown to be a special case of the proposed models for POLSAR And finally these proposed models are validated against real-life practical data. Mathematical derivations of the proposed models are presented in the Appendix.

4.1 POLSAR statistical analysis

In this section, the POLSAR scattering vector is denoted as s . In the case of partial polarimetric SAR (single polarization in transmit and dual polarization in receive), the vector is two-dimensional ($d = 2$) and is normally written as:

$$s_{part} = \begin{bmatrix} S_h \\ S_v \end{bmatrix}$$

In the case of full and monostatic POLSAR data, the vector is three-dimensional ($d = 3$)

and is presented as:

$$s_{full} = \begin{bmatrix} S_{hh} \\ \sqrt{2}S_{hv} \\ S_{vv} \end{bmatrix}$$

Let $\Sigma = E[ss^{*T}]$ denotes the population expected value of the POLSAR covariance matrix, where s^{*T} denotes the complex conjugate transpose of s . Assuming all the elements in s are independent and s is jointly circular complex Gaussian with the given covariance matrix Σ , then the probably density function (PDF) of s can be written as:

$$pdf(s; \Sigma) = \frac{1}{\pi^d |\Sigma|} e^{-s^{*T} \Sigma^{-1} s} \quad (4.1)$$

where $|M|$ denotes the determinant of the matrix M .

As the covariance matrix is only defined on multiple data points, the sample covariance matrix of POLSAR data is commonly presented in “ensemble” format. These are formed as the mean Hermitian outer product of single-look scattering vectors

$$C_v = \langle ss^{*T} \rangle = \frac{1}{L} \sum_{i=1}^L s_i s_i^{*T}$$

with s_i denotes the single-look scattering vector, which equals s_{part} in the case of partial POLSAR and s_{full} in the case of full polarimetry, and L is the number of looks.

Complex Wishart distribution statistics, however, are normally written for the scaled covariance matrix $Z = LC_v$, whose PDF is given as:

$$pdf(Z; d, \Sigma, L) = \frac{|Z|^{L-d}}{|\Sigma^L| \Gamma_d(L)} e^{-tr(\Sigma^{-1} Z)} \quad (4.2)$$

with $\Gamma_d(L) = \pi^{d(d-1)/2} \prod_{i=0}^{d-1} \Gamma(L-i)$ and d is the dimensional number of the POLSAR covariance matrix.

Our approach differs by applying the homoskedastic log transformation on the determinant of the covariance matrix. In [89], it has been proven that the ratio between the observable and the expected values of the sample covariance matrix’s determinants behaves like a product of d chi-squared random variables with different degrees of freedom

$$\chi_L^d = (2L)^d \frac{|C_v|}{|\Sigma_v|} \sim \prod_{i=0}^{d-1} \chi^2(2L - 2i) \quad (4.3)$$

Its log-transformed variable consequently behaves like a summation of d log-chi-squared random variables with the same degrees of freedom

$$\Lambda_L^d = \ln \left[(2L)^d \frac{|C_v|}{|\Sigma_v|} \right] \sim \sum_{i=0}^{d-1} \Lambda^\chi(2L - 2i) \quad (4.4)$$

where $\Lambda^\chi(k) \sim \ln [\chi^2(k)]$

4.2 Heteroskedastic POLSAR data and the Homoskedastic Log-Transformation

In this section the multiplicative nature of POLSAR data is illustrated. Log-transformation is shown able to convert this into a more familiar additive model. Heteroskedasticity, which is defined as the dependence of variance upon the underlying signal, is proved to be the case for the original POLSAR data. In log-transformed domain, the case for a homoskedastic model, whose variance is fixed and be independent of the underlying mean, is demonstrated. To keep the section flowing, the mathematical derivation is only presented here in major sketches. For more detailed derivation, please refer to Appendix A.

From Eqn. 4.3 and Eqn. 4.4 we have:

$$|C_v| \sim |\Sigma_v| \cdot \frac{1}{(2L)^d} \cdot \prod_{i=0}^{d-1} \chi^2(2L - 2i) \quad (4.5)$$

$$\ln |C_v| \sim \ln |\Sigma_v| - d \cdot \ln(2L) + \sum_{i=0}^{d-1} \Lambda(2L - 2i) \quad (4.6)$$

Over a given homogeneous POLSAR area, the parameters Σ_v , d and L can be considered as constants. Thus Eqn. 4.5 gives the theoretical explanation that, in the original POLSAR domain, a multiplicative speckle noise pattern is present. At the same time, Eqn. 4.6 shows that the logarithmic transformation converts this into a more familiar

additive noise.

Since chi-squared random variables $X \sim \chi^2(k)$ follows the PDF:

$$pdf(x; k) = \frac{x^{(k/2)-1} e^{-x/2}}{2^{k/2} \Gamma\left(\frac{k}{2}\right)} \quad (4.7)$$

Applying the variable change theorem, its log-transformed variable follows the PDF of:

$$pdf(x; 2L = k) = \frac{e^{Lx - e^x/2}}{2^L \Gamma(L)} \quad (4.8)$$

Given the probability distribution function, the characteristic function of both the chi-squared and log-chi-squared random variables can be written as:

$$CF_\chi(t) = (1 - 2it)^L \quad (4.9)$$

$$CF_\Lambda(t) = 2^{it} \frac{\Gamma(L + it)}{\Gamma(L)} \quad (4.10)$$

Subsequently their means and variances can be computed from the given characteristic functions as:

$$\begin{aligned} avg [\chi(2L)] &= 2L \\ var [\chi(2L)] &= 4L \\ avg [\Lambda(2L)] &= \psi^0(L) + \ln 2 \\ var [\Lambda(2L)] &= \psi^1(L) \end{aligned}$$

where $\psi^0()$ and $\psi^1()$ stands for digamma and trigamma functions respectively.

Since the average and variance of both chi-squared distribution and log-chi-squared distribution are constant, the product and summation of these random variables also has fixed summary statistics. Specifically:

$$\begin{aligned}
\text{avg} \left[\prod_{i=0}^{d-1} \chi^2(2L - 2i) \right] &= 2^d \cdot \prod_{i=0}^{d-1} (L - i), \\
\text{var} \left[\prod_{i=0}^{d-1} \chi^2(2L - 2i) \right] &= \prod_{i=0}^{d-1} 4(L - i)(L - i + 1) - \prod_{i=0}^{d-1} 4(L - i)^2, \\
\text{avg} \left[\sum_{i=0}^{d-1} \Lambda(2L - 2i) \right] &= d \cdot \ln 2 + \sum_{i=0}^{d-1} \psi^0(L - i), \\
\text{var} \left[\sum_{i=0}^{d-1} \Lambda(2L - 2i) \right] &= \sum_{i=0}^{d-1} \psi^1(L - i)
\end{aligned}$$

Combining these results with Eqns. 4.5 and 4.6, we have:

$$\text{avg} [|C_v|] = \frac{|\Sigma_v|}{L^d} \prod_{i=0}^{d-1} (L - i) \quad (4.11)$$

$$\text{var} [|C_v|] = \frac{|\Sigma_v|^2 \left[\prod_{i=0}^{d-1} (L - i)(L - i + 1) - \prod_{i=0}^{d-1} (L - i)^2 \right]}{L^{2d}} \quad (4.12)$$

$$\text{avg} [\ln |C_v|] = \ln |\Sigma_v| - d \cdot \ln L + \sum_{i=0}^{d-1} \psi^0(L - i) \quad (4.13)$$

$$\text{var} [\ln |C_v|] = \sum_{i=0}^{d-1} \psi^1(L - i) \quad (4.14)$$

For a real captured image, while the parameters d and L do not change for the whole image, the underlying Σ_v is expected to differ from one region to the next. Thus over an heterogeneous scene, the stochastic process for $|C_v|$ and $\ln |C_v|$ varies depending on the underlying signal Σ_v . In such a context, Eqn. 4.12 indicates that the variance of $|C_v|$ also differs depending on the underlying signal Σ_v , which indicates its heteroskedastic property. At the same time, in the log-transformed domain, Eqn. 4.14 shows that the variance of $\ln |C_v|$ is invariant and independent of Σ_v , hence exhibiting its homoskedastic nature.

4.3 Consistent Measures of Distance for POLSAR data

This section introduces the consistent sense of distance from a few different perspectives. First assuming that the true value of the underlying signal Σ_v is known *a priori*, the following random variables, namely ratio (\mathbb{R}) and log-distance (\mathbb{L}), are observables according to their definitions:

$$\mathbb{R} = \frac{|C_v|}{|\Sigma_v|} \quad (4.15)$$

$$\mathbb{L} = \ln |C_v| - \ln |\Sigma_v| \quad (4.16)$$

From another perspective where the POLSAR is known as having come from an homogeneous area, but the true value of the underlying signal Σ_v is *unknown*, consider the dispersion (\mathbb{D}) and contrast (\mathbb{C}) random variables being defined as:

$$(4.17)$$

$$\mathbb{D} = \ln |C_v| - \text{avg}(\ln |C_v|) \quad (4.18)$$

$$\mathbb{C} = \ln(|C_{v1}|) - \ln(|C_{v2}|) \quad (4.19)$$

Applying Eqns. 4.5, 4.6 and 4.13, Eqns 4.15 to 4.19 becomes:

$$\mathbb{R} \sim \frac{1}{(2L)^d} \cdot \prod_{i=0}^{d-1} \chi^2(2L - 2i) \quad (4.20)$$

$$\mathbb{L} \sim \sum_{i=0}^{d-1} \Lambda(2L - 2i) - d \cdot \ln(2L) \quad (4.21)$$

$$\mathbb{D} \sim \sum_{i=0}^{d-1} \Lambda(2L - 2i) - d \cdot \ln 2 + k_D \quad (4.22)$$

$$\mathbb{C} \sim \sum_{i=0}^{d-1} \Delta(2L - 2i) \quad (4.23)$$

with $\Delta(2L) \sim \Lambda(2L) - \Lambda(2L)$ and $k_D = \sum_{i=0}^{d-1} \psi^0(L-i)$

Also given the characteristic functions (CF) for the elementary components $\Lambda(2L)$ written in Eqn. 4.10, the characteristic functions for the summative random variables can be derived as:

$$\begin{aligned} CF_{\Lambda_L^d}(t) &= \frac{2^{idt}}{\Gamma(L)^d} \prod_{j=0}^{d-1} \Gamma(L-j+it) \\ CF_{\mathbb{L}}(t) &= \frac{1}{L^{idt}\Gamma(L)^d} \prod_{j=0}^{d-1} \Gamma(L-j+it) \\ CF_{\mathbb{D}}(t) &= \frac{e^{ikt}}{\Gamma(L)^d} \prod_{j=0}^{d-1} \Gamma(L-j+it) \\ CF_{\Delta(2L)} &= \frac{\Gamma(2L)B(L-it, L+it)}{\Gamma(L)^2} \\ CF_{\mathbb{C}}(t) &= \prod_{j=0}^{d-1} \frac{\Gamma(2L-2j)B(L-j-it, L-j+it)}{\Gamma(L-j)^2} \end{aligned}$$

Since each elementary simulation component follows fixed distributions (i.e. $\chi^2(2L), \Lambda(2L), \dots$), it is natural that these variables also follow fixed distributions. Moreover, they are independent of Σ_v . This serves as conclusive evidence that these random variables follow consistent and fixed distributions, regardless of the underlying signal Σ_v .

4.4 SAR as the Special Case of Polarimetric SAR

The previous section has validated the use of our models for 3-dimensional ($d = 3$) full polarimetric and 2-dimensional ($d = 2$) partial polarimetric SAR cases. In this section, the focus is on the limit case where the dimensional number is reduced to 1, i.e. $d = 1$. Physically this means that when the multi-dimensional POLSAR dataset is collapsed into the one dimension, it becomes conventional SAR data. Mathematically, the sample covariance matrix is reduced to the sample variance and the determinant equates the scalar value. Since it is well known that, for SAR data, variance equals intensity, the special case of the $d = 1$ result should be consistent with previous results for SAR intensity data. This can be thought of either as a cross-validation evidence for the proposed POLSAR models, or alternatively as having SAR as the special case

of POLSAR.

The results so far for our models can be summarized as:

$$\begin{aligned}
\mathbb{R} &= \frac{|C_v|}{|\Sigma_v|} \sim \frac{1}{(2L)^d} \prod_{i=0}^{d-1} \chi^2(2L - 2i) \\
\mathbb{L} &= \ln |C_v| - \ln |\Sigma_v| \sim \sum_{i=0}^{d-1} \Lambda(2L - 2i) - d \cdot \ln 2L \\
\mathbb{D} &= \ln |C_v| - avg(\ln |C_v|) \sim \sum_{i=0}^{d-1} \Lambda(2L - 2i) - d \ln 2 + k \\
\mathbb{C} &= \ln |C_{1v}| - \ln |C_{2v}| \sim \sum_{i=0}^{d-1} \Delta(2L - 2i) \\
\mathbb{A} &= avg(\mathbb{L}) = \sum_{i=0}^{d-1} \psi^0(L - i) - d \cdot \ln L \\
\mathbb{V} &= var(\mathbb{L}) = \sum_{i=0}^{d-1} \psi^1(L - i) \\
\mathbb{E} &= mse(\mathbb{L}) = \left[\sum_{i=0}^{d-1} \psi^0(L - i) - d \cdot \ln L \right]^2 + \sum_{i=0}^{d-1} \psi^1(L - i)
\end{aligned}$$

Upon setting $d = 1$ into the above models, Section A.3 shows that the reduced results are consistent with not only the following results for single-look SAR derived earlier, i.e. $d = 1, L = 1$,

$$\begin{aligned}
I &\sim \bar{I} \cdot pdf \left[e^{-R} \right] \\
\log_2 I &\sim \log_2 \bar{I} + pdf \left[2^x e^{-2^x} \ln 2 \right] \\
\mathbb{R} &= \frac{I}{\bar{I}} \sim pdf \left[e^{-x} \right] \\
\mathbb{L} &= \log_2 I - \log_2 \bar{I} \sim pdf \left[2^x e^{-2^x} \ln 2 \right] \\
\mathbb{D} &= \log_2 I - avg(\log_2 I) \sim pdf \left[e^{-(2^x e^{-\gamma})} 2^x e^{-\gamma} \ln 2 \right] \\
\mathbb{C} &= \log_2 I_1 - \log_2 I_2 \sim pdf \left[\frac{2^x}{(1 + 2^x)^2} \ln 2 \right] \\
\mathbb{A} &= avg(\mathbb{L}) = -\gamma / \ln 2 \\
\mathbb{V} &= var(\mathbb{L}) = \frac{\pi^2}{6} \frac{1}{\ln^2 2} \\
\mathbb{E} &= mse(\mathbb{L}) = \frac{1}{\ln^2 2} (\gamma^2 + \pi^2 / 6) = 4.1161
\end{aligned}$$

but also the following well-known results for multi-look SAR, i.e. $d = 1, L > 1$:

$$I \sim pdf \left[\frac{L^L x^{L-1} e^{-Lx/\bar{I}}}{\Gamma(L) \bar{I}^L} \right]$$

$$N = \ln I \sim pdf \left[\frac{L^L}{\Gamma(L)} e^{L(x-\bar{N}) - L e^{x-\bar{N}}} \right]$$

Furthermore, the following results for multi-look SAR data, which can be thought of either as extensions of the corresponding single-look SAR results or as simple cases of the POLSAR results can also be derived and shown to be as follows:

$$\mathbb{R} = \frac{I}{\bar{I}} \sim pdf \left[\frac{L^L x^{L-1} e^{-Lx}}{\Gamma(L)} \right]$$

$$\mathbb{L} = \ln I - \ln \bar{I} \sim pdf \left[\frac{L^L e^{Lt - Le^t}}{\Gamma(L)} \right]$$

$$\mathbb{D} = \ln I - avg(\ln I) \sim pdf \left[\frac{e^{L[x - \psi^0(L)] - e^{[x - \psi^0(L)]}}}{\Gamma(L)} \right]$$

$$\mathbb{C} = \ln I_1 - \ln I_2 \sim pdf \left[\frac{e^x}{(1 + e^x)^2} \right]$$

$$\mathbb{A} = avg(\mathbb{L}) = \psi^0(L) - \ln L$$

$$\mathbb{V} = var(\mathbb{L}) = \psi^1(L)$$

$$\mathbb{E} = mse(\mathbb{L}) = [\psi^0(L) - \ln L]^2 + \psi^1(L)$$

This newly derived model for multi-look SAR data can also be validated against real-life data. Fig. 4.1 presents the the results of an experiment carried out for the stated purpose. In the experiment, the intensity of a single-channel of SAR data (HH) for an homogeneous area in the AIRSAR Flevoland dataset is extracted. Then the histograms for the log-distance and and contrast are plotted against the theoretical PDF given above. The ENL is set to the nominal number of 4. A good visual match is apparent in the final plotted results.

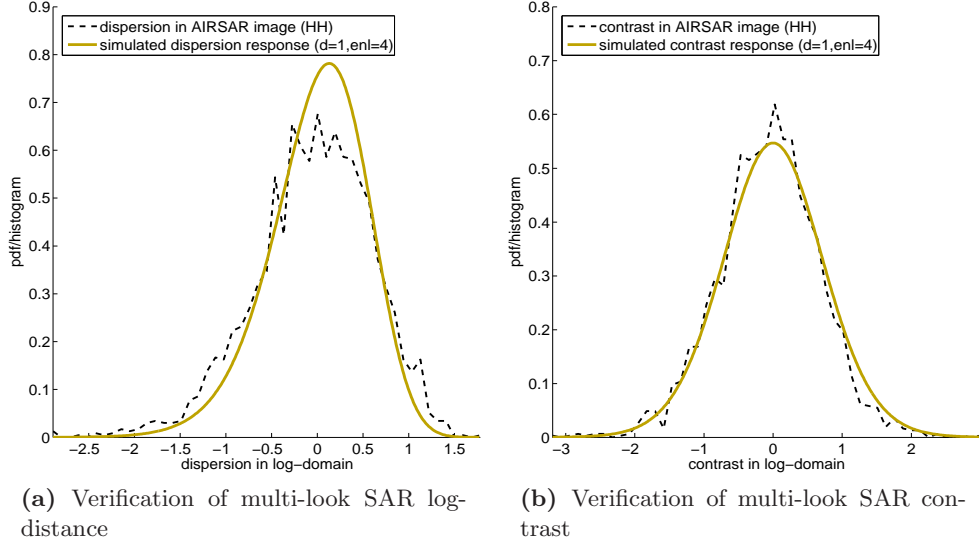


Figure 4.1: Multi-Look SAR dispersion and contrast showing that the modelled response matches very well with the histograms from real-life captured data.

4.5 Validating the models against real-life data

4.5.1 Explaining practical data with the given Number-of-Looks

This section describes the test to validate the proposed models against real-life captured data. The validation procedure is as follows. Using the stochastic models derived in the previous sections, histogram plots of its simulated data are generated graphically. This is then compared against the histogram plots of the real-life captured data samples extracted from an homogeneous area.

As such, the theoretical models can be validated if, for the same parameters, the two plots match each other reasonably well. For this verification, an homogeneous area was chosen from the AIRSAR Flevoland POLSAR data. Theoretical models are then verified against the real life data. The validations include the following models: the determinant and its log-transformed models, together with the various dissimilarity measures, namely: the determinant ratio, the log-distance, the dispersion and the contrast measures of distance.

These models are also closely related. Given the same parameter set, the determinant and determinant ratio are just scaled versions of each other. Meanwhile, the log-

determinant, the log-distance and the dispersion are also just shifted versions of each other. Thus ideally speaking, if one model is validated all the other models can also be, assuming that all the parameters of the image are known exactly. Nevertheless, all the models will be investigated separately in this section.

Among all these models, the least-assumed stochastic process for dispersion and contrast measures of distance are validated first. From the real-life data, for each pixel in the region, the determinant of the covariance matrix is computed and the log-transformation is applied. The average of POLSAR covariance matrix determinants in the log-transformed domain, i.e. $\text{avg}(\ln|C_v|)$, is then used to calculate the dispersion. Next, the observable samples of dispersion and contrast are computed according to Eqns. 4.18 and 4.19. Finally, their histograms are generated.

Theoretical simulations of the models based on Eqns. 4.22 and 4.23 are also performed. The nominal value of 4 was taken as the dataset's number of looks, L , while the dimensional number d is set to 3 for the full polarimetric SAR dataset, and 2 for the partial polarimetric SAR dataset. The histogram plots of the theoretical models and the real-life dataset are presented in Fig. 4.2. A visual match is clearly observable which verifies the applicability of the theoretical models for the dispersion and contrast measures of distance.

Apart from dispersion and contrast, the other four models to be investigated require an estimation of the “true” underlying signal $|\Sigma_v|$. There are two ways to estimate this quantity over an homogeneous area. The traditional way is to simply assume that the true signal is equal to the average of the POLSAR covariance matrix in its original domain, i.e. $\Sigma_v = \text{avg}(C_v)$. Another approach is to estimate the true signal from the average of the log-determinant of the POLSAR covariance matrix (i.e. $\text{avg}[\ln|C_v|]$) using Eqn. 4.13. Both approaches will be explored in this section. However, given that the log-determinant average has already been computed earlier, the second approach is used first for the validation of determinant-ratio and log-distance.

Fig. 4.3 shows the various plots for the models of determinant-ratio and log-distance against real-life data. In this test, the theoretical models are simulated from Eqns 4.20 and 4.21, while the observable samples are computed using Eqns 4.15 and 4.16 with the true signal estimated from the log-determinant average, i.e. $\text{avg}(\ln|C_v|)$. Again a reasonable match is observed, which validates the models for log-distance and determinant ratio.

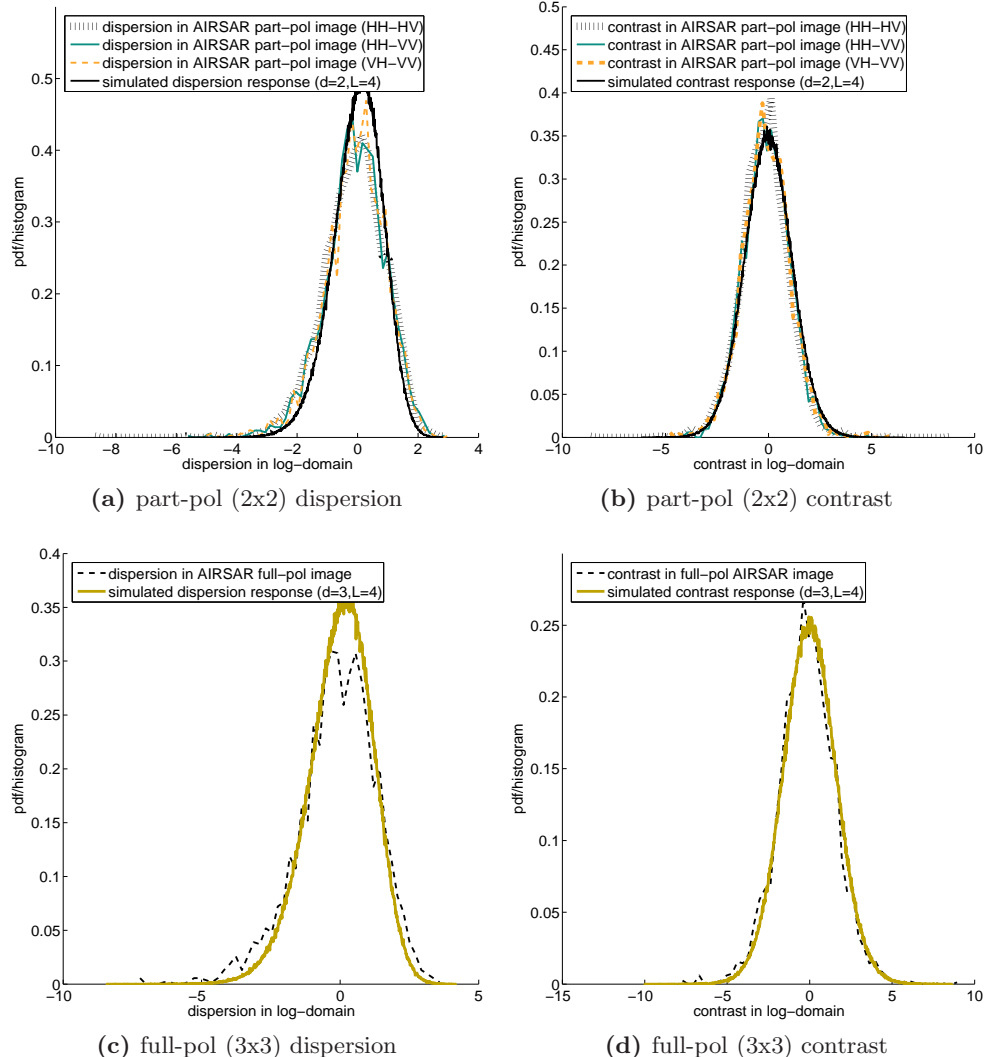


Figure 4.2: Validating the dispersion and contrast models against both partial and full polarimetric AIRSAR Flevoland data.

Since the models for the determinant and log-determinant are just scaled or shifted versions of the models for determinant-ratio and log-distance, similar validation results are to be expected. And if the true signals are computed in the same manner as described before then in fact a similar match can be easily observed.

However, a more interesting phenomena is to be described. It happens in the validation process for determinant and its log-transformed model, where the theoretical response is taken from the simulated stochastic process described by Eqns. 4.5 and 4.6. The

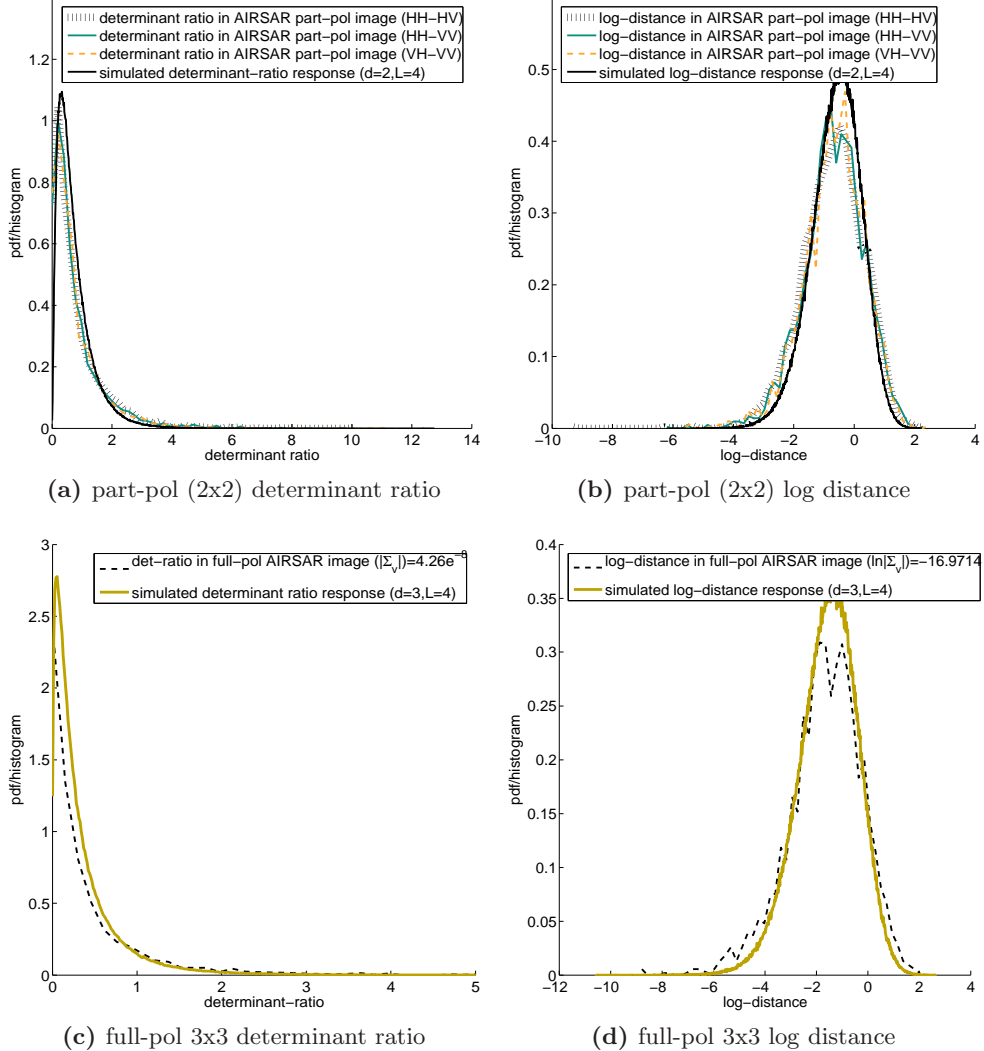


Figure 4.3: Validating determinant-ratio and log-distance models with $|\Sigma_v|$ is computed using $\text{avg}(\ln |C_v|)$

phenomena occurs when the true signal is estimated by the first approach i.e. equal to the average of the sample covariance matrix in its original domain. Using this approach, a different estimation for the true signal arises.

Subsequently the validation plots, which are presented in Fig 4.4d, exhibit some small discrepancies. The differences are easier to observe in the log-determinant plots. Except for the shifted effect, the shapes of the models and the real-life data are practically similar.

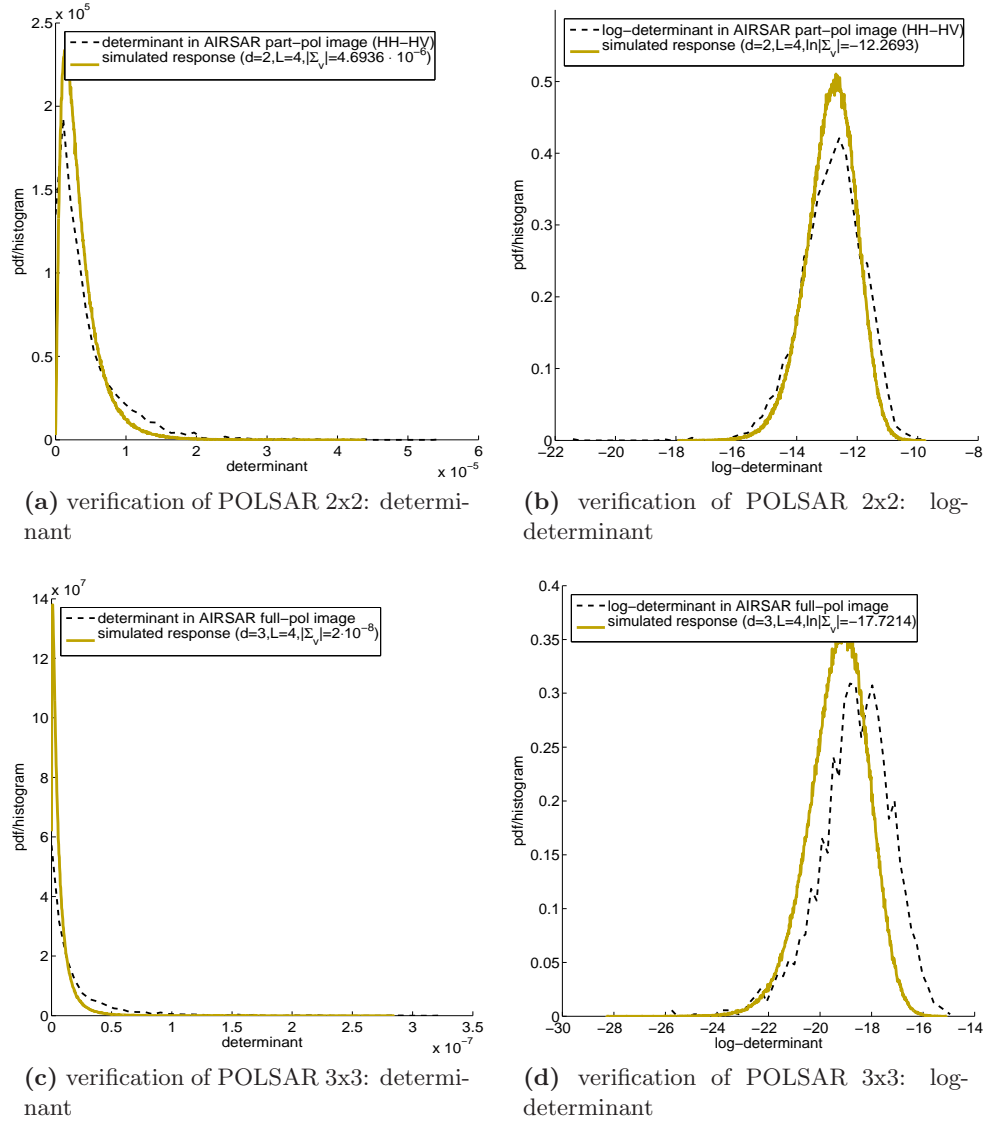


Figure 4.4: Validating determinant and log-determinant models with $\Sigma_v = \text{avg}(C_v)$

In summary, the dispersion and contrast measures of distance are shown to match reasonably well with the real-life data. The same can be stated for the other four models, namely: determinant, log-determinant, determinant ratio and log-distance, if the underlying parameters can be estimated reasonably well for the given image. However as described above a single “true signal” $|\Sigma_v|$ can have two different estimated values, depending on which estimation method is chosen. The discrepancy suggests that at least one parameter for the models was wrongly employed. But which model

parameter was used wrongly, and even if that can be corrected, would a better match become observable? This question will be discussed further in the next section.

4.5.2 Comparing Theoretical Assumptions and Practical Implementations

While the assumptions used for the proposed models are intentionally kept to the minimum, like all other similar models, they are still built upon certain presumptions. Practical conditions however may not always satisfy these prerequisites. In this section, certain gaps between the conditions found in practical real-life data and the theoretical assumptions are discussed. It will be shown that the theoretical model proposed can handle the practical data, even when these “imperfections” are taken into account.

There are two main “imperfections” that are usually found in practical POLSAR data with reference to the theoretical model. The first is the mutually independent assumption for each component in the POLSAR target vector s . However, in practice, high correlation is routinely observable between the POLSAR data components, specifically between S_{hh} and S_{vv} . This phenomena is also present in our AIRSAR dataset, where

$$\Sigma_v = \text{avg}(C_v) = \begin{vmatrix} 0.0084 & 1 \cdot 10^{-6} + 4 \cdot 10^{-4}i & 0.0071 - 0.0017i \\ 1 \cdot 10^{-6} - 4 \cdot 10^{-4}i & 0.0017 & -3 \cdot 10^{-4} - 2 \cdot 10^{-4}i \\ 0.0071 + 0.0017i & -3 \cdot 10^{-4} + 2 \cdot 10^{-4}i & 0.0122 \end{vmatrix}. \quad \text{De-}$$

spite the mismatch, the proposed model is still valid under such conditions, as observed in the part-pol (HH-VV) and full-pol plots in Figs. 4.2 to 4.4.

Another assumption of the model (for both SAR and POLSAR) is that the samples are statistically independent of each other. This is a reasonable assumption given that the transmission and receipt of analogue signals are done independently for each radar pulse, i.e. for each resolution cell. Thus theoretically speaking, adjacent pixels in an image can be assumed to be statistically independent.

However, the actual imaging mechanism of a real-life (POL)SAR processor is that of digital nature, where the analogue signal is to be converted into a digital data-set. Specifically, the analogue signal in SAR which is characterized by the pulse bandwidth measurement, is fed into an analogue-to-digital sampling and conversion process which is characterized by its sampling rate. Theoretically it is possible to define a sampling rate to ensure that each digital pixel corresponds exactly to an analogue physical cell resolution. Practically however, to ensure “perfect reconstruction” of the analogue

signal, the sampling rate is normally set at a slightly higher value than the theoretical mark. This results in a higher number of samples / pixels than the number of physical cells available in the scene.

Stated differently, in practical data, each physical radar cell influences more than one pixel, and each pixel is not completely defined by one physical analogue cell. This high sampling rate results in a significantly higher correlation between pairs of pixels that would be found between within a single physical cell resolution, compared to the correlation between pairs of pixels that are further away and hence having less physical relation to each other. It also results in a reduction in the effective number of looks, which means for example that a window of 3x3 pixels actually contains less than 9 physical analogue cells.

The former phenomena is partially explained in [90] for SAR, while the later has been experimentally observed for POLSAR data in [27] and [91]. The oversampling practice is also documented by the producers of SAR processors. For AIRSAR, the sampling rate and pulse bandwidth combinations are either 90/40MHz or 45/20MHz [92]. While for RadarSat2, the pixel resolution and range–azimuth resolutions for SLC fine-quad mode is advertised as $(4.7 \cdot 5.1)m^2/(5.2 \cdot 7.7)m^2$ [93]

The proposed model in this thesis can handle this imperfection that is found in practical data through the use of an ENL estimation procedure, as will be described in the next section.

4.5.3 Estimating the Effect Number-of-Looks (ENL)

A number of techniques are available to estimate the Effective Number of Looks (ENL) for a given POLSAR dataset. The common approach is by investigating the summary statistics of a known homogeneous area in the given data before making inferences about the inherent ENL. The summary statistics for $|C_v|$ and $\ln |C_v|$ have been derived in Section 4.2. In fact Eqn. 4.13 indicates that there is a relationship among $|\text{avg}(C_v)|$, $\text{avg}(\ln |C_v|)$, d , L . Recall that in carrying out validation process for AIRSAR Flevoland data using the nominal look number of 4, this relationship was broken. The reason for such broken relationship is due to an inexact look number being taken. In a given POLSAR dataset, since values of $|\text{avg}(C_v)|$, $\text{avg}(\ln |C_v|)$, d are all known, it is possible to estimate the “effective” number of look, by finding L that ensures the above relationship is valid.

This approach was also used in [91], where the same equation as Eqn. 4.13 was used to estimate the ENL. Unfortunately, the only known way to solve the equation for the unknown L requires the use of an “iterative numerical method”. Instead of relying on the equations for statistical mean to find ENL, the approach here makes use of the variance statistics in the homoskedastic log-domain to find ENL. Specifically, Eqn. 4.14 can be rewritten as:

$$\text{var}[\ln|C_v|] = f(L) = \sum_{i=0}^{d-1} \psi^1(L - i)$$

where $\psi^1()$ denotes tri-gamma function.

Thus theoretically, given some measurable value for $\text{var}[\ln|C_v|]$, one could solve the above equation for the unknown L . However, that would also require some iterative computations. A more practical approach is to use a look-up graph approach where for each value of $\text{var}[\ln|C_v|]$, a corresponding pre-computed value for L can be found by referencing the variance value on the graph. An approximation can also be used to find the L value based on a back-of-the-envelope calculation using the following equation

$$\hat{L} = d \left(\frac{1}{\text{var}(\ln|C_v|)} + 0.5 \right) \quad (4.24)$$

Fig. 4.5 shows the shapes of the function defined in Eqn. 4.14 for SAR and partial-POLsar data $f_{d=1}(L)$ and $f_{d=2}(L)$, together with the approximation formula (Eqn. 4.24). It can be seen that they are practically the same, hence the validity of Eqn 4.24. In the next section, the estimated ENL will hence be used to demonstrate the accuracy of the proposed model.

4.5.4 Using the estimated ENL to better explain practical data

For this test a sample RADARSAT2 dataset is used. The dataset is in its Fine-Quad mode Single-Look format, and nine-look processing is applied. The dispersion histogram in the log-transformed domain is computed over an homogeneous area. The histograms generated by the theoretical models for nominal ENL value of 9 are then plotted in Fig. 4.6. The nine-look histogram is the narrower and higher curve. As can be seen, the match is not very good between this and the observed data, displayed as points.

A much better match can be achieved by estimating the ENL from the observable

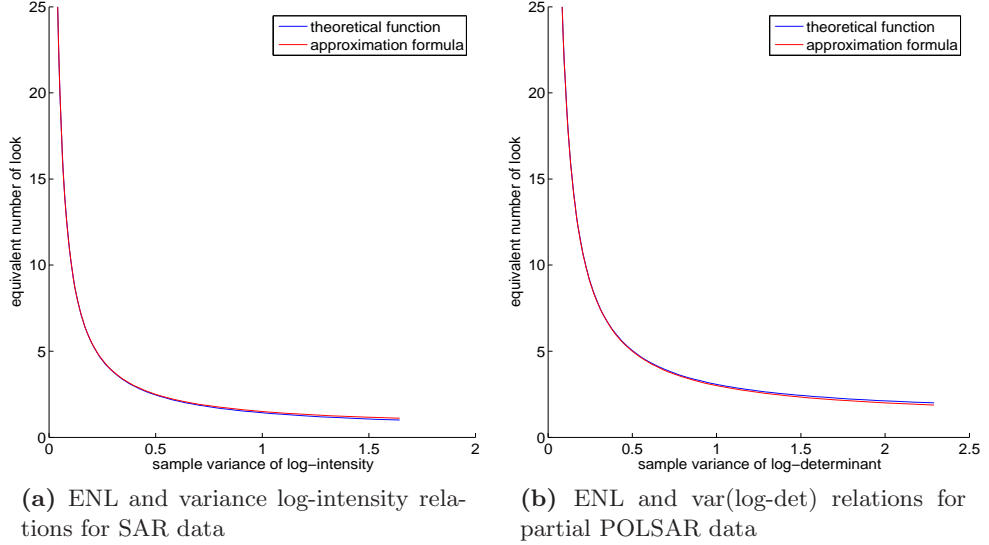


Figure 4.5: The relationships between ENL and the sample variance of log-determinant and log-intensity

variance of the log-determinant, using the approximation formula given in Eqn. 4.24. This is then used to re-calculate the histogram, which is plotted in the same figure (Fig. 4.6). As can be seen, the $L = 3.4241$ curve exhibits a much closer match to the real-life data. This procedure can always be carried out for any given dataset, as long as an area of homogeneous area can be identified.

Fig. 4.7 shows that the over-sampling issue is also present in AIRSAR Flevoland dataset, although to a much lesser extent. Using the effective number-of-looks value, the reconstructed model exhibits a better match to the real-life data.

In summary, this chapter proposes the determinant of the POLSAR covariance matrix as the scalar and representative observable for the both partial and full polarimetric SAR data. Out of many different scalar projections of the multi-dimensional POLSAR data, this observable is proposed together with its underlying statistical model, from which consistent discriminant measures are also proposed. The derived models are shown to be heteroskedastic in the original domain, and logarithmic transformation is shown to convert these into homoskedastic models. The representative power of the observable is explained in a few different ways. Firstly, the determinant observable neatly transforms into the representative and widely-used SAR intensity when the dimensional number is collapsed to one, putting the commonly-used statistical models

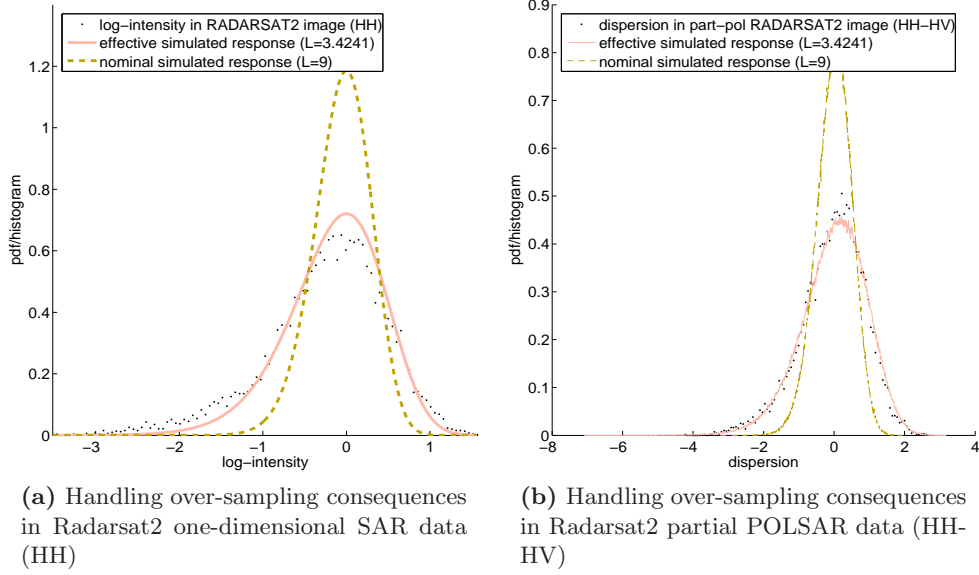


Figure 4.6: 9-look processed Radarsat2 data does not exactly exhibit 9-look data characteristics. An homoskedastic model in the log-transformed domain can be used to successfully estimate the effective ENL and thus offer a better model of the data.

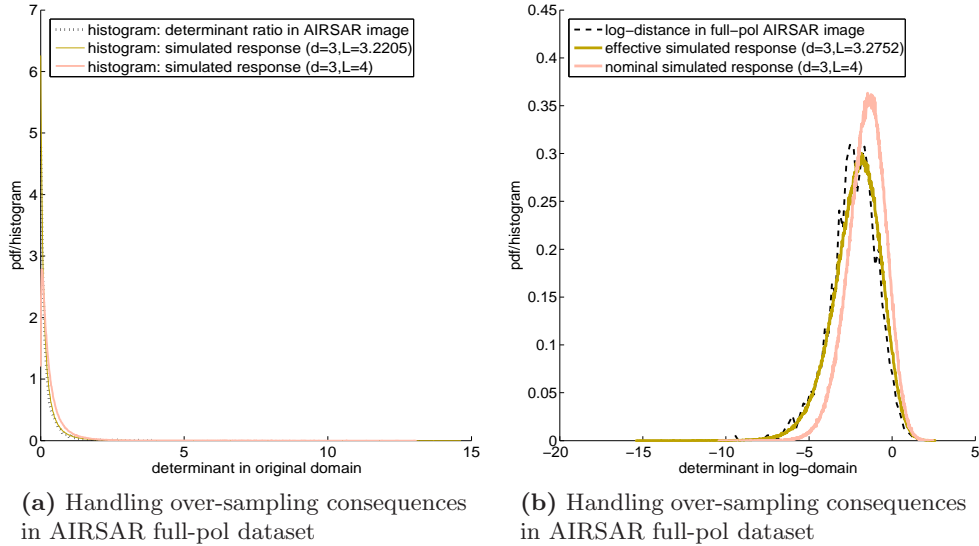


Figure 4.7: AIRSAR Flevoland also exhibits the over-sampling phenomena, though to a much smaller extent than the RADARSAT 2 data.

for SAR intensity to fall within this generic proposed models. Secondly, this observable is also widely used in existing discrimination measures for POLSAR. In fact, this chap-

ter also proposes several new discrimination measures for POLSAR, which together with the proposed statistical models help to link the existing discriminant measures for POLSAR to the widely-used intensity ratio for SAR. Thus this theory should help in a wide range of applications, where a single scalar observable is required to represent the complex, multi-dimensional and inter-correlated POLSAR data. It also builds a bridge allowing certain existing classes of SAR data processing technique to be applicable towards POLSAR data. The next chapter will briefly explore such applications as well as presents further validation of the proposed models.

Chapter 5

Applications of The Proposed Models

In this chapter, some beneficial applications of the proposed models are presented, which demonstrate how the models' consistent sense of variance capability can help to break the vicious circle encountered in SAR speckle filtering. This chapter also shows how the MSE can then be applied in the additive and homoskedastic domain to evaluate SAR speckle filters, and further extends the concept to also evaluate POLSAR speckle filters.

5.1 Clustering SAR images using the consistent measures

Given an area to be analyzed, the question of whether it is homogeneous or not can be investigated using the statistical hypothesis test described in chapter 3. If that is found to be the case, a clustering algorithm can then be applied to partition the area into smaller regions. Thus an image can be segmented into homogeneous areas by applying the process repeatedly.

5.1.1 Developing k-MLE clustering Algorithm

5.1.1.1 Homogeneous Maximum Likelihood Estimation

In a window of analysis, intensity dataset $X^I = \{x_1^I, \dots, x_n^I\}$ follows the exponential distribution given in Eqn. 2.3. Assuming prior knowledge of it being homogeneous, thus having a single σ , the objective then is to estimate σ . This section shows how σ can be estimated in the log-transformed domain.

It has already been proven that the log-transformed dataset $X^l = \log_2 \sigma$ follows a Fisher-Tippet distribution $pdf(x) = \ln 2 \frac{2^d}{e^{2^d}}$, with $d = x - \mu$, and $\mu = 2 \log_2 \sigma$. Thus the problem of estimating σ , casting into the log-transformed domain, equals to the problem of estimating μ . The PDF given in Eqn. 5.1 can then be interpreted as the conditional probability of observing a single value of x_i^l when the underlying coefficient equals μ :

$$P(x_i^l | \mu) = \ln 2 \frac{2^{x_i^l - \mu}}{e^{2^{x_i^l - \mu}}} \quad (5.1)$$

Since log-transformed variables are biased, an MLE approach is used to estimate μ . The MLE strategy aims to maximize the conditional (likelihood) probability of observing a set of values X found in the area, given that the underlying coefficient equals μ : $P(X^l | \mu)$. Assuming the values of x_i^l are independent, the statistical product rule indicates that $P(X^l | \mu) = \prod_{i=1}^n P(x_i^l | \mu)$, with $P(x_i^l | \mu)$ as given in Eqn. 5.1. Maximizing $P(X^e | \mu)$ also maximizes $\ln[P(X^l | \mu)]$, which can be written as:

$$\ln[P(X^l | \mu)] = \sum_{i=1}^n \ln(P(x_i^l | \mu)) = \sum_{i=1}^n \ln \left[\ln 2 \frac{2^{x_i^l - \mu}}{e^{2^{x_i^l - \mu}}} \right]$$

The parameter μ which maximizes the likelihood is found by setting its derivatives to

zero:

$$\begin{aligned}\frac{\partial \ln[P(X^l|\mu)]}{\partial \mu} &= 0 \\ \frac{\partial}{\partial \mu} \sum_{i=1}^n \ln(2^{x_i^l - \mu}) - \ln(e^{2^{x_i^l - \mu}}) &= 0\end{aligned}$$

Thus μ can be found by:

$$2^\mu = \frac{1}{n} \sum_{i=1}^n 2^{x_i^l} \quad (5.2)$$

This result in the log-transformed domain is consistent with the analysis result in the original domain where $\sigma^2 = \frac{1}{n} \sum_{i=1}^n x_i^e$, with $x_i^e = 2^{x_i^l}$

5.1.1.2 Heterogeneous k-MLE Clustering

In order to apply MLE into a given heterogeneous analysis window (L^w), one would need to partition the area into groups of homogeneous pixels (G). Assuming for now that the number of homogeneous groups ($c = \text{size}(C)$) is known *a priori*, this section will describe the proposed clustering algorithm. The basic template is similar to the k-means clustering algorithms (Listing 5.1)

1. Initialize the cluster centres
2. Assign each sample to a centre C_i that has the highest probability $P(x|C_i)$ (as in equation 5.1)
3. Recalculate cluster centres for each C_i (as in equation 5.2)
4. Iterate above 2 steps until there is no more changes in cluster centres' locations

Listing 5.1: k-MLE Clustering Algorithm Template

```
function optimized_clusters = k_mle_clustering(l, c_init)
    c_prev = c_init;
    c_new = find_new_centers(l, c_prev);

    while (c_new != c_prev) do
```

```

c_prev = c_new;
c_new = find_new_centers(l, c_prev);
end while

return optimized_clusters = c_new
end function

```

Due to the characteristics of the log-transformed domain, an MLE estimator is used in lieu of the standard averaging estimation for cluster centers. Consequently the k-MLE algorithm is presented in Listing 5.2.

Listing 5.2: Iteratively find better cluster centers

```

function c_new = find_new_centers(l, c)
    for (i = 1 to size_of(l))
        for (j = 1 to size_of(c))
            m[i, j] = 0; %reset memberships
            p[i, j] = conditional_probability_of( l[i] | c[j] );
        end for

        j_0 = argmax( p[i, :] );
        m[j_0] = 1; %assign membership to a cluster
    end for

    for ( j = 1 to size(c) )
        c_new[j] = maximum_likelihood_of( l[i] with m[i, j]==1 );
    end for

    return c_new;
end function

```

Compared with using the standard k-means algorithm, the following differences are noted:

1. In k-means, data points are grouped into clusters with minimum distance. In our specific situation, as the dispersion PDF is non-symmetric around the cluster centre, log-transformed data points are assigned to the cluster that gives them

highest likelihood probability.

2. The calculation of new cluster centres is also different. In k-means, new cluster centres are estimated as the average of all membered data points. Here, due to the bias of the PDF, maximum likelihood estimations are preferred.
3. All the design decisions are made possible by the knowledge of the statistical PDF in the log-transformed domain.

5.1.1.3 Determining number of clusters

In the last section the algorithm was designed with the assumption that the number of clusters are known *a priori*. In practice, this is not the case. This section will describe how the issue can be tackled with real world data.

The basic idea is to start with an assumption that the whole area is homogeneous. Then such an assumption is put to test using the hypothesis testing procedure described earlier. If the assumption appears to be violated, the area is broken down by introducing a new cluster centre. The clustering algorithm is again performed and the new clusters are again assumed to be homogeneous, and tested. The process iterates until all partitions are confirmed to be homogeneous. The pseudo code for such a procedure is given in Listing 5.3

Listing 5.3: Homogeneous partitions number growing

```

function centers = partition_into_homogenous_groups(1, threshold)
    c_init = maximum_likelihood_of(1);
    [further_partition_needed, c_new] =
        check_homogeneity_status(1, c_init, threshold);

    while (further_partition_needed) do
        c_prev = c_new;
        c_new = k_mle_cluster(1, c_prev);
        [further_partition_needed, c_new] =
            check_homogeneity_status(1, c_prev, threshold);
    end while
    %after this: all partitions are homogenous

    return centers = c_new;
end function

```

```

function [ further_partition_needed , c_new ]
    = check_homogeneity_status(l , c , threshold_vector);

    m[i,j] = get_membership_assignments(l , c);
    all_partitions_homogenous = true;
    c_new = c;
    for (j = 1 to size_of(c))
        g = {L[i] with m[i,j]==1};
        this_partition_homogenous =
            (variance(g) < threshold_vector[ size_of(g) ]);

        if (NOT this_partition_homogenous) then
            % split non-homogenous partition
            c_new[j] = min(g);
            c_new[size_of(c_new) + 1] = max(g);

            all_partitions_homogenous = false;
        end if
    end for

    further_partition_needed = NOT all_partitions_homogenous;
end function

```

5.1.2 Evaluating the k-MLE algorithm

5.1.2.1 Using the k-MLE clustering algorithm for speckle filtering

In the context of statistical hypothesis testing, there is a difference between accepting the null hypothesis and simply failing to reject it. However, in the section that follows, the decision rule in use is that if the sample variance is lower than the cut-off value, the null hypothesis is accepted. This section illustrates that for the purpose of speckle-filtering the difference is negligible.

The principle of speckle filtering is to group pixels into homogeneous areas so that the stochastic noise can be removed. Hence the k-MLE clustering algorithm can be used to form the basis of a speckle filter. Specifically, the clustered areas directly serve as the grouping of pixels into homogeneous areas, and the cluster centres serve as the

estimated backscattering coefficient for the analysis window.

Considering the case where some extreme threshold-values are used as the homogeneous criteria, if threshold-value is set to be very high (close to 100%), then a given partition would almost never be broken down. The kMLE speckle filter effect would then equals to a box-car filter. Conversely, if the threshold-value is set to a very low value (close to 0%), then a given partition would almost always be broken down to a single value. The kMLE speckle filtering effect then would be virtually negligible.

Fig. 5.1 shows various degrees of speckle filtering controllable by using different threshold-values. Using the same moving window size of 3×3 , the effect of filtering is clearly proportional to the threshold values employed. This can be observed from Figs. 5.1a to 5.1d where the visual quality reflects the effects of the kMLE speckle filter when its threshold is set at 0% (i.e. left untouched), 25%, 80% and 100% (i.e. equals to the boxcar filter) respectively.

One way to improve the speckle filtering performance is to use a larger window size. Fig. 5.2a shows the visual quality performance of k-MLE filtering on 5×5 window. As can be seen, the blurring effect in comparison to the 3×3 filter is clearly visible. To reduce the associated blurring effect, a threshold-value lower than 100% would help by providing an adaptive partitioning of the analysis window (via the k-MLE clustering algorithm).

Another way to improve the raw k-MLE speckle filter is to apply it iteratively. As can be seen in Fig. 5.1, a normal 3×3 k-MLE filter would not filter as much noise as a 3×3 boxcar filter. At the same time, a 5×5 boxcar filter, while having better speckle suppression power, would lose out by its blurring effects as can be seen in Fig. 5.2a. To improve k-MLE filtering power while avoiding the blurring effect, the k-MLE speckle filter can be used iteratively. Presented in the Fig. 5.3 is the result of a k-MLE filter configured in a 3×3 window with 25% threshold-value, being applied iteratively for four times. From the plot, the 3×3 iterative k-MLE filter appears to have similar quantitative performance with the 5×5 boxcar filter, while its visual imagery output appears much sharper, qualitatively speaking.

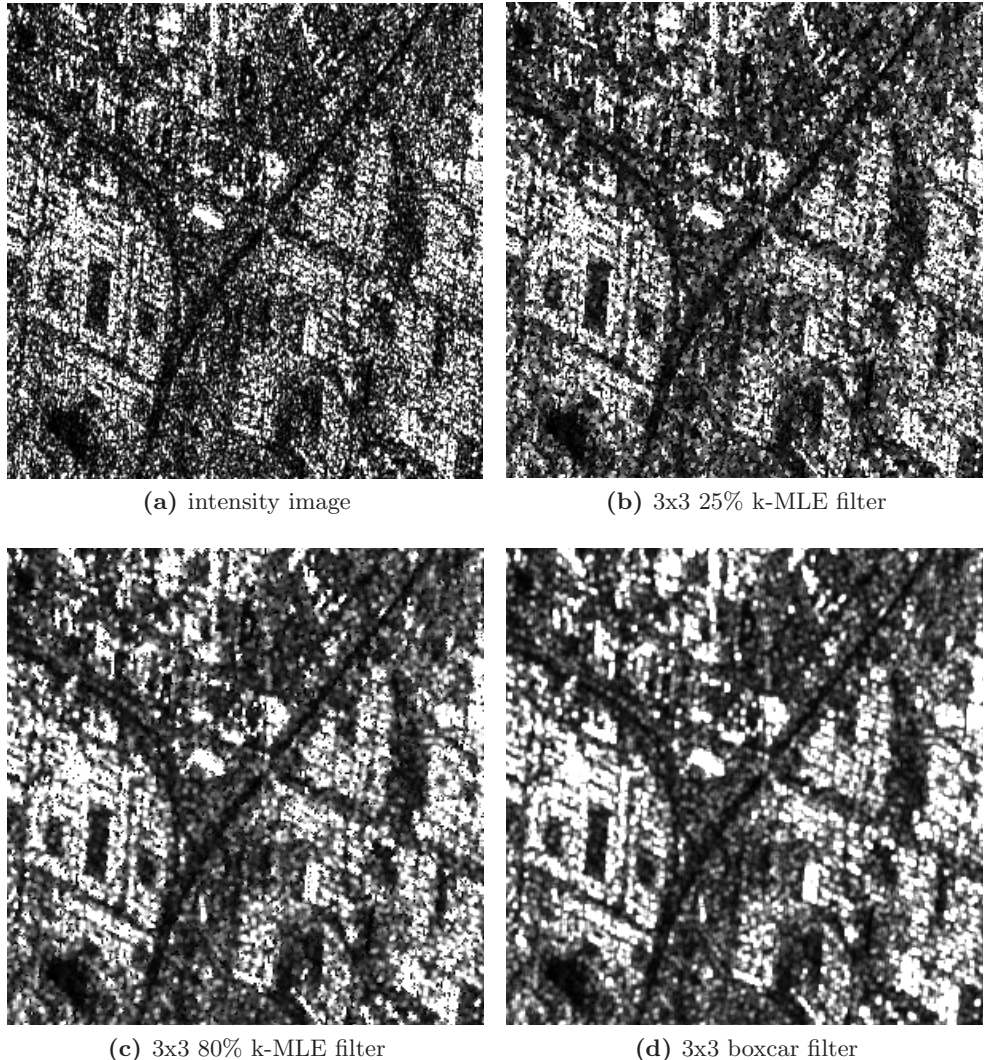


Figure 5.1: Speckle filtering effects by various threshold-value

5.1.2.2 Evaluation of the kMLE speckle filter on simulated targets

A number of point targets were simulated on a homogeneous background clutter. In this test, the SNR between the target and background clutter is fixed at 9dB. Subsequently, the kMLE speckle filter is to be benchmarked against the standard boxcar filters as shown in Fig. 5.4. Qualitatively speaking, it is clear that the kMLE speckle filter delivers a resultant image with both sharper edges than the 5×5 boxcar filter and a stronger visual contrast than the 3×3 boxcar filter. Quantitatively, the k-MLE also

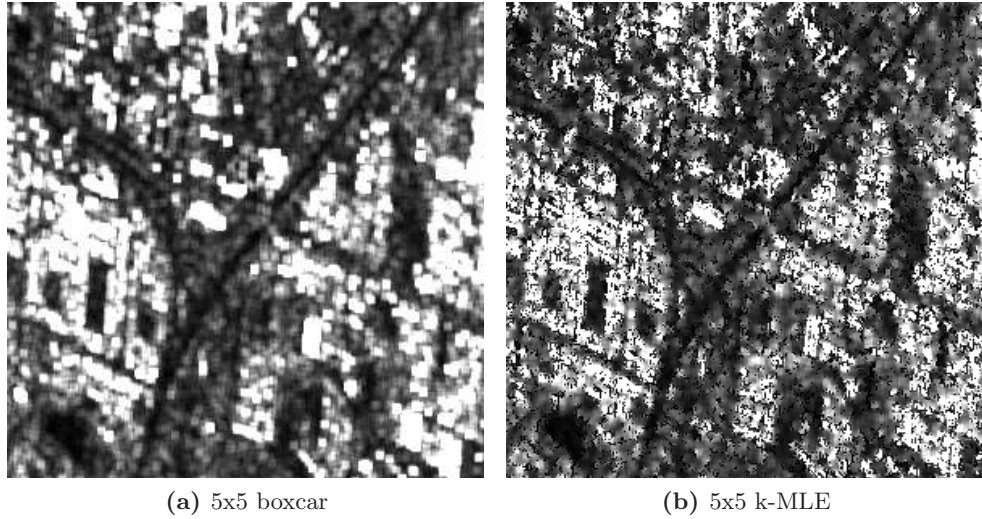


Figure 5.2: Blur effects of larger window size

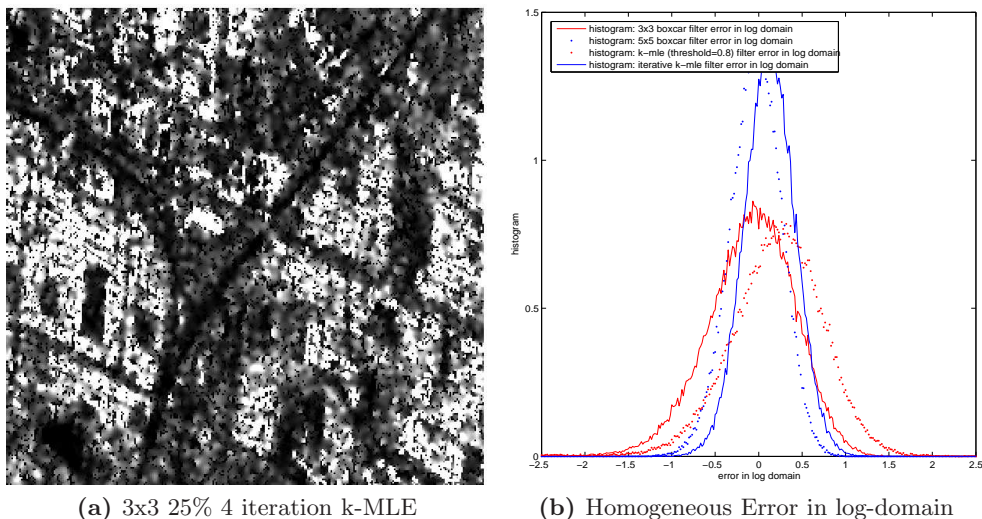


Figure 5.3: Improving Homogeneous error with iterative k-MLE filter

appears to have the best histogram response among the 3 filters compared.

5.1.2.3 Evaluation of the k-MLE speckle filter on Real Images

The k-MLE filters are also applied on a SLC RadarSat 2 image covering the Muada Merbok area of Malaysia. Fig. 5.5 shows the patches of original and filtered images of

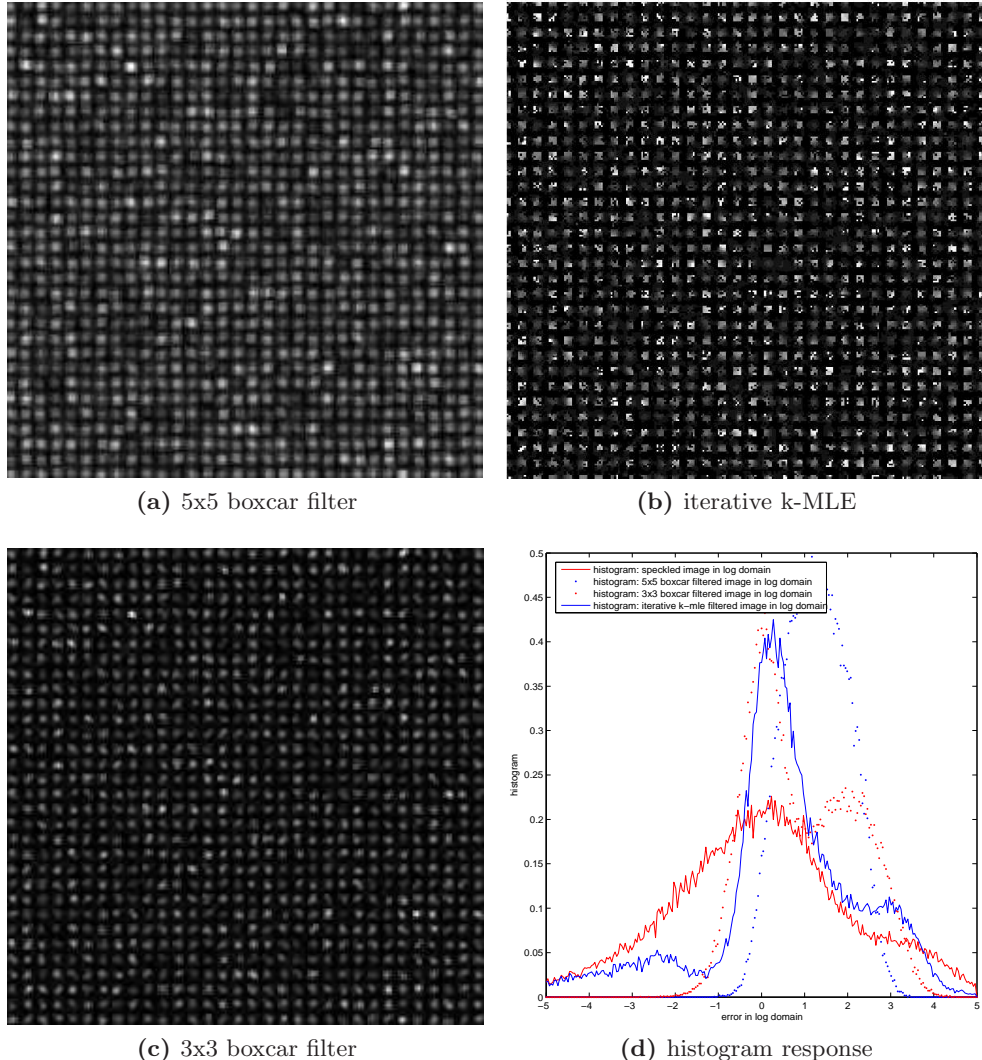


Figure 5.4: Qualitative evaluation on point targets

both natural and urban landscape. It is obvious that the k-MLE speckle filter delivers a significantly “better” image than the original data.

5.2 SAR Speckle filtering using the consistent measures

As mentioned earlier, speckle filters remove the stochastic noise by grouping data into homogeneous areas. In the boxcar filter, the filtering process can be described via Eqn.

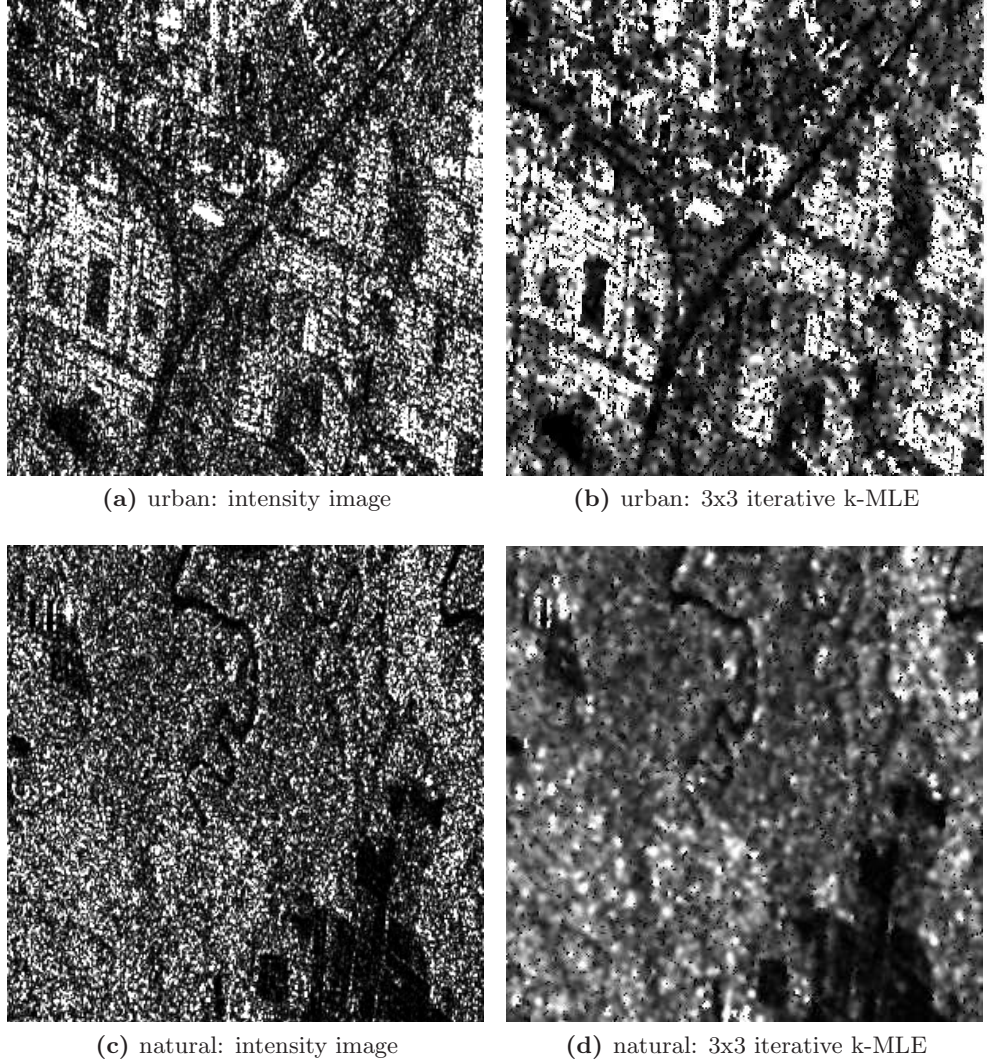


Figure 5.5: Qualitative evaluation on urban and agricultural areas

5.3, where I_i is the intensity value of pixel i and n is the total number of pixels in the surrounding areas. The implicit assumption for this filter is that ALL pixels in the surrounding area belongs to the same homogeneous area with the estimating central point. In the k-MLE filter presented in the previous section and in [88], the surrounding region is partitioned into homogeneous areas and the approximation is based on Eqn. 5.4, where I_i is the intensity value of pixel i and k is the total number of pixels in the

partitioned and homogeneous area covering the centre point.

$$f_{boxcar} = \sum_{i=1}^n I_i/n \quad (5.3)$$

$$f_{kMLE} = \sum_{i=1}^k I_i/k \quad (5.4)$$

While it appears logical to classify surrounding pixels as falling either inside or outside the same homogeneous area with the central point, the concept of “homogeneous area” lacks precise definition and boundaries. In fact, the classification decisions between homogeneity and heterogeneity are probabilistic in nature. This is evident in the statistical hypothesis testing used to support these decision makings [88].

In this section, a fuzzy logic approach is followed where, instead of fixing on a rigid two-member set of logical values (i.e. true and false), the system embraces truth values that range from 1 to 0. Thus instead of making a YES/NO decision on whether or not a data point is in the same homogeneous region as the estimated central point, a fuzzy probabilistic scale is calculated. Then the noise-removal impact of the surrounding data points will be scaled with this probability value. This fuzzy logic approach give rise to the f-MLE speckle filter presented next, and its main benefit is that: we no longer need to worry about the homogeneous / heterogeneous problem.

5.2.1 The f-MLE SAR Speckle Filters

The foundation of the fuzzy-estimation approach is the consistent sense of distance found in the log-transformed domain. The consistent measure of distance states that given two SAR intensity samples coming from the same background, their distance in the log transformed domain follows a fixed distribution according to Eqn. 3.24.

The base-2 log transformation is defined as: $L_I^i = \log_2(I^i)$ where I^i is the i^{th} intensity sample in the originally measured domain, L_I^i is the value of that sample in the log-transformed domain. The contrast is then defined as: $C = L_I^1 - L_I^2$. Assuming that I^i follows a negative exponential distribution [6], then this dissimilarity distance will follow the distribution $pdf(C) = \frac{2^C}{(1+2^C)^2} \ln 2$, which is consistent. This analysis is confirmed by real-life data validations (see [88]) and visually demonstrated in Fig. 5.6a.

5.2.1.1 f-MLE Estimation

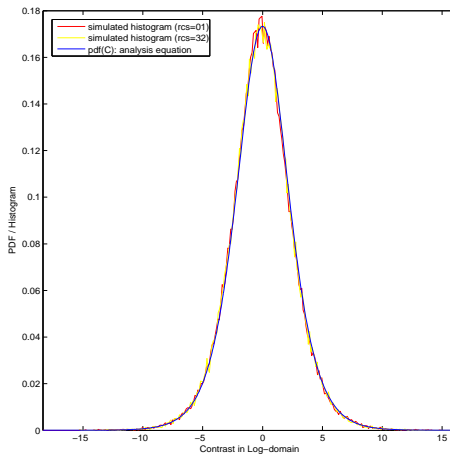
In this fuzzy logic approach, a pixel with intensity value I_i in the surrounding area of the centre point I_0 has a likelihood of being in the same homogeneous area given as: $p_i = \text{pdf}(C_i)$, with $C_i = \log_2(I_i) - \log_2(I_0)$. The f-MLE approximation is then proposed as written in Eqn. 5.5.

In implementing this statistical estimator, there are very noticeable black dots in the filtered output image. These dots can be explained by the long-tailed nature of the intensity PDF, which manifests itself in the significant existence of very small values in the population. In this all-inclusive scheme, there is a single $C_0 = 0$ (at I_0) in the middle of other very large $C_{i,(i>0)}$, which results in a single significant p_0 (at I_0), and other probably insignificant $p_{i,(i>0)}$. This marginalizes the filtering power of surrounding pixels. One way to counter this effect is to exclude the centre point I_0 from its estimation, which results in the exclusive scheme written in Eqn. 5.6.

$$FMLE_{incl} = \frac{\sum_{i=0}^n p_i * I_i}{\sum_{i=0}^n p_i} \quad (5.5)$$

$$FMLE_{excl} = \frac{\sum_{i=1}^n p_i * I_i}{\sum_{i=1}^n p_i} \quad (5.6)$$

For visualization and comparison purposes, both filtering schemes are applied to an simulated single-look homogeneous scene. The histogram of the filtered images are plotted in Fig. 5.7a and Fig. 5.7b, where the speckle suppression power is clearly visible. And it is apparent that the filtering performance of the excluding-centre-point scheme is at least as good as that of the centre-point-included scheme and the skewness in the histogram of the exclusive scheme is less than that of the inclusive estimation.



(a) Intensity histogram

Figure 5.6: Consistent Distance Property and the f-MLE Estimations

5.2.1.2 Preservation of Log-Distance Histogram Consistency

Fig. 5.7c and 5.7d plot the filtering treatment described above when applied on the inputs depicted in Fig. 5.7a. They clearly demonstrate that the f-MLE speckle filters preserve the consistent sense of distance. This can be explained from the consistent histogram of the input log distance PDF.

Unfortunately, the filtering formula given in Eqn. 5.5 and Eqn. 5.6, especially when applied to large image areas, involves a large number of random variables. This renders the task of deriving an analytical PDF expression impractical for the log-distance output. However, large scale computer simulations can be used to provide a usable histogram, from which a PDF can be estimated. Specifically, given a distance d , its corresponding probability $pdf(d)$ can be simulated by interpolating from the saved histogram $y \equiv hist(x)$ at the value of $x \equiv d$.

5.2.1.3 Recursively Applying The f-MLE Filters

The preservation of consistent distance property is the enabling factor that allows the recursive application of f-MLE filters. Additional execution of the filtering process is be expected to further reduce the random noise power / variance even further.

In subsequent application of the filtering algorithm, the main different when compared

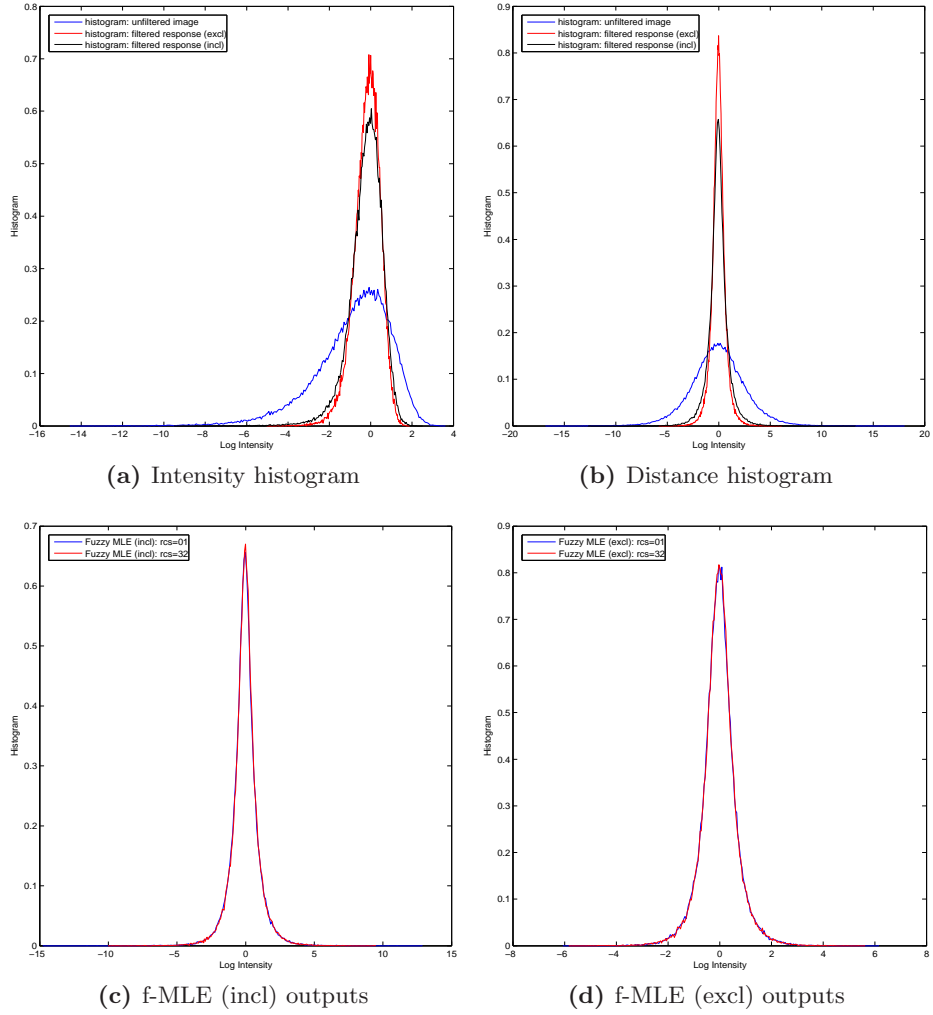


Figure 5.7: Consistent Distance Property and the f-MLE Estimations

with the initial iteration is the way the new fuzzy probabilities being calculated. This subsequent computation of fuzzy probabilities is based on the output distance PDF, whose computation process is described in the previous section. This process is repeated iteratively, with the histogram obtained from the previous iteration serves as the input fuzzy probability PDF in subsequent application of the filter. Fig. 5.8 illustrates the extra speckle suppression power of this scheme.

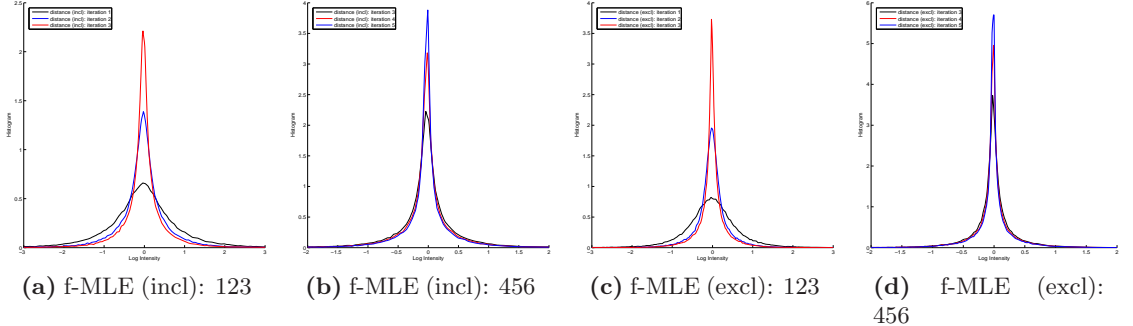


Figure 5.8: Iteratively Improving in Distance Histograms

5.2.2 Evaluating the f-MLE SAR speckle filters

The performance of speckle filters are normally evaluated based on a number of criteria [68]. The most widely used criteria is speckle suppression, which is often evaluated over homogeneous area. The other important criteria include radiometric preservation, something obviously desirable in the filtered output. In practical terms, the most common usage of speckle filtered imagery include target and feature detection and classification. In this section, the use of the ROC curve and the area under it as the statistical evidence of separability between target and clutter PDFs is briefly explored.

The performance of the f-MLE filter is evaluated both qualitatively against real images and quantitatively via simulated experiments. Let us start with a qualitative visual evaluation of the speckle filter on real-captured images.

5.2.2.1 Qualitative Evaluation on Real Images

The filters are applied to a SLC RadarSat 2 image covering the Muda Merbok area of Malaysia. Fig. 5.10 shows the patches of original and filtered images of both natural and urban landscape. The filtering effects are clearly visible. Apparently the second iteration outputs appears much better than the initial application. Furthermore, they offer roughly the same level of speckle suppression power in comparison to that of boxcar filter.

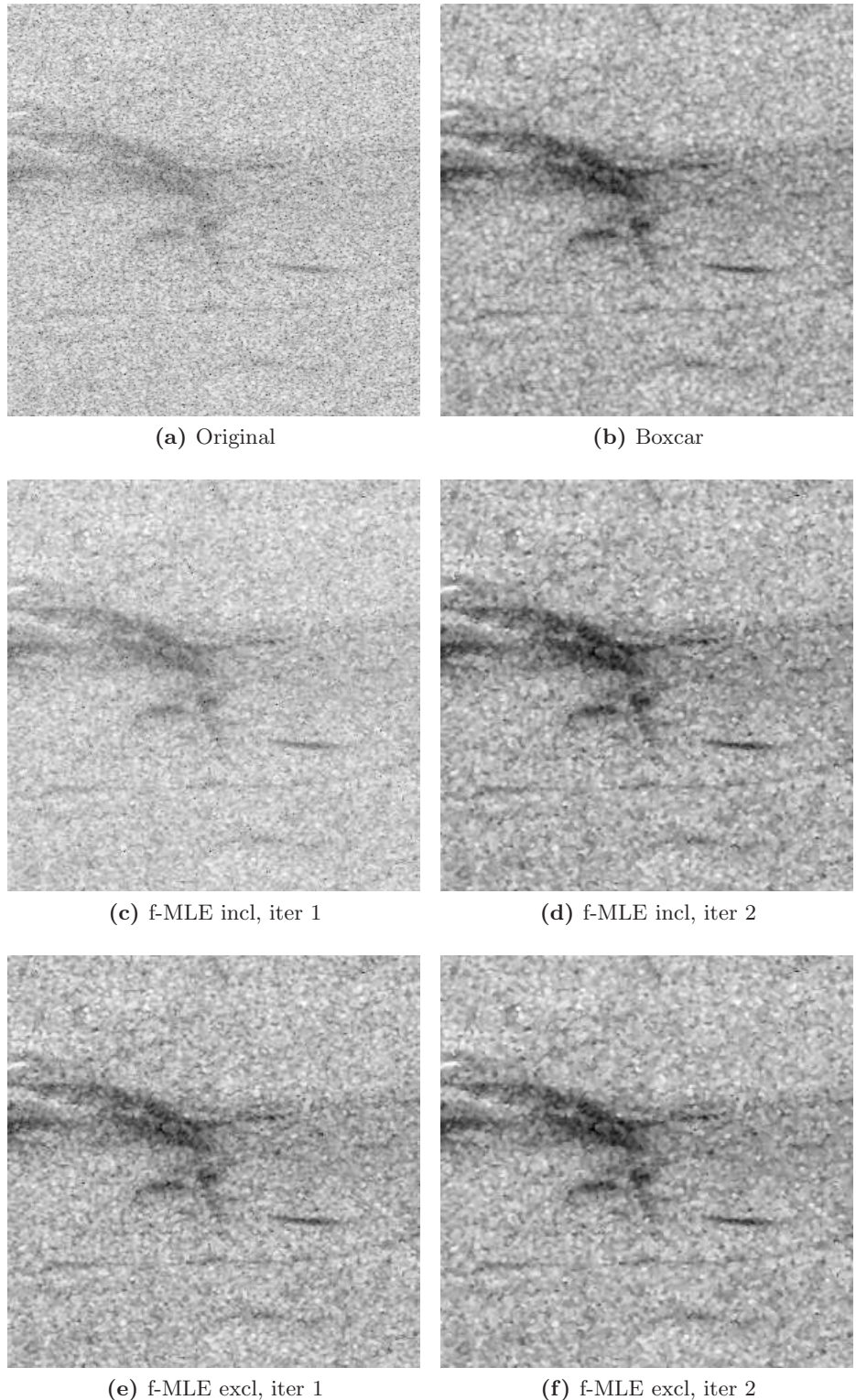


Figure 5.9: Qualitative Evaluation of f-MLE filter on Real Life Scene of Natural Surface

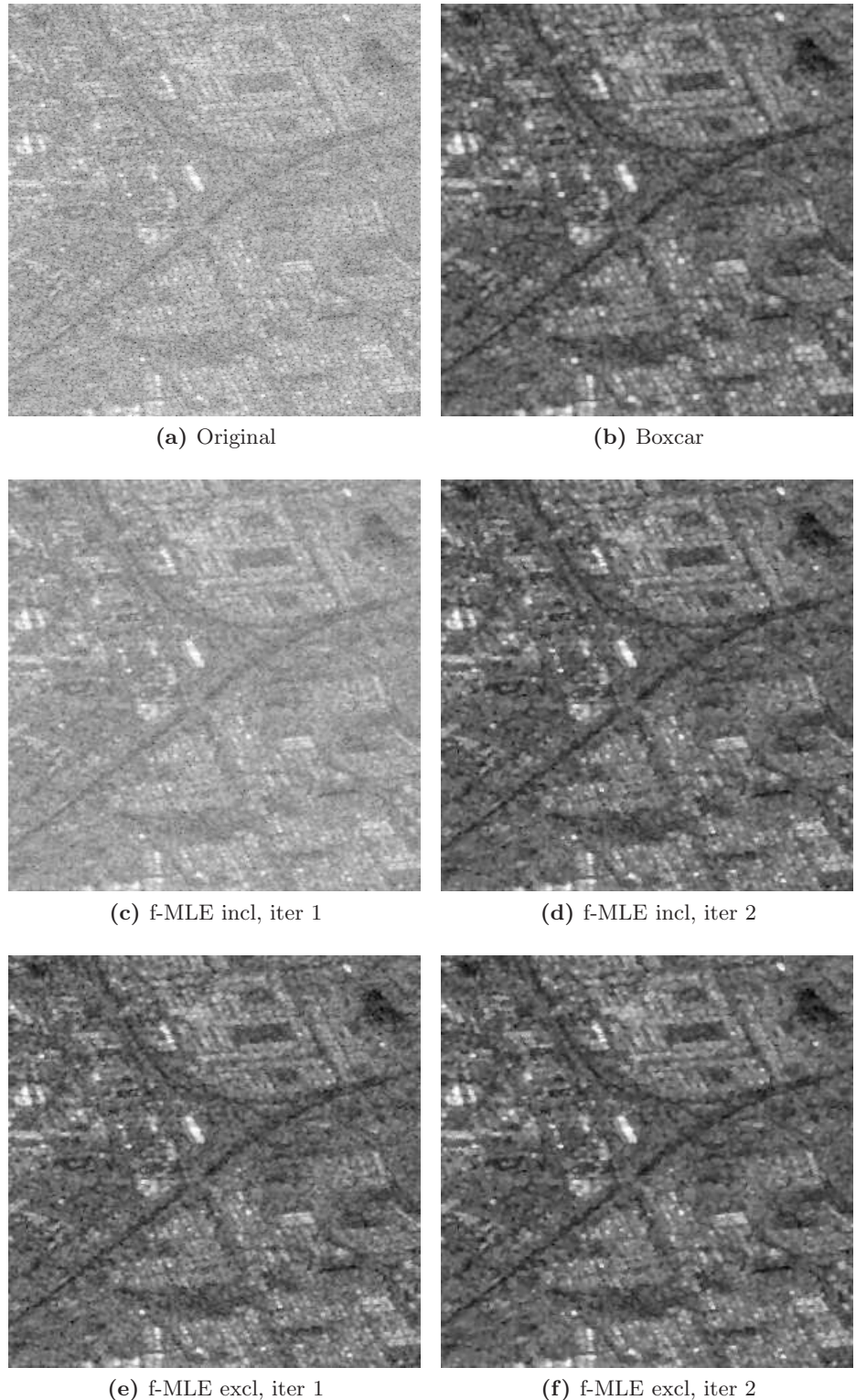


Figure 5.10: Qualitative Evaluation of f-MLE filter on Real Life Scene of Urban Landscape

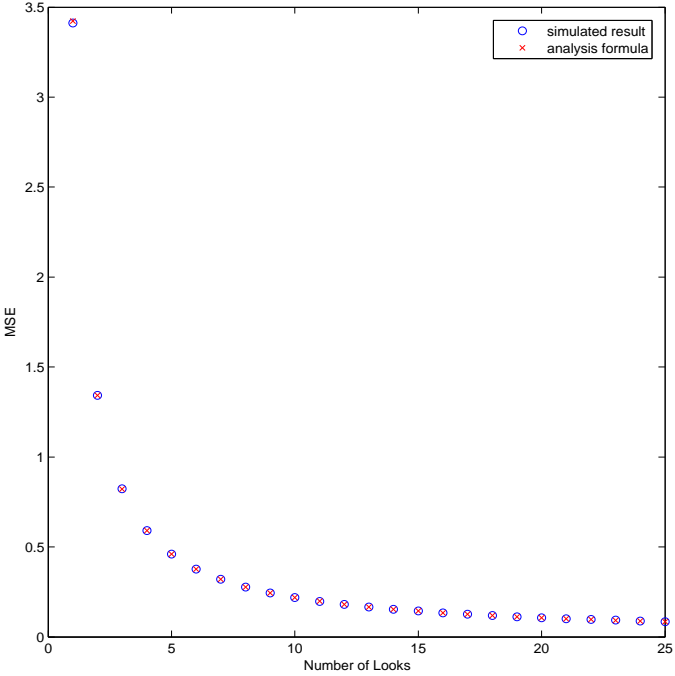


Figure 5.11: MSE in the log-transformed domain is related to the ENL index

5.2.2.2 Evaluating Speckle Suppression Effects

We have found that variance in the log-transformed domain is related to the standard Equivalent Number of Looks value. Deriving from the results of [94] and [95], the formula is given as: $MSE = \frac{1}{(ENL-0.5)\ln^2(2)}$. Fig. 5.11 demonstrates the relationship. The use of iterative Fuzzy MLE estimations allows further suppression of speckle. This is illustrated with “tighter” distance histograms and reducing MSE, as plotted in Fig. 5.12

5.2.2.3 Evaluating Target Detection Performance

The normal application after applying filters on SAR images is to detect the existence of certain target within its surrounding clutters or other similar classification / discrimination tasks. The most common type of detector (or classifier) employs a threshold based approach in determining whether an abnormal value signifies the existence of a target. The Receiver Characteristic Curve (ROC) and the area under it (AUC) is typically used to evaluate the detectability of target features [96].

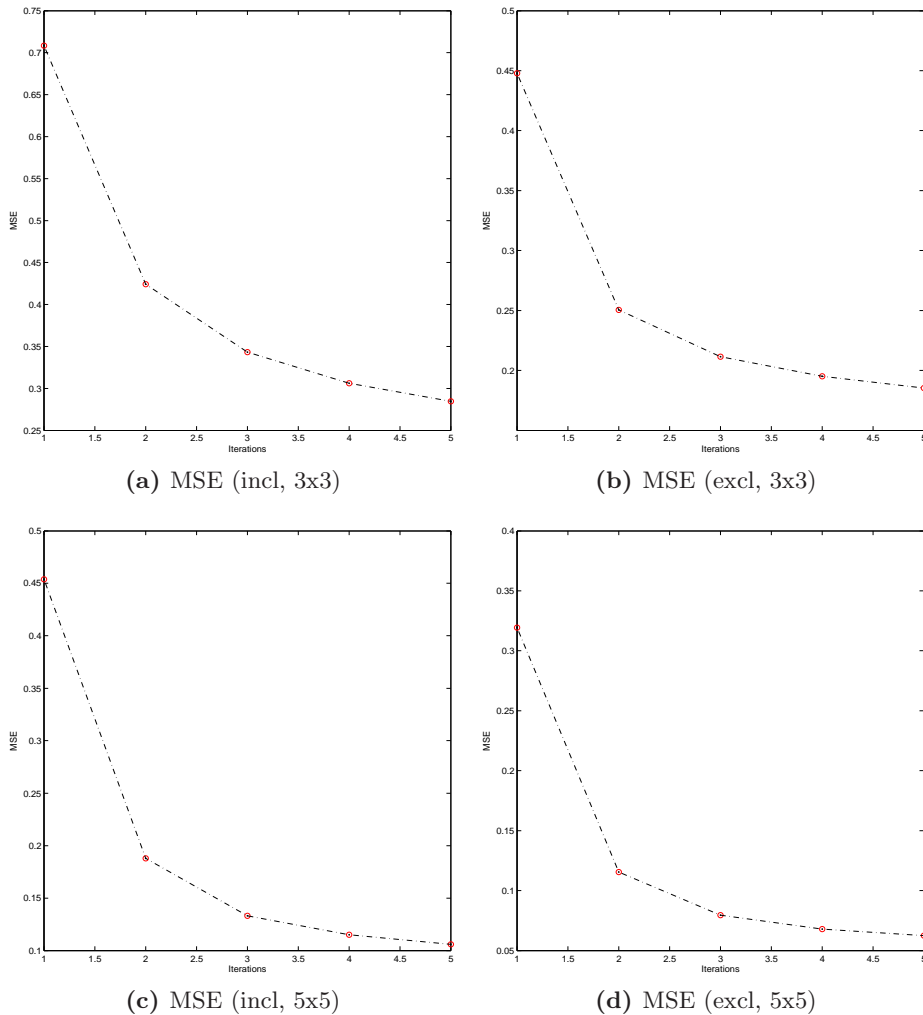


Figure 5.12: Homogeneous Area: MSE criteria and speckle suppression power of f-MLE filters

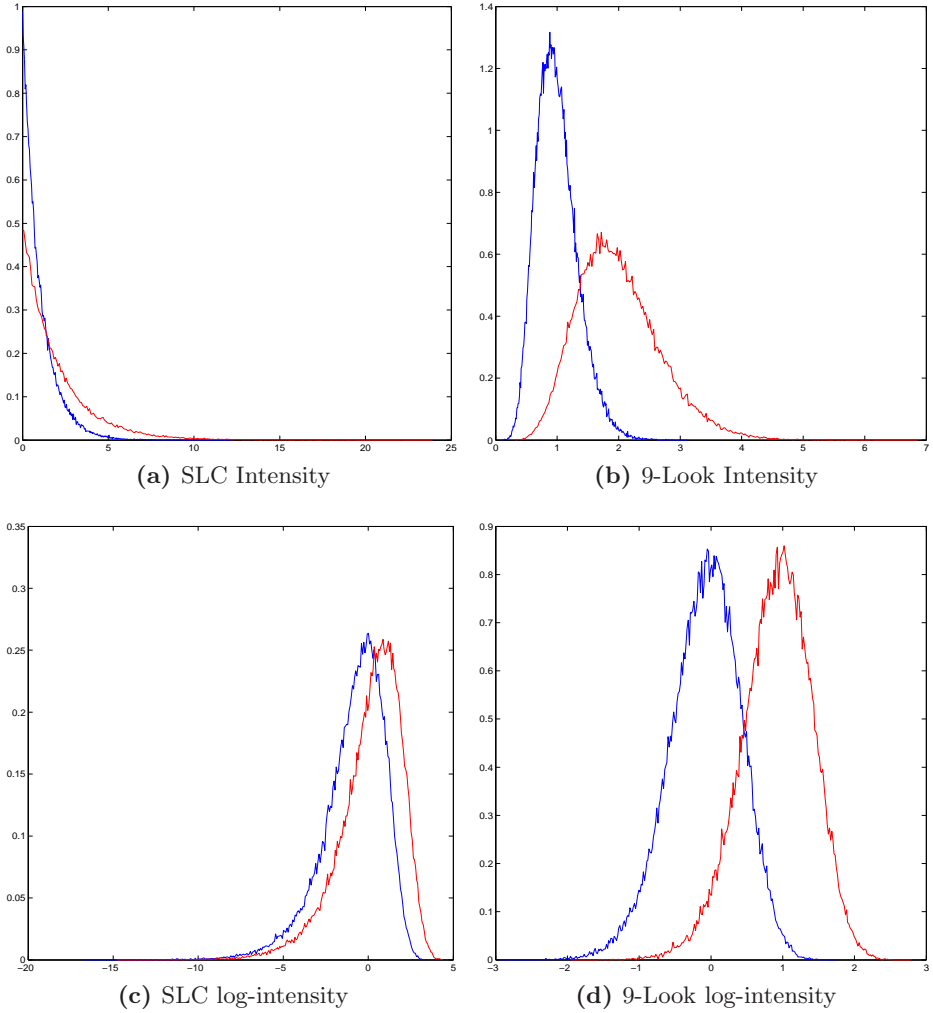


Figure 5.13: Histogram discriminability and the ROC Curve

It is normally claimed that applying speckle filters increases the performance of subsequent target detection tasks. The following experiment illustrates this point. In this experiment, we apply a simple 3×3 boxcar filter to two different homogeneous and SLC noise corrupted scenes that are known to be 3dB apart. And then the histograms as well as the resulting ROC curve are plotted between the pairs of target and background histogram for both cases of unfiltered and filtered data. We note that the ROC curve for the histograms in original domain matches perfectly with the ROC for the histograms in the log-transformed domain (see Fig. 5.13), as expected from theory.

The most common types of target to be detected in image processing are point targets,

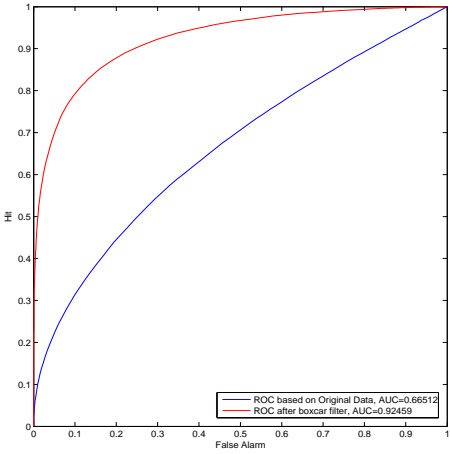
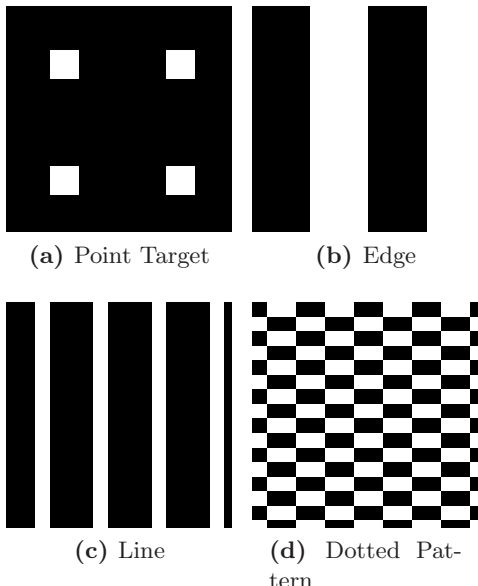


Figure 5.14: Invariant ROC Curve

line targets, and edge targets. The detectability of these targets are measured using the AUC index which is tabulated against the MSE. Fig. 5.15 illustrates the evaluation result in benchmarking the performance of f-MLE filters for artificially-generated heterogenous test regions. Apparently the f-MLE filters have better performance than boxcar filters. Also noticeable is the correlation between MSE and the Area Under the ROC curve criteria, which is an interesting phenomena that will be investigated further in the next section.



Scene	Filter	MSE	AUC
Point Target	f-MLE (incl, 3x3)	1.38	0.901
Point Target	f-MLE (excl, 3x3)	1.47	0.893
Point Target	boxcar (3x3)	1.56	0.826
Point Target	boxcar (5x5)	2.67	0.502
Edge	f-MLE (incl, 3x3)	0.68	0.969
Edge	f-MLE (excl, 3x3)	0.73	0.964
Edge	boxcar (3x3)	1.03	0.942
Edge	boxcar (5x5)	1.51	0.934
Line	f-MLE (incl, 3x3)	1.89	0.791
Line	f-MLE (excl, 3x3)	2.02	0.767
Line	boxcar (3x3)	2.27	0.658
Line	boxcar (5x5)	2.88	0.375
Dotted	f-MLE (incl, 3x3)	2.28	0.639
Dotted	f-MLE (excl, 3x3)	2.32	0.621
Dotted	boxcar (3x3)	2.92	0.431
Dotted	boxcar (5x5)	3.35	0.382

Figure 5.15: Heterogeneous Patterns: MSE criteria and f-MLE performance

5.2.2.4 Summary

The nature of SAR speckle is stochastic. The speckle filtering problem has been cast into a statistical estimation theory framework. Speckle filtering, by and large, means the removal of stochastic components from SAR images. Log-transformation is shown to provide homoskedasticity in statistical models. Using speckle filtering as an application example, these homoskedastic features are shown to be useful.

The log-transformed domain provides a consistent sense of distance. By embracing a probabilistic approach, the proposed Fuzzy Maximum Likelihood Estimator makes use of this consistency. Experimental results suggest that the estimator output also exhibits this consistency property, which allows recursive application of the filter discussed above.

The speckle filtering technique proposed here has been shown to work for single-look SAR images. Multi-look processed image speckle filtering should be possible to use this technique with some minor adaptations. The f-MLE approach is developed from an easy to understand winner-take-all k-MLE clustering approach. With the fuzziness be taken to a new level, fuzzy probabilistic speckle filters which requires no clustering have been specified and designed.

The filter is rigorously evaluated. Over homogeneous regions, the speckle suppression power is evaluated by measuring the ubiquitous MSE on simulated and truth-grounded experiments. The results suggest that by applying the estimation recursively, this value can be reduced arbitrarily low, assuming that the number of iterations, and hence the available computational power, is sufficiently large. For heterogeneous scenes, the robust Area Under the ROC Curve criteria is used as statistical evidence for better performance in the subsequent tasks of target detection and surface classification. Experiments confirm the power of f-MLE filters in various heterogeneously simulated areas. A good correlation between the MSE and the AUC index is also exhibited. The result suggests that lower MSE achievable by f-MLE filters does lead to better performance in the subsequent tasks of target detection and classification.

5.3 Evaluating SAR Speckle Filters using the consistent measures of distance

The nature of SAR speckle is that it is stochastic even if the underlying radiometry is constant. And when there is spatial radiometric variation, not only its expected value changes, but its heteroskedastic variance changes as well. Nevertheless, statistical models have been developed to derive the underlying back-scattering coefficient (σ) from measured SAR data. As such, speckle filters are, by and large, estimators that attempt to determine this unknown coefficient from observable SAR data.

SAR speckle-filtering can be, and has been, positioned within the context of estimation theory [83]. The stages in this statistical framework consist of statistical modelling, estimator development and evaluation of the estimators' performance. Estimators are typically evaluated based on the bias and variance properties of their estimates: with lower bias and/or lower variance lead to lower MSE, which then indicates better accuracy. Ideally, the evaluation of SAR speckle filters' performance should be based both qualitatively on some real data and quantitatively through simulated experiments. In addition, due to the stochastic nature of SAR-processing, and its simulating process, statistical summaries of repeatedly-simulated experiments are preferred to single-run results.

However, current SAR speckle filter performance evaluations uses a different approach from the standard practice of the statistical estimation framework. Due to the multiplicative and heteroskedastic nature of speckle noise, bias and variance evaluation would not be the most useful measures. Thus, the standard evaluation metric of mean-squared-error is not easily applicable, prompting alternative evaluation criteria to be proposed. Although there are alternative evaluation criteria being proposed, there is currently no single universally agreed quantitative metric for the performance of speckle filters.

Most commonly, each newly proposed speckle filter tends to be published along with its own methodology for evaluating its performance. As such, many papers lack a comparative basis beyond simple visual qualitative comparison on a few image scenes. While such visual comparison is useful, as an evaluative methodology, regrettably it lacks scientific objectivity. Some papers do present quantitative measurements. However, due to the lack of a standardized performance criteria, the evaluation metrics can change significantly from one paper to the next.

To do quantitative evaluation of different speckle filters, it is necessary to compare a filtered result with a ground-truth image. Furthermore, it is desirable that the error, i.e. the difference between the filtered output and the original input, should be consistent and independent to the particular simulated scenario.

In general, the measure of difference for evaluation should be based on the original SAR intensity or amplitude domain. However owing to the additive and homoskedastic effects of the log-transformation, the error measured in the log-transformed domain is preferred here. This is because homoskedasticity would allow the use of standard Minimum Squared Error as a performance index. In this section, the use of MSE in the homoskedastic log-transformed domain to evaluate SAR speckle filters is proposed and validated.

5.3.1 Speckle Filtering Process And The Homoskedastic Log-transformed Domain

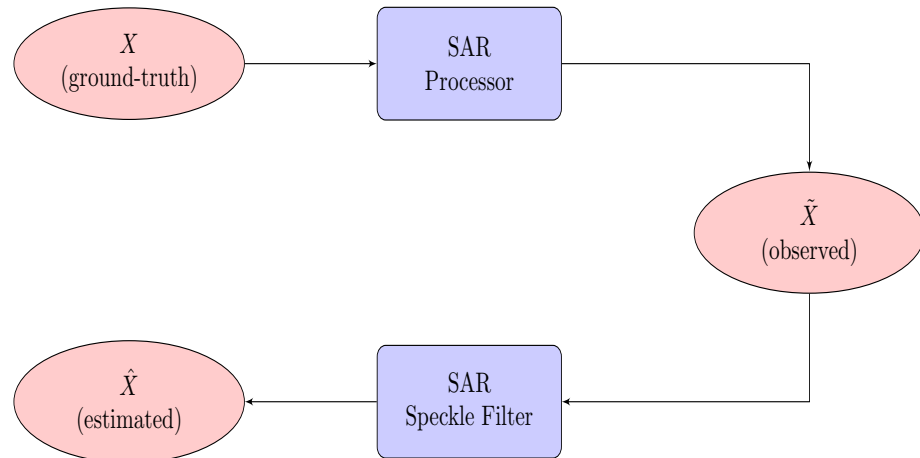


Figure 5.16: SAR simulation, processing and filtering schema

Fig. 5.16 illustrates the general schema of SAR simulation / processing and SAR speckle filtering process. There are two approaches that can be used to implement the indicated “SAR processor” block. First is the normal process of SAR processing where the unknown ground radiometric attribute (X) is recorded in \tilde{X} . Second is the simulation process where the noisy SAR data \tilde{X} is simulated from a known ground-truth pattern X .

The “SAR Speckle Filter” block indicates the speckle filtering process, which takes

the noisy speckled SAR data \tilde{X} as input and outputs \hat{X} as a better estimation of the ground-truth (i.e. X). The speckle filters employed in this section include: the boxcar filter, the enhanced Lee filter, the enhanced Kuan filter, the enhanced Frost filter, the Gamma Map filter and the PDE filter [97].

Logarithmic transformation offers several consistent measures of distance, which is hypothesized to be significant in evaluating speckle filters. A case in point is in visual evaluation of filtered results obtained from real captured SAR images. Since the radiometric ground-truth is not available, the most common way to evaluate speckle filters then is by qualitative visual evaluation. A conventional method is to investigate the ratio images between the filtered output and the noisy input images. Since logarithmic transformation converts these ratio into subtractive residual which are consistent, residual analysis can be used to analyse and evaluate the performance of speckle filters. The benefit of using log-residual over original-ratio is that the additive and homoskedastic nature of the log-residual signal fits better with the digital nature of imagery visualization.

For visual comparison, Fig. 5.17 depicts the residual image in the log-transformed domain and the ratio images in the original domain, where a simple boxcar filter has been applied to data obtained from a real RADARSAT SAR image. “Visible” structure appears to be more easily discernable in the log-2 residual random pictures than in the ratio images, although this conclusion is of course itself a subjective one.

$$MSE_{true} = E \left[(\hat{X}^L - X^L)^2 \right] \quad (5.7a)$$

$$MSE_{base} = E \left[(\tilde{X}^L - X^L)^2 \right] \quad (5.7b)$$

$$MSE_{noise} = MSE_{residual} = E \left[(\hat{X}^L - \tilde{X}^L)^2 \right] \quad (5.7c)$$

$$MSE_{benchmark} = |MSE_{residual} - MSE_{base}| \quad (5.7d)$$

Compared to qualitative visual evaluation which is subjective by nature, quantitative measurements are more objective and hence are usually preferred. In quantitative evaluation, it is important that the quantitative metric is computable and relevant. Different metrics to evaluate speckle filters, which will be investigated in subsequent sections, are given in Eqns. 5.7, all in the log-transformed domain. When the ground-truth is available, either in simulated experiments or over homogeneous areas where

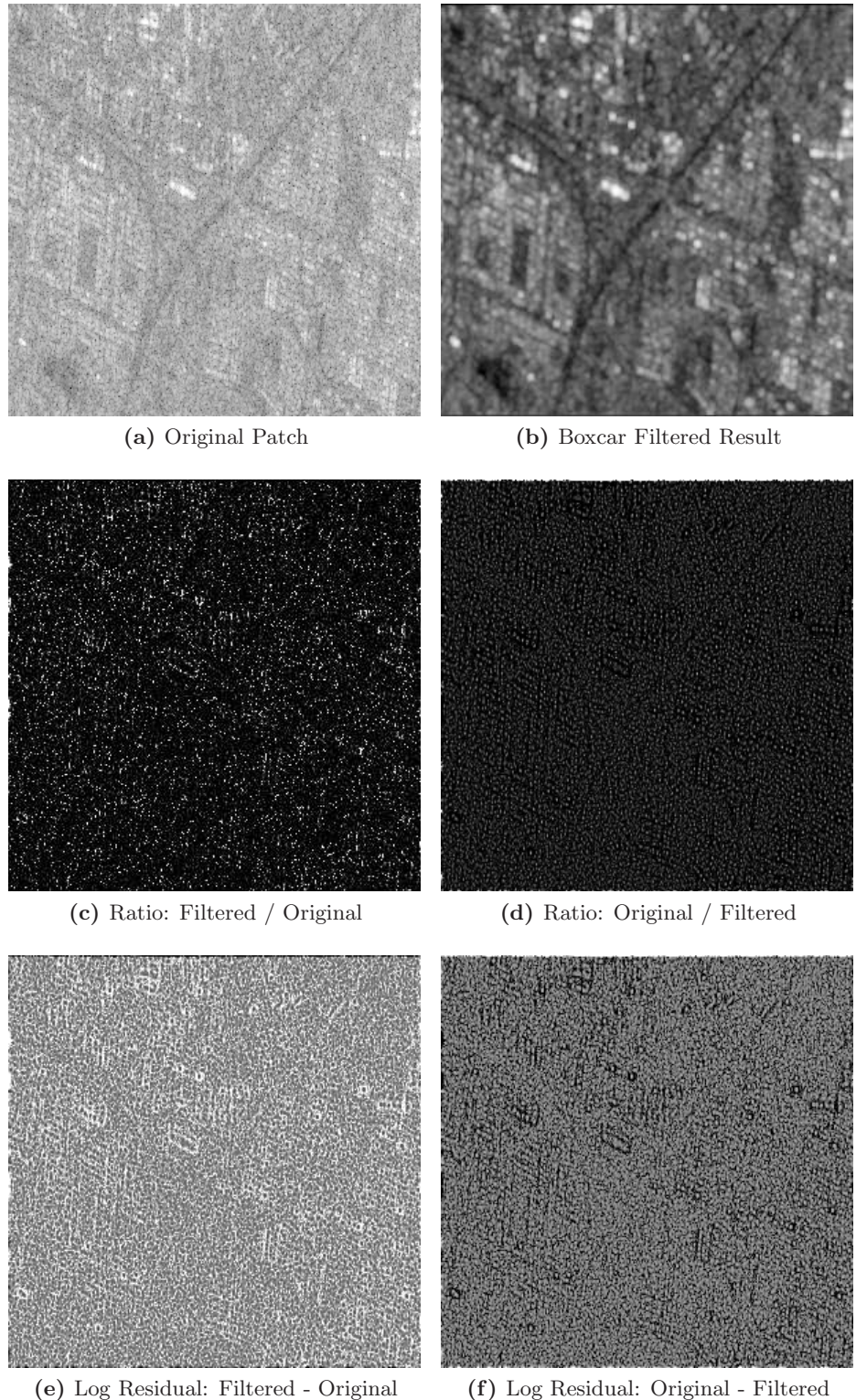


Figure 5.17: Visualising Removed “Noise”: Ratio images in the original domain vs. Residual images in the log-transformed domain

it can be reasonably estimated, true MSE is the expected squared error between the estimated and true values.

However, in real captured SAR images where such ground truth is unknown, the evaluation can only be carried out through a benchmarked MSE. The idea is that since both the speckled values and the estimated values are available, the residual MSE_{noise} can be computed, which can be thought of as the level of noise being removed by a speckle filtering process. Even as the ground-truth is not known in real SAR images, their speckle level (i.e. ENL) may be known or can be estimated reasonably well. Thus the base MSE level, which is also a measure of the speckle noise level, can also be estimated. Naturally, while the speckle filter should remove as much noise as possible, it also should not remove more variations than that caused by the speckle noise. That is, MSE_{noise} should track the base MSE as close as possible, making the $MSE_{benchmark}$ as close to 0 as possible.

5.3.2 Evaluating SAR Speckle Filters Over Homogeneous Areas

In this section, a methodology to evaluate speckle filters over homogeneous areas in the log-transformed domain is illustrated. Under the condition of homogeneity, speckle filters are supposed to estimate with negligible bias. Then the filters are traditionally compared by measuring their speckle suppression power using the ENL index. Consequently, in the log-transformed domain, the first component of MSE evaluation (i.e. bias evaluation) is probably insignificant in comparison to the other components, namely, variance evaluation. The next section will give a theoretical justification for our methodology where variance methods of evaluation are shown to be mathematically related to the ENL index. over homogeneous areas.

5.3.2.1 Estimating ENL from the log-variance index in homogeneous areas

Let us consider the multi-look processing effect in the log-transformed domain. Hoekmen [94] and Xie et. al. [98] have given the variance for L-look log-transformed random variables as:

$$var(\hat{X}^L) = \frac{1}{\ln^2(2)} \left(\frac{\pi^2}{6} - \sum_{i=1}^{L-1} \frac{1}{i^2} \right).$$

Based on the Euler proof for the Basel problem, we have

$$\frac{\pi^2}{6} = \sum_{i=1}^{\infty} \frac{1}{i^2}$$

then:

$$var(Y^L) = \frac{1}{\ln^2(2)} \left(\sum_{i=L}^{\infty} \frac{1}{i^2} \right)$$

Noting that:

$$\frac{1}{i} - \frac{1}{i+1} = \frac{1}{i(i+1)} < \frac{1}{i^2} < \frac{1}{i(i-1)} = \frac{1}{i-1} - \frac{1}{i}$$

then:

$$\frac{1}{L} - \frac{1}{\infty} < \sum_{i=L}^{\infty} \frac{1}{i^2} < \frac{1}{L-1} - \frac{1}{\infty}$$

In fact, we could estimate:

$$var(\hat{X}^L) = \frac{1}{(L-0.5)\ln^2(2)} \quad (5.8)$$

Thus the ENL, i.e. L , can be estimated as:

$$\hat{L}_{est} = \frac{1}{var(\hat{X}^L)\ln^2(2)} + 0.5 \quad (5.9)$$

The above analysis can be verified experimentally as follows. First, a 512×512 homogeneous area is generated and corrupted with single look SAR-speckle PDF. Different multi-look processing filters are then applied to the image patch. The observable variance in the log-transformed domain is recorded, and ENL is then estimated from Eqn. 5.9 for each simulation. This simulation is performed multiple times. The results in terms of mean and standard deviation are consolidated in Table 5.1. The theoretical variances are calculated from Equation 5.3.2.1, together with the analytical values from Eqn. 5.8. These experimental results evidently validate the analysis given above. They also show that while the approximation in Eqn. 5.9 may not be perfect, since ENL is supposed to be an integer, the value obtained actually corresponds very closely with the nearest correct integer result.

The relationship proposed here may also help to unite other seemingly unrelated results.

ENL	Var (Theory)	Var (Analysis)	Var (Observed)	\hat{L}_{est}
2	1.3423	1.3876	1.3452 (0.0031)	2.047 (0.0036)
3	0.8221	0.8326	0.8191 (4.2e-5)	3.041 (0.0001)
4	0.5907	0.5947	0.5941 (0.0059)	4.004 (0.0351)
5	0.4607	0.4625	0.4622 (0.0010)	5.003 (0.0099)
6	0.3774	0.3784	0.3800 (0.0009)	5.977 (0.0131)
7	0.3196	0.3202	0.3188 (0.0037)	7.029 (0.0769)
8	0.2771	0.2775	0.2786 (0.0002)	7.970 (0.0065)
9	0.2446	0.2449	0.2455 (0.0007)	8.979 (0.0244)
10	0.2189	0.2191	0.2183 (0.0012)	10.035 (0.0538)
11	0.1981	0.1982	0.1975 (0.0001)	11.038 (0.0063)
12	0.1809	0.1809	0.1810 (0.0022)	12.001 (0.1419)
13	0.1664	0.1665	0.1661 (0.0002)	13.031 (0.0191)
14	0.1541	0.1542	0.1534 (0.0016)	14.068 (0.1387)
15	0.1435	0.1435	0.1432 (0.0019)	15.036 (0.1967)
16	0.1342	0.1343	0.1342 (0.0009)	16.006 (0.0987)
17	0.1261	0.1261	0.1249 (0.0005)	17.159 (0.0636)
18	0.1189	0.1189	0.1192 (0.0010)	17.959 (0.1406)
19	0.1125	0.1125	0.1126 (0.0004)	18.976 (0.0788)
20	0.1067	0.1067	0.1074 (0.0005)	19.889 (0.0937)
21	0.1015	0.1015	0.1017 (0.0002)	20.975 (0.0357)
22	0.0968	0.0968	0.0970 (0.0002)	21.952 (0.0337)
23	0.0925	0.0925	0.0924 (0.0006)	23.027 (0.1386)
24	0.0886	0.0886	0.0887 (0.0002)	23.957 (0.0507)
25	0.0849	0.0849	0.0846 (0.0007)	25.094 (0.1934)

Table 5.1: Speckle Suppression Power: ENL and Variance

For example, Solbo [99] used standard deviation in the log-transformed domain to measure homogeneity, while Lopes [86] proposed the use of variation co-efficient index $C_v = std(I)/avg(I)$ to evaluate scene heterogeneity.

5.3.2.2 Using MSE criteria to evaluate speckle filters

Over an homogeneous area, the ground-truth is unchanged, i.e. $X_i^L = X^L \forall i$. Assuming the filters achieve negligible bias, i.e. $E(\hat{X}^L) = X^L$, then the MSE evaluation is reduced to variance evaluation. Since the log-variance is related to the ENL, this evaluation approach is equivalent the established ENL evaluation methodology. In fact, a few more observations and analysis can be carried out as follows.

Fig. 5.18 plots the histograms of homogeneous SAR data over different radiometric

values. Both single-look simulated and multi-look processed/box-car filtered data is displayed. Specifically the plots show that the log-transformed domain is consistent, i.e. they retain similar shapes regardless of the underlying signal value, while the plots from the original domain are not.

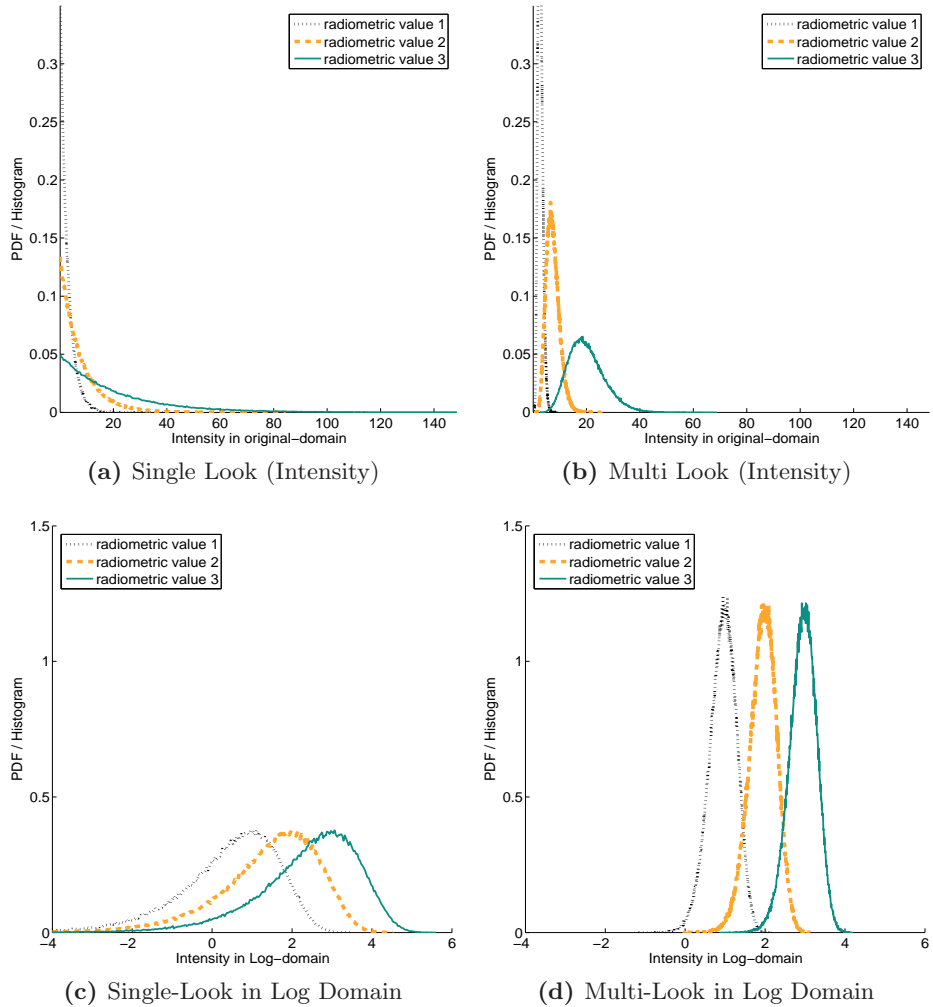


Figure 5.18: The Inconsistency evident in the original SAR domain and the Emerged Consistency demonstrated in the log-transformed domain

Fig. 5.19 shows that all of the standard filters (Lee, Kuan, Frost and Gamma MAP) preserve this consistency in their filtered output. Intuitively, as the boxcar filter is actually similar to multi-look processing, its output also exhibits this consistency. The preservation of this consistent property is important in evaluating SAR speckle filters as it leads to the consistent sense of distance, contrast and variance described earlier.

It also ensures applicability of various target detection/classification algorithms which employ statistical properties in the unfiltered data, such as the ratio based discriminator in the original domain or the differential based discriminator in the log-transformed domain. The consistent log-variance also leads to consistent and thus reliable ENL evaluation, regardless of the underlying radiometric value.

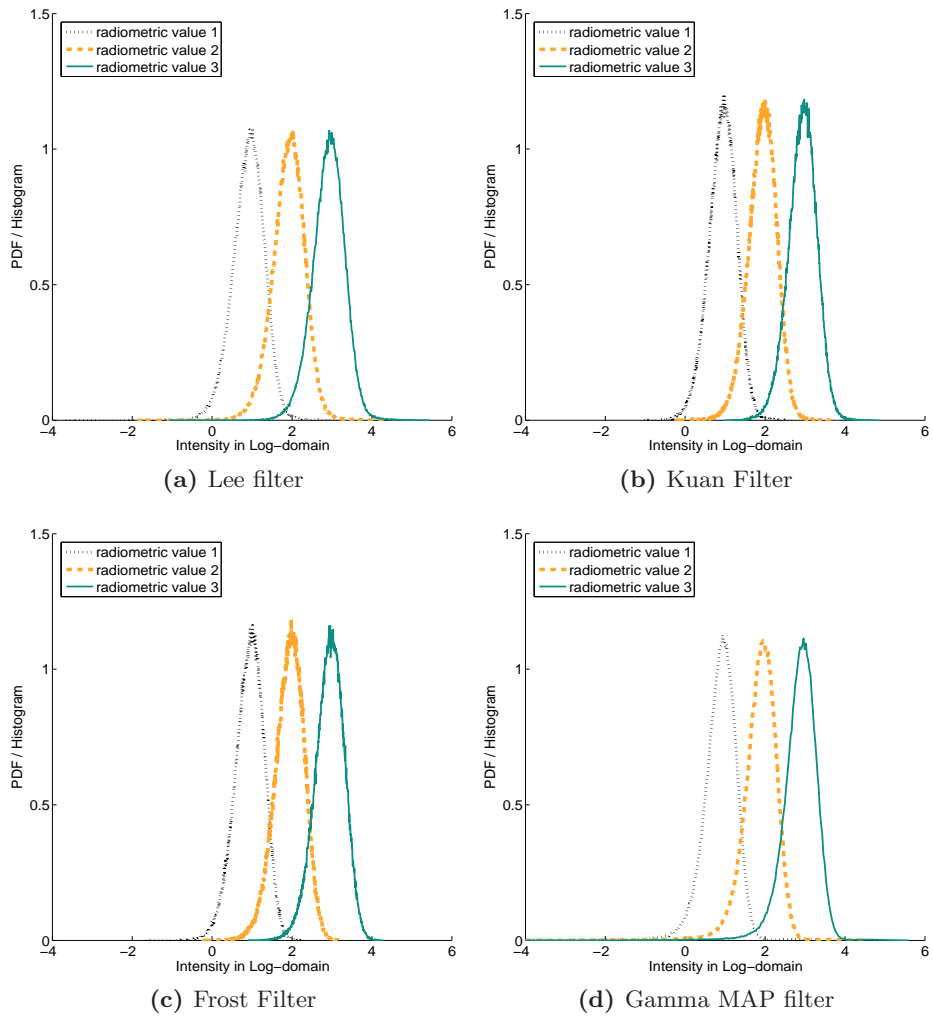


Figure 5.19: Filtered results: consistency in log-transformed domain

Table 5.2 provides a quantitative comparison among the filters. It shows that the filters can all preserve the underlying radiometric values, while their speckle suppression power can be equivalently measured using either variance in the log-transformed domain, or the standard ENL index.

Filter	Set	Log-Variance	\hat{L}_{est}	Avg Intensity
none	1	3.4149 (0.0003)	1.1095 (5.8e-5)	3.4795 (0.0029)
pde	1	1.2674 (0.0014)	2.1423 (0.0018)	3.4806 (0.0029)
map	1	1.2651 (0.0055)	2.1454 (0.0072)	3.1627 (0.0002)
lee	1	0.4604 (0.0027)	5.0206 (0.0268)	3.4835 (0.0022)
kuan	1	0.2979 (0.0024)	7.4864 (0.0574)	3.4748 (0.0054)
frost	1	0.2852 (0.0012)	7.7975 (0.0299)	3.4799 (0.0027)
boxcar	1	0.2513 (0.0011)	8.7819 (0.0353)	3.4799 (0.0027)
none	2	3.4191 (0.0068)	1.1088 (0.0012)	9.4925 (0.0049)
pde	2	1.6071 (0.0026)	1.7952 (0.0021)	9.4930 (0.0048)
map	2	1.2646 (0.0023)	2.1459 (0.0029)	8.6091 (0.0162)
lee	2	0.4653 (0.0026)	4.9731 (0.0254)	9.4936 (0.0080)
kuan	2	0.2999 (0.0026)	7.4391 (0.0602)	9.4761 (0.0014)
frost	2	0.2867 (0.0005)	7.7595 (0.0128)	9.4912 (0.0039)
boxcar	2	0.2532 (0.0006)	8.7203 (0.0193)	9.4914 (0.0040)
none	3	3.4203 (0.0187)	1.1068 (0.0033)	25.6234 (0.0389)
pde	3	2.0353 (0.0021)	1.5226 (0.0010)	25.6236 (0.0389)
map	3	1.2799 (0.0091)	2.1263 (0.0116)	23.2628 (0.0304)
lee	3	0.4633 (2.4e-5)	4.9926 (0.0002)	25.6406 (0.0488)
kuan	3	0.2964 (0.0010)	7.5225 (0.0244)	25.6112 (0.0226)
frost	3	0.2862 (0.0008)	7.7714 (0.0202)	25.6263 (0.0409)
boxcar	3	0.2529 (0.0005)	8.7296 (0.0178)	25.6261 (0.0407)

Table 5.2: Performance of various filters over homogeneous areas

5.3.3 Evaluating SAR Speckle Filters over Heterogeneous Scenes

From a statistical estimation framework point of view, the use of MSE to evaluate statistical estimators is natural. In this section, the MSE criteria (MSE_{true}) in the log-transformed domain is validated through experiments and analysis.

The test patterns used in this section include the following pattern: point targets, line targets, edge targets and a heterogeneous checker board. These test patterns could of course be concatenated into a larger composite test image, although they will be considered separately to allow easier analysis of the results. Each pattern comprises two classes of ground-truth: background and target areas, with the target signified by the brighter area of the image as conventionally used in the radar community. Fig 5.20 shows a small section (32×32 window) of each pattern.

Large patches of these patterns (512×512) are first corrupted with single look speckle. The speckle filters are then applied onto these noised images. Since the filters are

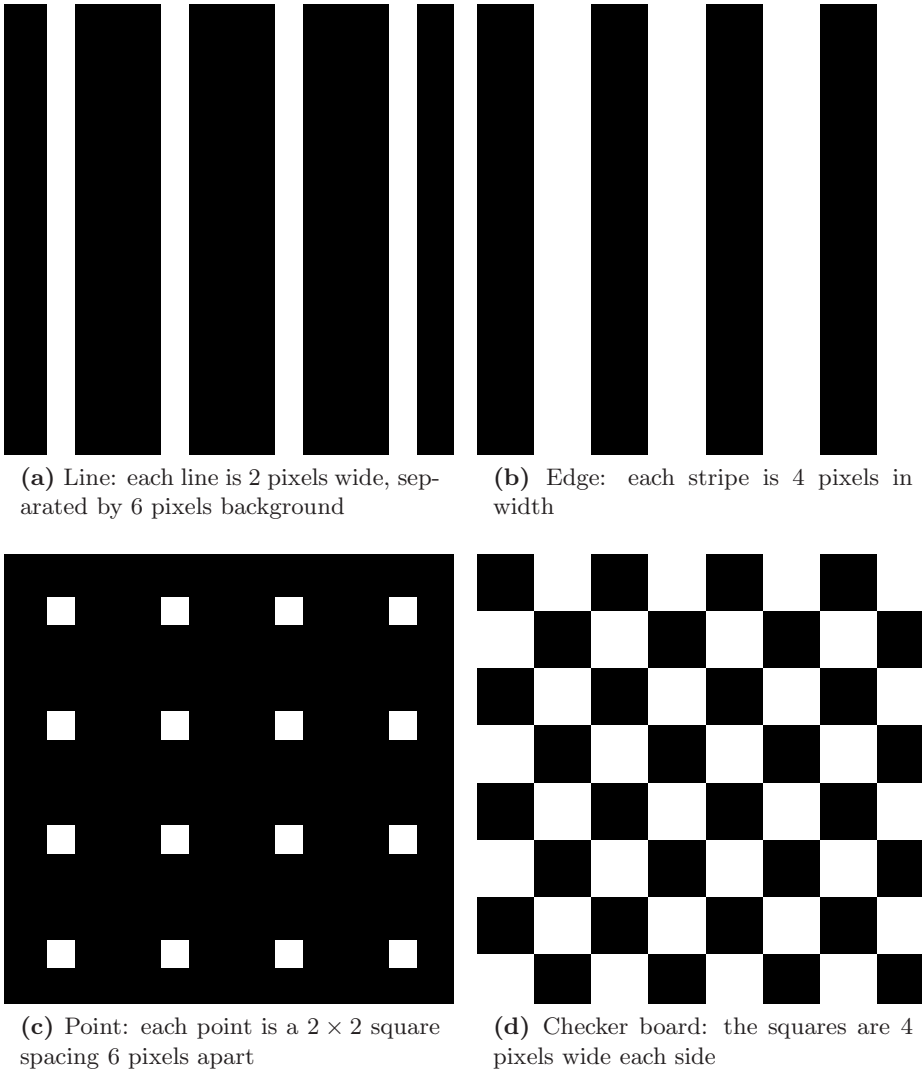
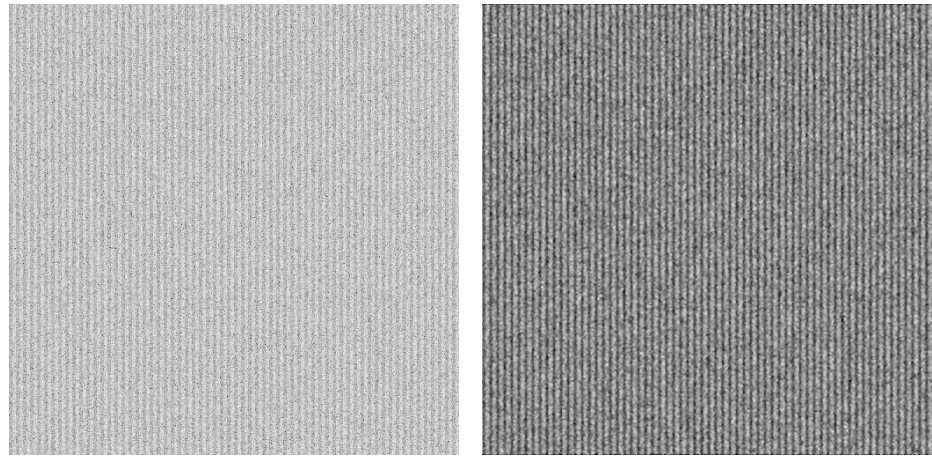


Figure 5.20: Example windows of ground truth patterns, each 32×32 pixels in size.

expected to be consistently behaved in the log-transformed domain, as we repeat a pattern multiple times, the histograms of the target and background areas can be reliably obtained. The target and background can then be separated using a simple threshold based classification model. Using this method, the separability of the two stochastic populations are judged by the standard ROC, and the normalized metric of AUC can then be used as an evaluation criteria.

Fig. 5.21 shows that feature preservation can be evaluated by examining the separability of the two background and target populations. Figs. 5.21c and 5.21d allows



(a) Simulated Image

(b) Kuan Filtered Image

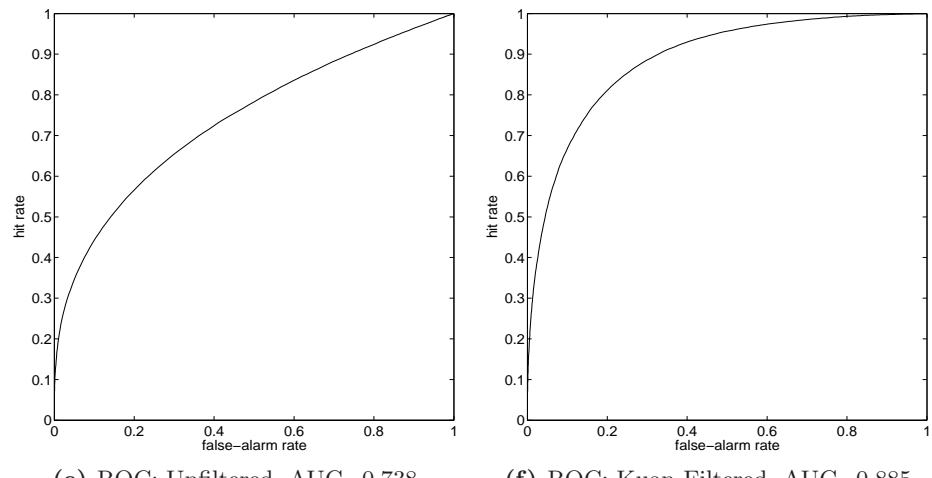
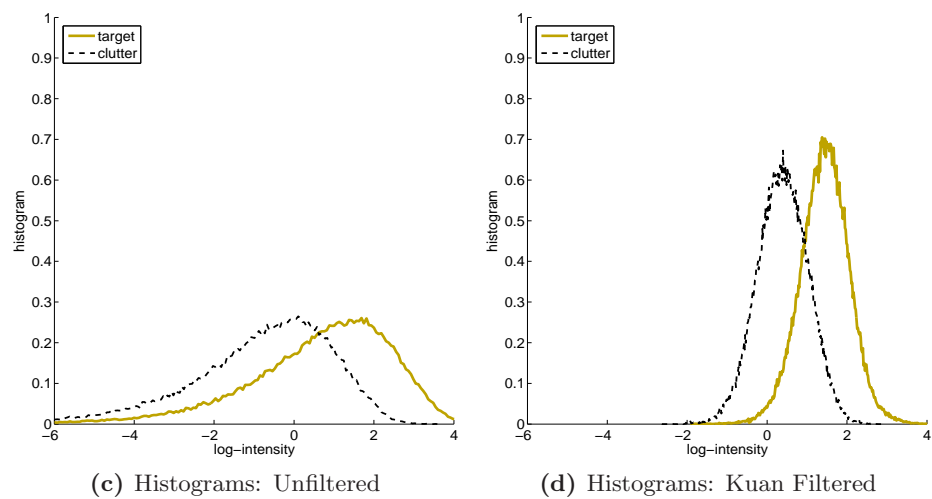


Figure 5.21: Target and Clutter Separability: Histograms and resulting ROC Curve visualisation

visual evaluation of target and clutter histograms and their separability. Quantitative evaluation of these separability is carried out by plotting the Receiver Operating Curve (ROC), in Figs. 5.21e and 5.21f respectively, and is measured by computing the Area Under these Curves (AUC).

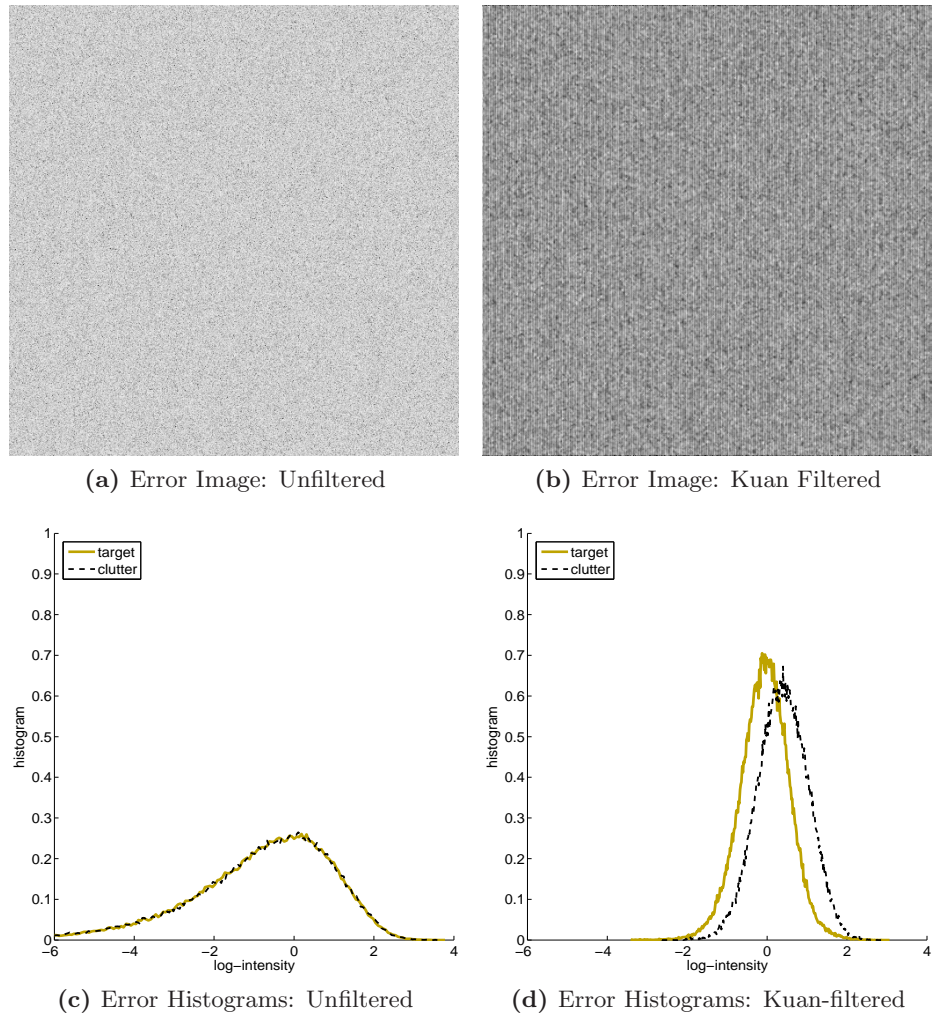


Figure 5.22: Bias Error Investigation: Image and Histogram Visualisation

Detailed examination of Figs. 5.21 and 5.22 can help to explain how the MSE is related to the histograms' separation capability. In pre-filtered images, shown in Figs. 5.21c and 5.22c, there is no bias error visible. Then the separability of background and target populations depends only on the variance of the additive noise. This variance is visualized as the horizontal spread of the histograms. Naturally, given a fixed location (i.e. expectation) of the two populations, the smaller the spread (i.e. variance) of these

sample histograms, the better the separation capability.

In post-filtered images, shown in Figs. 5.21d and 5.22d, the situation is more complicated. Here, besides the effect of the histogram spread, one also needs to take into account the bias error. A closer examination of Fig. 5.22d indicates that the output of the Kuan filter, and in fact the outputs of all other filters (which are not reproduced here due to space constraints), also introduce bias errors. Specifically, the target (brighter) populations are always under-estimated and the clutter (darker) population are always over-estimated. This is probably due to the entropy reduction effect of the speckle filters. Apparently, assuming that the variances are fixed, the lower these bias errors, the better the separation capability.

In SAR domain terminology, the general requirements of feature preservation for SAR speckle filters can be broken down into the requirements of radiometric preservation and speckle suppression. In the log-transformed domain, these smaller requirements are equivalent to the bias and variance evaluation of statistical estimators respectively. Overall, while the MSE index combines the measurements of bias and variance evaluation, the feature preservation requirement, in the context of simple target and clutter scenes, can be measured by the standard metric for target detectability: the Area Under the ROC Curve (AUC).

Next the MSE is experimentally shown to be inversely correlated with the AUC index, for all simulated patterns. Table 5.3 provides the measurements of MSE and AUC performance for various filters and patterns. It suggests that the MSE is inversely correlated to this separability index. This statistical correlation is quantitatively measured in the first column of Table 5.4. The results suggest that the lower MSE achievable by a SAR speckle filter would, in general, lead to better feature preservation in its filtered output.

Thus in this section, the MSE criteria in the log-transformed domain is validated through experiments and analysis. Analytically, on clear-cut simple target-background patterns, MSE is shown to be related to the target / background separation capabilities. Because the log-transformation converts heteroskedastic SAR speckle into a homoskedastic distribution model, the log-transformed domains MSE is much preferred to MSE in the original SAR domain. Experimentally, the results that follow will indicate that the lower the MSE achievable by a speckle filter, the better the feature preservation performance recorded for its output.

Pattern	Filter	AUC	MSE_{true}	MSE_{noise}
point	unfiltered	0.741 (0.7e-3)	4.101 (1.3e-3)	2e-33 (4e-36)
	pde	0.789 (1.3e-3)	1.291 (5.1e-3)	1.817 (2.2e-3)
	map	0.813 (1.4e-3)	1.679 (2.2e-3)	2.183 (7.4e-3)
	frost	0.836 (1.8e-3)	0.536 (2.4e-3)	4.976 (6.9e-3)
	lee	0.857 (0.9e-3)	0.615 (3.1e-3)	3.189 (0.9e-3)
	boxcar	0.871 (1.5e-3)	0.471 (1.7e-3)	4.503 (5.4e-3)
	kuan	0.882 (1.1e-3)	0.448 (2.3e-3)	3.859 (3.4e-3)
edge	unfiltered	0.738 (1.5e-4)	4.128 (9.0e-3)	2e-33 (1e-35)
	pde	0.783 (0.6e-4)	1.409 (0.3e-3)	1.589 (0.4e-2)
	map	0.830 (0.6e-4)	1.712 (3.5e-3)	2.184 (0.8e-2)
	frost	0.841 (0.6e-4)	0.551 (0.1e-3)	5.035 (1.3e-2)
	boxcar	0.871 (0.2e-4)	0.486 (0.2e-3)	4.560 (1.3e-2)
	lee	0.872 (0.7e-4)	0.619 (2.2e-3)	3.233 (1.3e-2)
	kuan	0.885 (0.4e-4)	0.471 (2.0e-3)	3.909 (1.1e-2)
checker	unfiltered	0.738 (4.5e-4)	4.11 (7.8e-3)	2e-33 (5e-36)
	pde	0.785 (6.2e-4)	1.445 (2.6e-3)	1.586 (2.4e-3)
	map	0.836 (4.0e-4)	1.663 (1.1e-3)	2.213 (4.6e-3)
	frost	0.855 (5.6e-4)	0.528 (2.2e-3)	4.965 (9.3e-3)
	lee	0.879 (2.2e-4)	0.605 (1.7e-3)	3.229 (2.8e-3)
	boxcar	0.883 (6.4e-4)	0.466 (2.4e-3)	4.493 (9.1e-3)
	kuan	0.894 (4.2e-4)	0.453 (0.9e-3)	3.860 (9.5e-3)
line	unfiltered	0.737 (1.1e-3)	4.129 (7.3e-3)	2e-33 (6e-36)
	pde	0.752 (1.2e-3)	1.339 (2.0e-3)	1.885 (3.7e-3)
	map	0.801 (1.6e-3)	1.706 (5.8e-3)	2.188 (3.5e-3)
	frost	0.831 (1.3e-3)	0.551 (1.1e-3)	5.023 (0.5e-3)
	lee	0.847 (1.5e-3)	0.623 (2.9e-3)	3.228 (4.8e-3)
	boxcar	0.865 (1.3e-3)	0.486 (0.9e-3)	4.549 (0.9e-3)
	kuan	0.874 (1.9e-3)	0.464 (1.9e-3)	3.897 (4.9e-3)

Table 5.3: Lower MSE suggest better feature detection, measured by the AUC index

Pattern	AUC - MSE_{true}	AUC - $MSE_{benchmark}$
edge	-0.8958 (1.5e-05)	-0.9778 (1.6e-09)
point	-0.9012 (1.1e-05)	-0.9816 (5.3e-10)
checker	-0.9077 (7.3e-06)	-0.9829 (3.5e-10)
line	-0.8223 (3.1e-04)	-0.9421 (4.8e-07)

Table 5.4: The correlation between MSE and AUC evaluation criteria (inside the brackets are corresponding p-values)

5.3.4 Using MSE to find the most suitable speckle filter for practical SAR images

In this section, our conjecture of using MSE in the log-transformed domain to find the most suitable speckle filter for practical real-captured SAR images is described. In these scenarios, the ground-truth, and hence the true MSE, is not available. Therefore, only the residual MSE is computable. Assuming the level of speckle noise (i.e. ENL or MSE_{base}) is known or can be estimated, then the benchmark MSE, which is defined as the absolute difference between the residual and the base MSE, is also measurable.

The proposed heuristic rule is that the best filtered results are those that have minimal benchmarked MSE. This heuristic rule allow us to choose the “best” filtered results from an array of standard speckle filters for a captured SAR image, where the ground-truth and hence true MSE is not available. The intuition for this conjecture is that the best speckle filter for a given scene is the one having its removed variation being closest to the inherent speckle noise.

Experimental results are presented as empirical evidence supporting the conjecture. The experiments in the previous sections are repeated on single-look SAR images which are simulated from given ground-truth aerial images. Then the filters are applied onto the simulated SAR images. Fig. 5.23 illustrates some of the images used for our experiments.

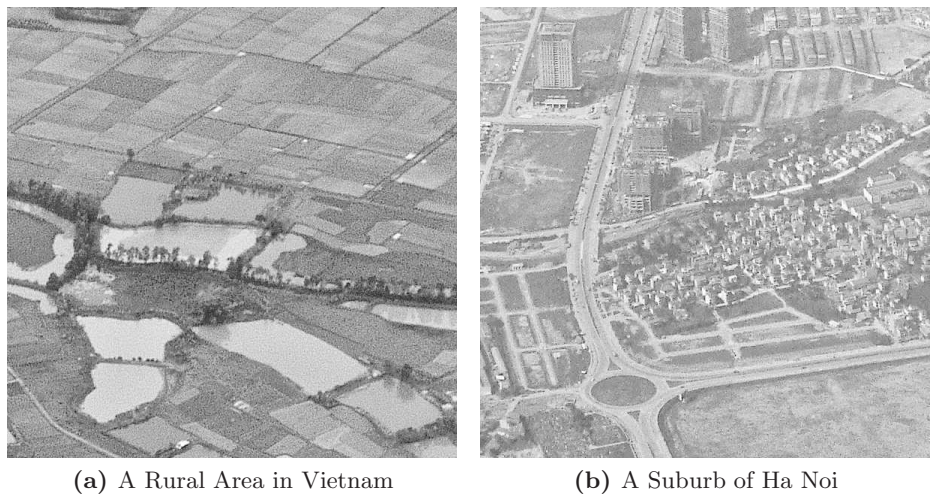


Figure 5.23: Ground Truth Images for simulation

The SAR speckle filters are then applied onto the simulated images, and the various MSE in the log-transformed domain are computed. With the use of MSE being validated from previous experiments, the most suitable filter is deemed as the one with the lowest true MSE. The use of residual MSE is validated by examining the values shown in Table 5.5. It shows that among the various filters used, the most suitable filter is also the filter that has its observable residual MSE value being closest to the noise MSE (4.1167 in the case of this example). The conjecture is also validated using visual evaluation, an example of which is presented in Fig. 5.24.

Pattern	Filter	MSE_{true}	MSE_{noise}
Vietnam rural	none	4.1174	4e-35
	pde	3.8022	0.0368
	lee	0.4984	3.2555
	frost	0.3490	4.6856
	kuan	0.3396	3.6877
	boxcar	0.3107	4.2328
Hanoi suburb	none	4.1321	4e-35
	pde	3.8004	0.0391
	lee	0.5261	3.2598
	frost	0.3811	4.7427
	kuan	0.3619	3.7270
	boxcar	0.3395	4.2882

Table 5.5: If the best filters are the ones with smallest true MSE, then their observable noise-MSE are also the ones closest to the MSE of inherent noise

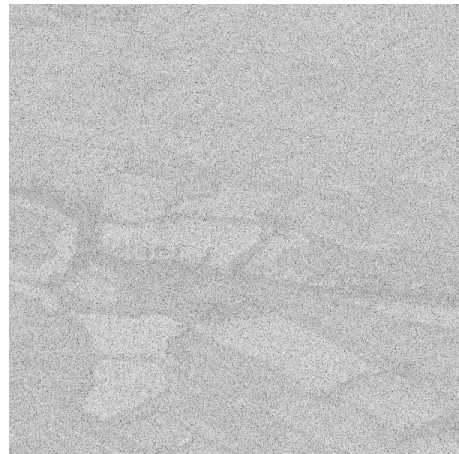
Filter	$MSE_{residual}$	$MSE_{benchmark}$
pde	0.2583	3.8584
map	2.6936	1.4231
kuan	3.3924	0.7243
lee	3.4172	0.6995
boxcar	3.6918	0.4249
frost	4.1191	0.0024
none	MSE_{base}	4.1167

Table 5.6: Our Conjecture: Most Suitable Speckle Filter For The Scene Can Be Chosen Using The Residual MSE.

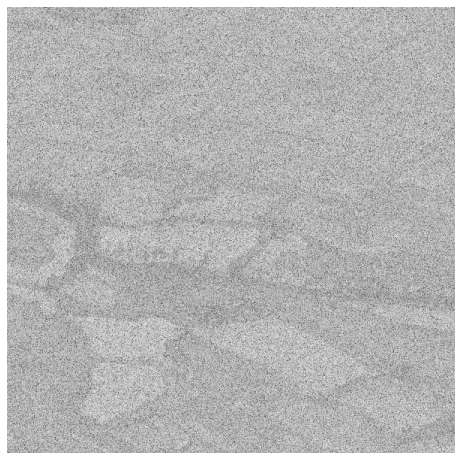
The results from the experiments in previous sections can also be used to validate the use of residual and benchmark MSE. The AUC- $MSE_{benchmark}$ column in Table 5.4 shows that the evaluation index is strongly correlated with feature classification capability, measured by the standard AUC index.



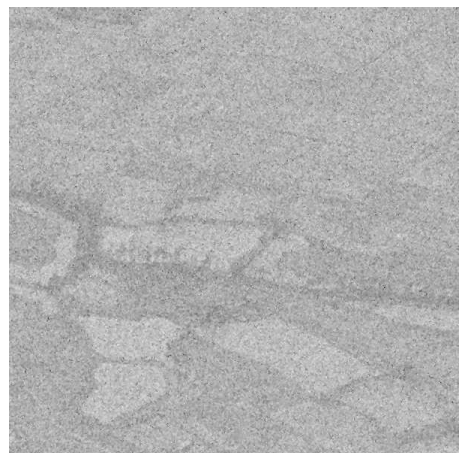
(a) Ground-Truth Image



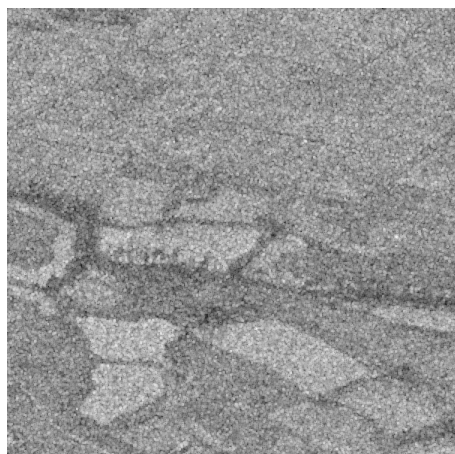
(b) Unfiltered Image $MSE_{true} = MSE_{base} = 4.1174$



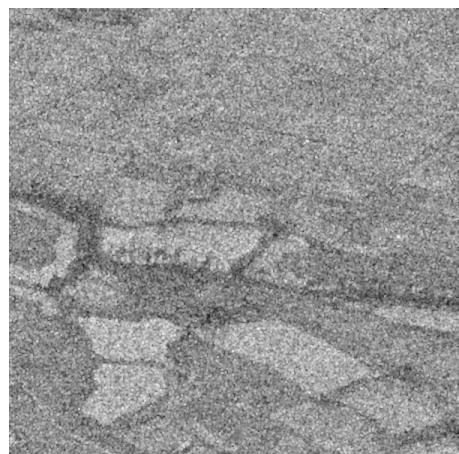
(c) PDE Result: $MSE_{true} = 3.8022$, $MSE_{noise} = 0.0073$



(d) Lee Result: $MSE_{true} = 0.4984$, $MSE_{noise} = 3.25553$



(e) Frost Result: $MSE_{true} = 0.3490$, $MSE_{noise} = 4.6856$



(f) Boxcar Result: $MSE_{true} = 0.3107$, $MSE_{noise} = 4.2328$

Figure 5.24: Filtering Simulated Real Images: Qualitative Validation

The conjecture is also validated in real SAR images. Different speckle filters are applied onto a real RADARSAT-2 image. In this case, since the ground-truth is not available, only visual evaluation can be used to validate our conjecture. Table 5.6 tabulates the computed MSE of the “removed” additive noise. Evidently all filters still leave some noise “unremoved”, in which case, the higher removed noise MSE would probably suggest a more suitable filter. Fig. 5.25 confirms this visually.

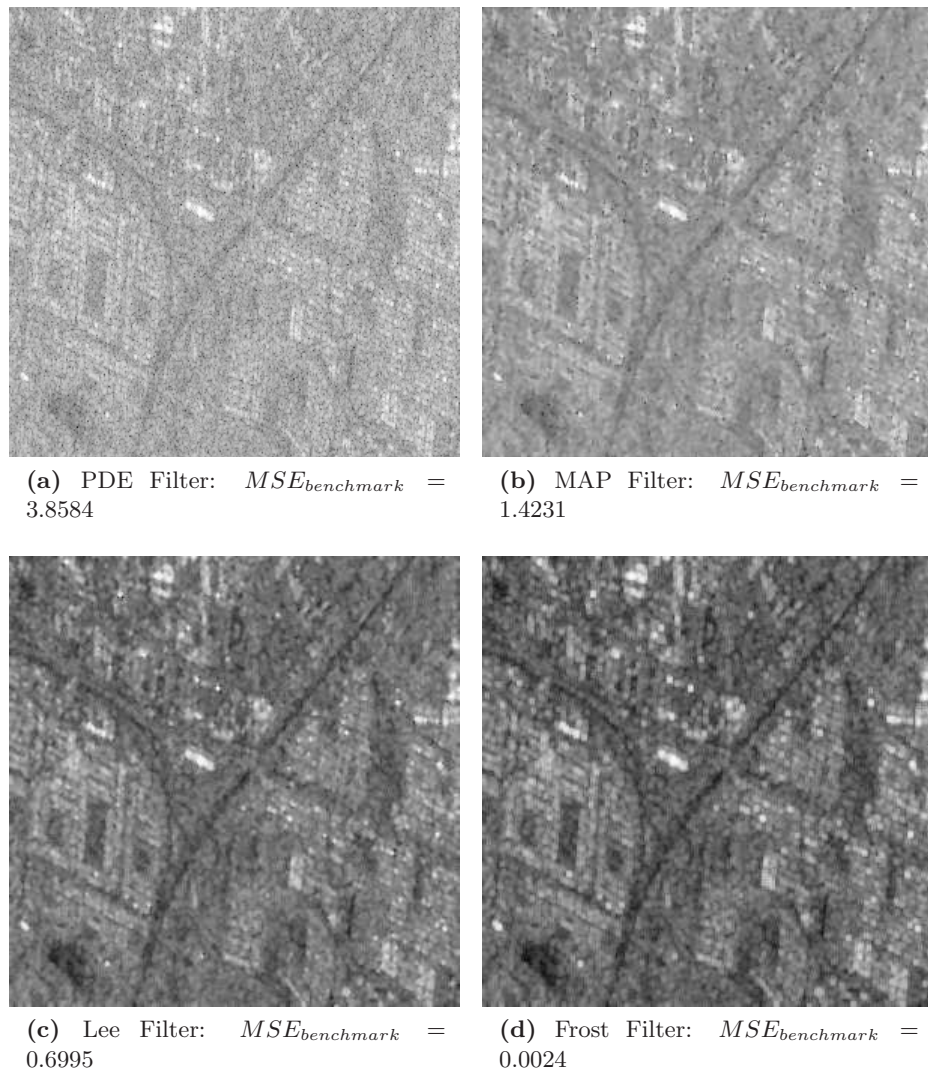


Figure 5.25: Filtering Real Images: Smaller $MSE_{benchmark}$ suggests visually better images

5.3.5 Discussion and Summary

5.3.5.1 Discussion

Although it is widely known that log transformation transforms multiplicative SAR speckle into additive noise, one should note that the noise is not Gaussian. In fact, figures presented in the previous sections show that they are not even centred around the origin. This may explain why averaging filters in the log-transformed domain (e.g. [87]) do not work very well in practice. To counter this, the use of maximum likelihood estimation, instead of simple averaging, is proposed in this thesis. Interestingly, averaging is also the MLE operator in the SAR's original domain.

Log transformation also brings about a few consistent measures of dissimilarity. This consistency can be found in single-look or multi-look SAR data, as well as in filtered outputs of various “standard” speckle filters. This allows a variety of target detection/classification algorithms - which exploit these consistent statistical properties - to perform brilliantly on pre-filtered as well as post-filtered data.

These consistent measures of distance in the log-transformed domain could probably have implications beyond speckle filtering. For example, in the subsequent tasks of designing target detectors or classifiers, it is normally desirable for the solution to work on both unfiltered and post-filtered SAR data. In such cases, these consistent dissimilarity measures found in the log-transformed domain could provide a sound theoretical basis. In fact, a number of proposed solutions have already appeared to exploit this feature. A case in point is the simple ratio based discriminator in the original SAR domain [2]. Looking backwards, in designing new speckle filters, by ensuring that the filtered output preserves these consistent properties, the newly designed filters would be eligible to be employed as pre-processing step for properly designed classifiers / detector. From a higher level perspective, the applicability of the Gauss-Markov theorem and consequently a meaningful MSE predict fruitful applications for a variety of least-squared-error algorithms in the homoskedastic log-transformed domain.

Of course, there are other speckle filters that do not preserve such consistency (e.g. the PDE filter [97]). One could argue that it would not be fair to judge such filters using the MSE criteria, which tend to favour the “standard” filters. While we respect other criteria that have been used, we reiterate the two salient points of our approach: Firstly, our MSE criteria is closely related to the basic ENL criteria. As shown in

previous sections, experimental results indicated that the ENL measures for such filter (i.e. the PDE filter) differ depending on the radiometric values. Secondly, speckle filters need to serve a purpose, and evaluation criteria should be relevant to such purpose. The MSE criteria is shown to be related to feature preservation requirements. Thus it is relevant towards subsequent target detection / classification processing, believed to be a common subsequent processing step. For these two reasons, the MSE criteria is advocated.

In the experiments above, speckle filters with a 3×3 sliding window were used even though we are aware that the normal window size employed is much larger. The reasons for maintaining such a small window is that smaller-sized filters facilitate the use of smaller patterns without too much concern for crosstalk among adjacent targets. In addition, we focused on the use of MSE in the log-transformed domain for the evaluation of speckle filters, and do not wish to advocate any particular “best” filter. In other words, we addressed the methodology of evaluating speckle filters, and did not directly address the design of speckle filters. However, interested filter designers are invited to download the open Matlab source code used in this chapter to evaluate their own designs ¹.

In this section, stochastic simulation is used extensively to evaluate the performance of statistical estimators (i.e. speckle filters). The use of small and simple patterns allows detailed analysis which can then be done repeatedly and reliably against the stochastic nature of SAR data. This also helps in mapping qualitative requirements for the speckle removal process into specific and quantitative requirements in the design of speckle filters. Its use also provides an absolute ground-truth which can serve as a solid base for comparison of results across different papers.

The main drawback, of course, is that ground truth often does not exist in real-captured SAR images. Thus the result extension towards real images is only analogical. While the proposed rule is heuristic, the experimental results presented in this chapter are shown to be valid empirically.

We distinctively divided evaluation of SAR speckle filters into two distinct scenarios, that of homogeneity and heterogeneity. While perfect homogeneous ground truth can be defined, different heterogeneous patterns exhibits different levels of heterogeneity. As such, different measures have been proposed to evaluate heterogeneity levels. Un-

¹This can be found at <http://www.lintech.org/Hai/Matlab>

fortunately, for real captured images, where the absolute ground-truth is not available, there is no known and certain way to assert a given image as being perfectly homogeneous or absolutely heterogeneous. Thus while the distinction helps in clarifying the concepts, it is probably a leaky abstraction.

The patterns used are chosen based on our experience, which may affects evaluation results. As different patterns result in different homogeneity/heterogeneity degrees, they also appear to affect the performance and ranking of each speckle filters. One extreme example is that of perfect homogeneity, where boxcar filters would exhibit a respectable performance. While, at the other end of the spectrum: that of high heterogeneity, it is common knowledge that the boxcar filter would not perform that well. While the ranking of the speckle filters may change, the methodology to compare and choose the “best” speckle filter should work regardless of the choice of patterns.

The current scheme of finding the most suitable speckle filter requires the application of all filters before a decision is made, which probably demands excessive processing. A possibly better alternative would be to predict the choice, escaping such massive requirements of computational power. This, however, is outside the scope of this section.

5.3.5.2 Summary

To summarize, speckle filters are generally evaluated using many different qualitative criteria. To compare the filters against each other, a methodology is needed to quantify these qualitative requirements, and subsequently to measure, compare and evaluate these quantities in the filtered results. Central to all these is the need for a consistent sense of distance.

Logarithmic transformation has been shown not only to convert multiplicative and heteroskedastic noise in the original SAR domain to additive and homoskedastic values, but also to offer a few consistent measures of distance. With the Gauss-Markov theorem becoming applicable in this domain, we describe and propose the use of MSE in the log-transformed domain as a unifying criteria to quantitatively measure different requirements for speckle filters.

Our contribution is mainly centred around a few points. Firstly, a mathematical equation is established to link the ENL index to the variance in the log-transformed domain. We also illustrate the use of log-variance evaluation - which is shown to be equivalent

to the standard ENL evaluation - in evaluating the speckle suppression effect of different speckle filters. Secondly we show that MSE is inversely correlated to the AUC index for simulated heterogeneous areas. The result suggests that the smaller MSE a filter could achieve, the better it would be at discriminating between the underlying radiometric features. Thirdly, the practical contribution is to suggest heuristic rules using the benchmark MSE to find the most suitable speckle filter for any given scene. Combined, we propose the use of MSE in log-transformed domain in evaluating the performance of different speckle filters in a variety of evaluation scenarios, and suggest several evaluation methodologies that may be useful in this regard.

It should also be noted that similar consistent measures of distance also exist in polarimetric SAR (POLsar) data. Thus future work may explore the applicability of MSE approaches to POLsar data analysis and processing.

5.4 Evaluating POLsar Speckle Filters using the consistent measures of distance

This section describes how POLsar filters can be evaluated using the consistent measures of distance found in the homoskedastic log-transformed domain. The next subsection first illustrates theoretically how the consistent variance is linked to the ENL index.

5.4.1 POLsar ENL Estimation using the Homoskedastic Property

This section discusses how ENL can be estimated using the log-variance approach in the homoskedastic, hence consistent variance, log-transformed domain. Theoretically speaking, the Eqn. 4.14 can be solved for the unknown L , which would require some iterative, and hence intensive, computation. Extending the result in the previous subsection for SAR, simpler estimation can be derived as:

$$L = d \left[\frac{1}{\text{var}(\ln |C_v|)} + 0.5 \right] \quad (5.10)$$

The subsequent paragraphs details the derivation of this approximation.

The previous section has discussed the one-dimensional case of SAR. The relation

between ENL and the log-variance is depicted in Eqns. 5.8 and 5.9. This relationship forms the special case of Eqn. 5.10 above, where $d = 1$.

In the case of partial POLSAR, d=2, then

$$var_2 [\ln |C_v|] = \psi^1(L) + \psi^1(L-1) = \sum_{i=L}^{\infty} 1/i^2 + \sum_{i=L-1}^{\infty} 1/i^2$$

Similar to the SAR case:

$$1/L + 1/(L-1) < var_2 [\ln |C_v|] < 1/(L-1) + 1/(L-2)$$

Thus, approximately:

$$var_2 [\ln |C_v|] = 2/(L-1)$$

Equivalently:

$$L = 2/var_2 [\ln |C_v|] + 1$$

In the case of full POLSAR, d=3, then

$$var_3 [\ln |C_v|] = \psi^1(L) + \psi^1(L-1) + \psi^1(L-2) = \sum_{i=L}^{\infty} 1/i^2 + \sum_{i=L-1}^{\infty} 1/i^2 + \sum_{i=L-2}^{\infty} 1/i^2$$

Again:

$$1/L + 1/(L-1) + 1/(L-2) < var_3 [\ln |C_v|] < 1/(L-1) + 1/(L-2) + 1/(L-3)$$

As $L > 3$

$$var_3 [\ln |C_v|] = 3/(L-1.5)$$

Or:

$$L = 3/var_3 [\ln |C_v|] + 1.5$$

In short, for all cases of SAR, partial-polarimetric and full-polarimetric SAR, Eqn. 5.10 relates the ENL for an homogeneous POLSAR area to the variance of the log-determinant computed from POLSAR covariance matrices. Since the ENL has routinely been used to evaluate (POL)SAR speckle filters, this mathematical relationship suggests that the same procedure applied in the log-transformed domain can, at the least, also be used to evaluate the performance of (POL)SAR speckle filters over homogeneous area. The next section will briefly explore this area.

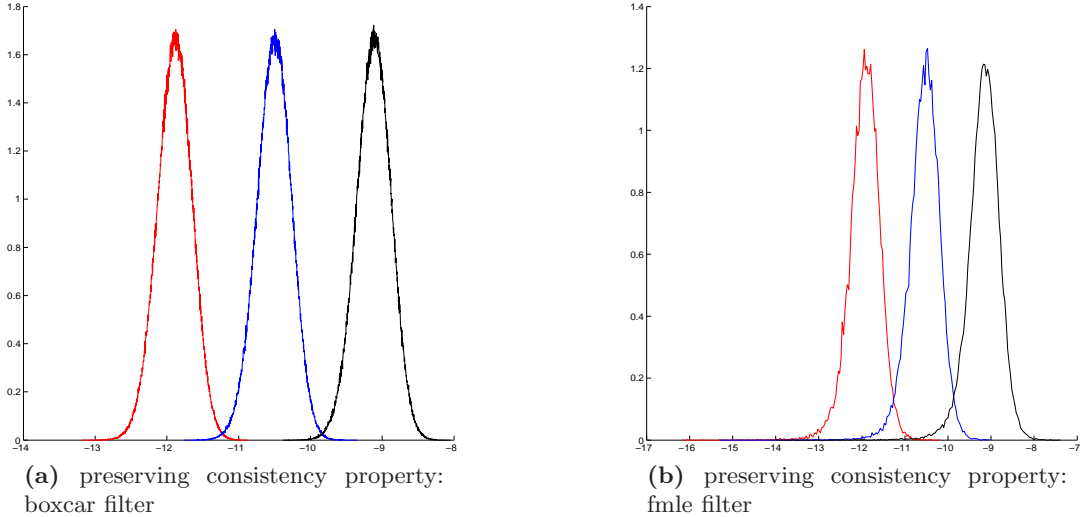


Figure 5.26: Checking the preservation of the consistency property for POLSAR speckle filters

5.4.2 Evaluating POLSAR Speckle Filters over Homogeneous Areas

It has also been found in [2] that for SAR dataset in its original domain: ratio offers a better dis-similarity measures than the standard subtractive residual. However, the ratio is not considered as being natural for digital display [45]. As shown earlier, in log-transformed domains, this ratio is transformed into a subtractive residual that is excellent at visual evaluation. This section describes how the performance of POLSAR filters over homogeneous area can be evaluated using the consistent measures of distance found in the homoskedastic log-transformed domain.

To evaluate a given POLSAR speckle filter over homogeneous areas, the filter is applied over any known homogeneous areas and the sample variance of log-determinant is measured. The Equivalent Number of Looks (ENL) is then estimated either by referencing the prepared graphs given by Eqn. 4.14. or alternatively by setting the measured variance value into $\text{var}[\ln |C_v|]$ in Eqn. 5.10. The estimated ENL and equivalently the measured log-variance is finally used to evaluate the speckle suppression power of the filters. It is common consensus that the higher the ENL estimated, implies the lower the log-variance measured, leading to better POLSAR speckle filters in terms of suppressing speckle noise.

However, in order for such a procedure to be generic, it is important that the given

POLSAR speckle filter preserve the consistency property in the log-transformed domain. That can be tested by applying the POLSAR filter into different sets of homogeneous areas and investigating the plots of the measures of distance presented above. An experiment is carried out as follows to show that the 3×3 POLSAR boxcar speckle filter preserves the consistency property. The boxcar filter is applied into 2 sets of part-pol AIRSAR data over Flevoland (HH-HV and VH-VV). Log-determinant and the contrast measure is computed for the inputs and outputs filtered POLSAR data, and their plots are presented in Fig. 5.27. It is clear that for the log-determinant histograms, while the location of the filtered plots differs depending on the underlying signal Σ_v , the shape of the plots, for both pre-filtered and post-filtered data, is invariant to the underlying signal. Contrast, and similarly dispersion, measures of distance have its location independent of Σ_v . Thus, the contrast plots for the filtered output should overlap each other to show consistency. Similar procedures can also be applied using any of the models presented above.

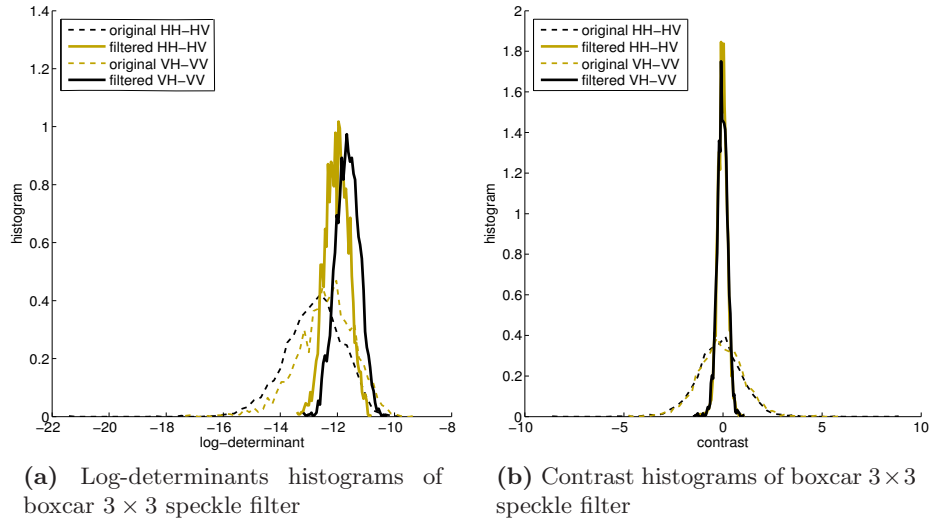


Figure 5.27: POLSAR 3×3 boxcar filter preserves the consistency property. Consistency means: as long as the area is homogeneous, regardless of the underlying signal Σ_v the shapes of the histograms should be the same.

The consistency property of POLSAR speckle filters is important not only to make the estimation of ENL become general enough. It is also important in ensuring that any classification / detection algorithm which is based on the scalar and consistent measures of distance would work on both pre-filtered and post-filtered data. Otherwise if a POLSAR speckle filter gives different plots for different homogeneous areas, then

not only its ENL estimation will be dependent on the underlying signal, its output also shall not be consistent and homoskedastic. In short, the preservation of this consistency is believed to be an important consideration for POLSAR speckle filter which should also be evaluated together with the evaluation of speckle suppression power of POLSAR speckle filters.

5.4.3 Evaluating POLSAR Speckle Filters over Heterogeneous Areas

Over heterogeneous areas, the consistent measures of distance may also be an important tool to help evaluate POLSAR speckle filters. For a start, since the model for log-determinant is additive and homoskedastic, log-determinant images is naturally more suitable for grey-level digital images. In particular for evaluation of statistical estimators, the estimators' error / residual plays an important role. Specifically, it is both important and convenient to investigate the estimator's error and/or residual image(s).

Ideally speaking, under the context of an additive model, the perfect estimators' residual should only consists of random noise. The Gauss-Markov theorem, which works under the assumption of homoskedasticity, states that the optimal estimator should have minimal Mean Squared Error. When the underlying signal is not known *a priori*, the second best gauge is possibly having the MSE of the residual being equal or being as close as possible to the MSE of the inherent noise.

To illustrate the above analysis, an experiment is carried out to evaluate the performance of boxcar 3×3 and boxcar 5×5 POLSAR filters on the AIRSAR Flevoland partial polarimetric data (HH-HV). A square 700×700 portion of the AIRSAR dataset is extracted, and the two POLSAR speckle filters are applied on to the patch. Then the log-determinant images of the filtered outputs are presented in Fig. 5.28. At the same time the residual is computed for both filters and the images are also displayed in the same figure. Assuming the quantitative evaluation of SAR speckle filters can also be extended to POLSAR speckle filters, the Mean Squared Error (MSE) of the filters residuals are computed and compared with the “optimal” value. This optimal value is computed by setting $d = 2, L = 4$ into Eqn. A.40 making the expected MSE being $mse(\mathbb{L}) = 1.0132$.

In visual and qualitative evaluation, Fig. 5.28 shows that not only can the log-determinant image offer a nice visualization of the scene, but the residual images also

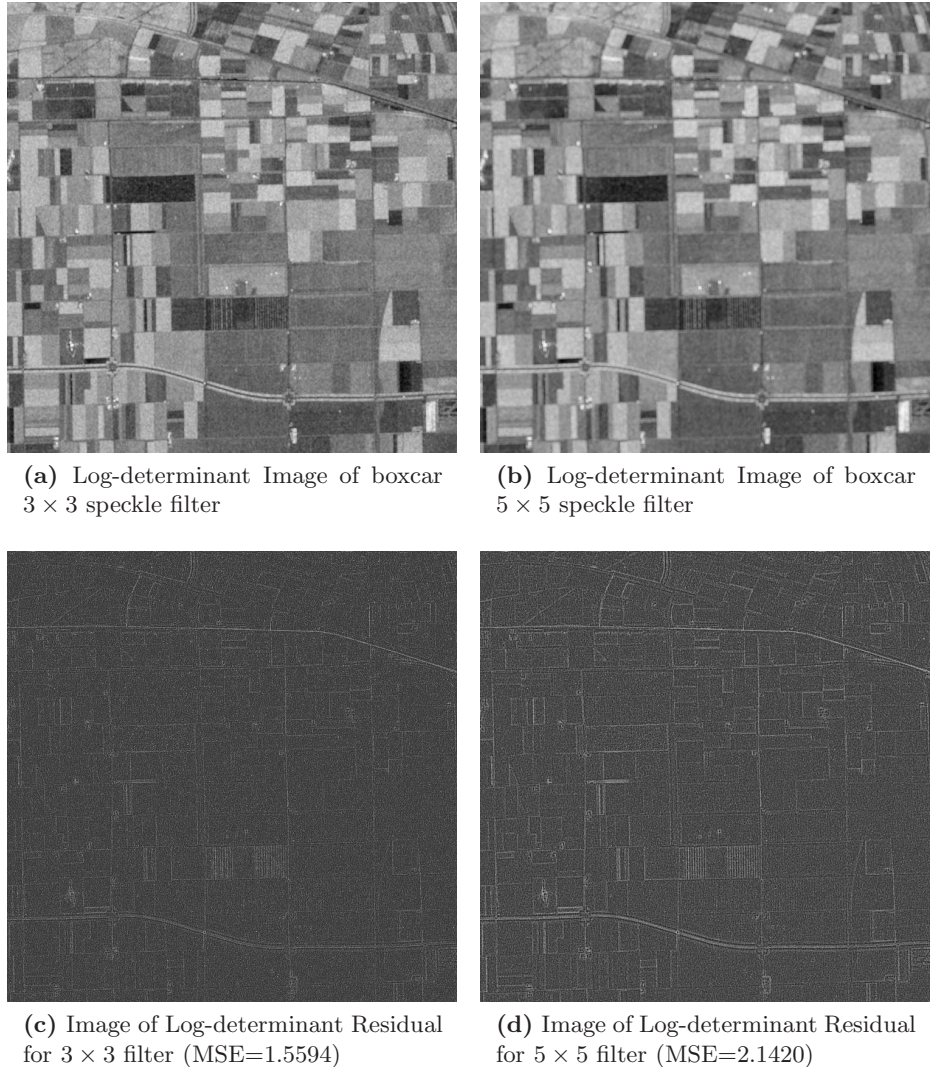


Figure 5.28: Visually Evaluating POLSAR Boxcar 3×3 vs. 5×5 Speckle Filters on AIRSA Flevoland part-pol data (HH-HV) with expected MSE=1.0312 at ENL=4.

help in visualizing the distortion impact of the filter. Specifically, while it is quite hard to observe the worsening blurring-effects of the 5×5 boxcar speckle filter as compared to the 3×3 filter in the additive log-determinant image of the filtered output, such a conclusion can be made relatively easier by visually investigating the residual image.

And when quantified evaluation is carried out where the residual MSE is compared with the expected level of noise to be removed, the excessive blurring effects of the 5×5 filter become crystal clear. In fact, even the 3×3 boxcar filter itself might be

also a bit blurry, as suggested by its relatively high residual values.

In summary, while it may be hard to make such a conclusion just by looking at the filtered imagery, by investigating the residual between the unfiltered input and the filtered results in the additive and homoskedastic model, both visual and quantitative evaluations offer conclusive evidence.

Specifically, this is an illustration of how the proposed theoretical model can possibly be applied to a practical scenario, rather than a full evaluation procedure proposal.

Chapter 6

Conclusions

This chapter concludes the work, summarizes main contributions and lists possible directions for future research.

6.1 Contributions of the Thesis

The research sets out to seek the solution for the dual-problem of 1) establishing scalar and representative statistical models for the multi-dimensional and inter-correlated POLSAR data and 2) developing novel additive and homoskedastic measures of distance for both SAR and POLSAR data, which allow the benefits of the homoskedastic statistical estimation framework to be demonstrated. After different scalar statistical models, together with many different data processing techniques, are reviewed for both SAR and POLSAR data, Chapter 2 highlights the needs for scalar, representative and homoskedastic statistical models for the multi-dimensional, complex and heteroskedastic data.

Chapter 3 then presents homoskedastic models that are derived for heteroskedastic SAR data. In Chapter 4, scalar and representative statistical models are proposed for the multi-dimensional and inter-correlated POLSAR data. These two seemingly disconnected results are unified, when the statistical models for POLSAR are shown to be the generic multi-dimensional extension of the commonly used statistical models for SAR intensity. This combination leads to the main result: the proposal of scalar, representative and homoskedastic models for both SAR and POLSAR data. These

theoretical results are applied in chapter 5 where a new clustering algorithm and a new SAR speckle filter are proposed together with our proposal of using MSE to evaluate both SAR and POLSAR speckle filters.

Generally speaking, this thesis contributes solutions for the problem of how to interpret and process the multidimensional and stochastic (POL)SAR data. Specifically, the main theoretical results obtained in this thesis are novel statistical models, which subsequently lead to derivation of consistent and homoskedastic measures of distance, for both SAR and POLSAR data. Compared to other scalar models for POLSAR the proposed models are highly representative of the multi dimensional data. Its representative power is demonstrated as it lead to consistent discrimination measures as well as it generalizes the traditional representative model for SAR intensity towards the multidimensional domain.

The proposal of using the determinant ratio as a POLSAR discrimination measure is also a novel contribution. It can be considered as the extension of the SAR intensity ratio, which have long been considered as the best discrimination measures for traditional SAR data [2]. It works consistently in the original multiplicative and heteroskedastic POLSAR domain, and the logarithmic transformation converts this ratio into a consistent subtractive measures of distance in the transformed additive and homoskedastic domain. This derived consistent measures of distance for SAR and especially for POLSAR are also a novelty. With regards to other existing discrimination measures for SAR and POLSAR, this thesis unite them, together with the new ones proposed herein, all into a consistent theory.

In summary, to address the dual-problem stated earlier, this thesis proposes several scalar, additive and homoskedastic models for the multi-dimensional, multiplicative and heteroskedastic POLSAR data. The dis-similarity measures are based on the determinant of the POLSAR covariance matrix, which when converted into one-dimensional data is gracefully transformed into the traditional SAR intensity. The models are shown to be theoretically powerful. Not only they include the one-dimensional SAR under their natural coverage, they are also able to provide alternative and simpler explanations to a range of theoretical concepts. Consequently, these measures of dis-similarity may be employed in a wide range of applications where a scalar number is required to represent the complex multi-dimensional POLSAR data. The proposed theoretical models are also versatile in practice as they cope well with imperfect conditions evident in real-life captured data.

The work in this research results in the following list of articles that has been prepared for public communication:

1. **Neural network-assisted reconstruction of full polarimetric SAR information.** Thanh-Hai Le, I. McLoughlin, Ken Yoong Lee, and T. Bretschneider. In *Communications, Control and Signal Processing (ISCCSP), 2010 4th International Symposium on*, pages 15, 2010. [100]
2. **SLC SAR speckle filtering using homoskedastic features of logarithmic transformation.** T. H. Le, I. V. McLoughlin, K. Y. Lee, and T. Brestchneider. In *Proceedings of the 31st Asian Conference on Remote Sensing (ACRS)*, Hanoi, Vietnam, Nov 2010. [88]
3. **SAR Fuzzy-MLE Speckle Filter using the Distance Consistency Property in Homoskedastic Log-Transformed Domain.** T. H. Le and I. V. McLoughlin. In *Proceedings of the 32nd Asian Conference on Remote Sensing (ACRS)*, Taipei, Taiwan, Nov 2011 [101]
4. **Scalar and Representative Models for Polarimetric SAR Data.** T. H. Le, I. V. McLoughlin, and C. H. Vun, Being finalized for submission to *IEEE Journal on Selected Topic in Applied Earth Observation and Remote Sensing*.
5. **Using MSE to evaluate SAR speckle filters.** T. H. Le, I. V. McLoughlin, and C. H. Vun. Being finalized for submission to *IEEE Journal on Selected Topic in Applied Earth Observation and Remote Sensing*

6.2 Discussion of the proposed models

Let us consider the different theoretical properties of the proposed models. First, the use of covariance matrix log-determinant may be related to the standard eigen-decomposition method of the POLSAR covariance matrices. In fact, the log-determinant can also be computed as the sum of log-eigenvalues. Specifically $\ln |M| = \sum \ln \lambda_M$ where λ_M denotes all the eigenvalues of M. Thus similar to other eigenvalue based approach (e.g. entropy/anisotropy, ...), the models presented here are invariant to polarization basis transformations.

Second, the models are developed for the POLSAR covariance matrix. However, since the POLSAR coherency matrix is related to the covariance matrix via a unitary transformation which preserves the determinant, the model should also be applicable to the coherency matrix.

It should be noted that the models are far from complete. While it is desirable to reduce the multi-dimensional POLSAR data to a scalar value for many applications, such a reduction is unlikely to be lossless. Thus the use of this technique could be complemented with some high-dimensional POLSAR target-decomposition techniques, such as the Freeman Durden decomposition [102] or the entropy/anisotropy decomposition [103] or similar.

Nevertheless the proposed models are promising. Even though initially developed for partial and monostatic POLSAR data, it was shown to be applicable to traditional SAR data as well. Since the models assumptions are quite minimal, they may potentially applicable to bi-static and interferometric data, although that would require further study.

6.2.1 Beneficial implications of the proposed models

The over-arching strategic benefit is to enable the application of existing and established techniques from one matured field into another less-than-developed new field. An example is between the fields of SAR and POLSAR, where obviously the SAR data is studied in much further details than the newly derived POLSAR data. By putting both SAR and POLSAR into one consistent theory, this thesis opens up the opportunities to apply many of the existing SAR processing technique to POLSAR. Another example is between the fields of computer science and SAR-based remote sensing. Evidently the number of different digital image processing, computational intelligence or signal processing techniques for digital input data is many times higher than the number of available techniques applicable to (POL)SAR data. And the proposed homoskedastic models, together with the consistent measures of distance, could potentially allows this currently small portion to grow larger.

The proposed homoskedastic statistical estimation framework also provides a firm foundation to overcome the various negative impacts of heteroskedasticity on statistical estimations. This is demonstrated in both stages of developing new statistical estimators (e.g. speckle filters) as well as evaluating their estimating performance. Specifically in

the context of SAR speckle filters: consistent variance and homoskedasticity is shown to help in breaking the vicious circle of speckle filtering.

At the same time, a consistently meaningful sense of distance leading to our proposal of using the familiar MSE in the homoskedastic domain to evaluate SAR speckle filters. Intuitively, this comes about as the speckle suppression power of speckle filters can be evaluated via variance estimation practice, while the radiometric preservation can be evaluated via the normal bias evaluation. Combined, while there are many different evaluation criteria in the heteroskedastic SAR speckle filter evaluation framework, the MSE is proposed as the single unified evaluation criteria for SAR speckle filters. In short, it is shown that in the homoskedastic domain, not only it is possible to find the equivalent of existing methods overcoming heteroskedastic drawbacks in the original domain, it is also possible to suggest further improvements based on existing techniques.

The proposed models for POLSAR also bring forward an important benefit. Since the models, especially those for discrimination measures, can be considered as the multi-dimensional extension of the models for SAR, it makes many existing SAR processing techniques extensible towards POLSAR data. The POLSAR determinant ratio, for example, can be considered as the extension of the ubiquitous SAR intensity ratio. This thesis also illustrates how the MSE evaluation criteria can also be extended from SAR to POLSAR.

From another angle, the theoretical models for POLSAR also offer several benefits. The theoretical models may also provide an alternative derivation for the widely used likelihood test statistics in POLSAR. In view of the models given in Eqns 4.5 & 4.6, the likelihood test statistics exposed in [37] and rewritten in Eqns 2.13 & 2.14 can be simulated as:

$$\begin{aligned} \ln Q &\sim k + L_x \Lambda_{L_x}^d + L_y \Lambda_{L_y}^d - (L_x + L_y) \Lambda_{(L_x + L_y)}^d \\ Q &\sim e^k \frac{(\chi_{L_x}^d)^{L_x} \cdot (\chi_{L_y}^d)^{L_y}}{(\chi_{L_x + L_y}^d)^{L_x + L_y}} \end{aligned}$$

where $k = d[(L_x + L_y) \ln(L_x + L_y) - L_x \ln L_x - L_y \ln L_y]$. As a by-product of this exact derivation, the current paper also proposed several simpler discrimination measures for the common case of $L_x = L_y$.

Similar to the way that other measures of distance can be used to derive POLSAR

classifiers [31], change detectors [37], edge detectors [104] or other clustering and speckle filtering techniques [88] [101], new algorithms can be derived using the proposed models.

6.2.2 Limitations of the proposed models

The proposed scalar models for POLSAR also have limitations. It calls for a dimensional reduction operation, which is probably not lossless. Thus while the determinant of POLSAR covariance matrix is said to be "highly representative", it is definitely not fully representative of the data. Intuitively, this is similar to the use of magnitude as being representative of a complex number, which also is not fully representative of the two-dimensional number. But it is important to emphasize that, just like the magnitude is invariant to the rotation of the reference frame, the POLSAR determinant is also invariant to polarization basis transformation.

While the proposed homoskedastic measures of distance have their own benefits, their biggest challenge probably lies in changing the hard learned lessons that previous generation of researchers have experienced tackling the multiplicative and heteroskedastic SAR data. At the same time, while the logarithmic transformation has the advantages of converting the multiplicative and heteroskedastic model into an additive and homoscedastic data, such transformation does not arrive conveniently to the common additive white noise model. In fact, figures presented in the previous chapters show that they are not even centred around the origin. This may explain why averaging filters in the log-transformed domain (e.g. [87]) do not work very well in practice, as the operation is biased and statistically inconsistent. To counter this, the use of maximum likelihood estimation, instead of simple averaging, is suggested [101]. While averaging is also the MLE operator in the SAR's original domain, the MLE operation in the log-transformed domain is admittedly more complex in comparison.

6.3 Possible Future Work

Although the proposed models may have certain limitations, its potentials still mostly stays undiscovered. Since the assumptions of partial and full monostatic POLSAR models are quite minimal, they are probably also applicable to other types of SAR-based data such as: Interferometric SAR (InSAR), Polarimetric Interferometric SAR (POLINSAR) or bistatic POLSAR data. In addition, further experiments can be done

to determine whether some existing SAR data processing techniques for SAR can be equally applicable to POLSAR data.

In the same vein, it is probably even more significant to investigate the applicability of some certain existing additive and homoskedastic based computational data processing techniques towards the multiplicative and heteroskedastic (POL)SAR data. As the additive noise PDF in log-domain has been worked out, we hypothesize that the true back-scattering coefficient PDF, also in log-domain, can be estimated through regularized deconvolution algorithms. If an algorithm could be designed to estimate such PDF, we believe this would present an improvement for a whole class of speckle filters, namely the Maximum-A-Priori (MAP) class, which up to now, still assumes the true PDF will follow certain known fixed distributions.

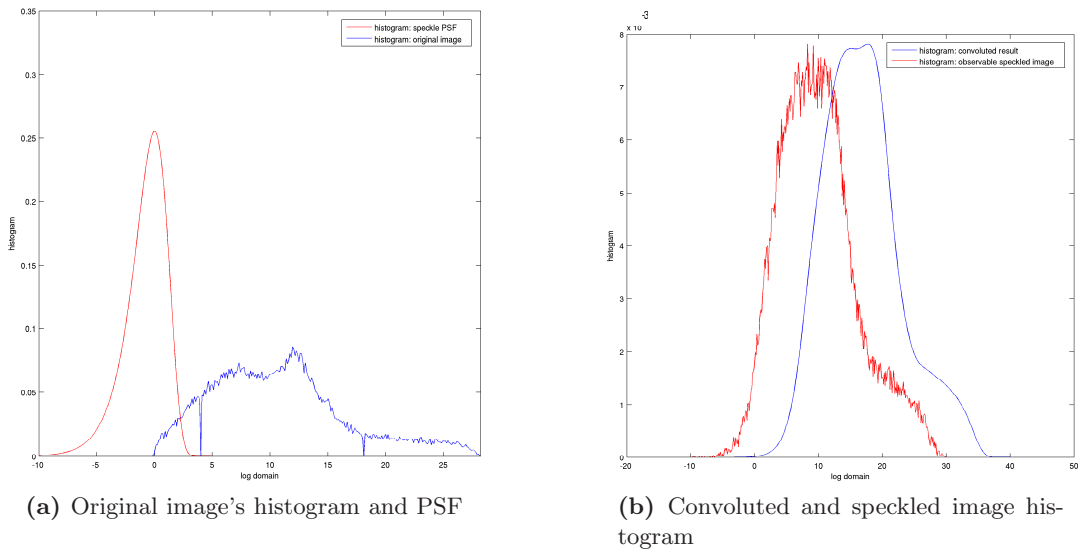


Figure 6.1: Observable convolution of PSF

Furthermore, as the point spread function (PSF) is available in the log-transformed domain, it appears that, for the first time, the histogram of the underlying back-scattering coefficient may become estimate-able. In Fig. 6.1a, the underlying single channel grey image histogram is presented along with the noise PDF, in the log-transformed domain. As the noise is additive, it is expected that the noise PDF will act as a point spread function. This makes the observable speckled image histogram mathematically equivalent to the convolution of the original image's histogram and the noise PDF. This characteristic is reflected clearly in Fig. 6.1b, where except for the un-calibrated shifting, the shapes of theoretical convolution and observed histogram are reasonably

similar. We hence hypothesize that: given the observable SAR data and its histogram, it should be possible to estimate the original underlying signal's histogram through some regularized deconvolution methods, such as using the Richardson-Lucy algorithm [105, 106].

For multi-channel SAR data, the short-term focus is to extend the existing statistical estimation framework for SAR towards POLSAR. Specifically, the F-MLE speckle filter for SAR should be extensible towards POLSAR. Similarly, the study to simulate POLSAR data as well as to use MSE to evaluate POLSAR speckle filters is also highly achievable. Lastly, the representative models for POLSAR may also be further explored, such as to explain if the additional channels provided in POLSAR do indeed lead to improved information being captured.

Appendix A

Log-Chi-Square Distribution

This appendix provides the mathematical proofs for the log-transformed version of chi-squared random variables.

Chi-squared random variables $\chi \sim \chi^2(k)$ follows the pdf:

$$pdf(\chi; k) = \frac{\chi^{(k/2)-1} e^{-\chi/2}}{2^{k/2} \Gamma\left(\frac{k}{2}\right)} \quad (\text{A.1})$$

Setting $L=k/2$ into Eqn. A.1

$$pdf(\chi) = \frac{\chi^{L-1} e^{-\chi/2}}{2^L \Gamma(L)} \quad (\text{A.2})$$

Applying the variable change theorem, which states that: if $y = \phi(x)$ with $\phi(c) = a$ and $\phi(d) = b$, then:

$$\int_a^b f(y) dy = \int_c^d f[\phi(x)] \frac{d\phi}{dx} dx \quad (\text{A.3})$$

into the log-transformation, which changes the random variables $\Lambda = \ln(\chi)$, we have:

$$\begin{aligned} d\chi &= e^\Lambda d\Lambda \\ \frac{\chi^{L-1} e^{-\chi/2}}{2^L \Gamma(L)} d\chi &= \frac{(e^\Lambda)^{L-1} e^{-e^\Lambda/2}}{2^L \Gamma(L)} e^\Lambda d\Lambda \end{aligned}$$

In other words, we have:

$$pdf(\Lambda; L) = \frac{e^{L\Lambda - e^\Lambda / 2}}{2^L \Gamma(L)} \quad (\text{A.4})$$

From the PDF given in Eqn. A.4, a characteristic function can be computed. By definition, the characteristic function (CF) $\varphi_X(t)$ for a random variable X is computed as:

$$\begin{aligned} \varphi_X(t) = \mathbb{E}[e^{itX}] &= \int_{-\infty}^{\infty} e^{itx} dF_X(x) \\ &= \int_{-\infty}^{\infty} e^{itx} f_X(x) dx \end{aligned}$$

with $\varphi_x(t)$ is the characteristic function, $F_X(x)$ is the CDF function of X and $f_X(x)$ is the PDF function of X . Thus the characteristic function for the log-chi-squared distribution is defined as:

$$\varphi_\Lambda(t) = \int_0^\infty e^{itx} \frac{e^{Lx - e^x / 2}}{2^L \Gamma(L)} dx \quad (\text{A.5})$$

The Gamma function is defined over the complex domain as: $\Gamma(z) = \int_0^\infty e^{-x} x^{z-1} dx$. Thus $\Gamma(L+it) = \int_0^\infty e^{-x} x^{L+it-1} dx$. Set $x = e^z / 2$ then $dx = e^z / 2 dz$, we have $\Gamma(L+it) = \int_0^\infty e^{itz} \frac{e^{Lz - e^z / 2}}{2^{L+it}} dz$

That is:

$$\varphi_\Lambda(t) = 2^{it} \frac{\Gamma(L+it)}{\Gamma(L)} \quad (\text{A.6})$$

Consequently, the first and second derivative of log-chi-squared distribution can be computed. The first derivative is given as:

$$\frac{\partial \varphi_\Lambda(t)}{\partial t} = \frac{i 2^{it} \Gamma(L+it)}{\Gamma(L)} [\ln 2 + \psi^0(L+it)] \quad (\text{A.7})$$

due to

$$\begin{aligned}\frac{\partial \Gamma(x)}{\partial x} &= \Gamma(x)\psi^0(x), \\ \frac{\partial \Gamma(L+it)}{\partial t} &= i\Gamma(L+it)\psi^0(L+it), \\ \frac{\partial 2^{it}}{\partial t} &= i2^{it}\ln(2), \\ \partial(u \cdot v)/\partial t &= u \cdot \partial v/\partial t + v \cdot \partial u/\partial t,\end{aligned}$$

where $\psi^0()$ denotes the di-gamma function.

Meanwhile, the second derivative can be written as:

$$\frac{\partial^2 \varphi_\Lambda(t)}{\partial t^2} = \frac{i^2 2^{it} \Gamma(L+it)}{\Gamma(L)} \left([\ln 2 + \psi^0(L+it)]^2 + \psi^1(L+it) \right) \quad (\text{A.8})$$

due to:

$$\begin{aligned}\frac{d2^{it}\Gamma(L+it)}{dt} &= i2^{it}\Gamma(L+it) [\ln 2 + \psi^0(L+it)], \\ \frac{d\psi^0(t)}{dt} &= \psi^1(t), \\ \frac{d\psi^0(L+it)}{dt} &= i\psi^1(L+it), \\ \partial(u \cdot v)/\partial t &= u \cdot \partial v/\partial t + v \cdot \partial u/\partial t,\end{aligned}$$

with $\psi^1()$ denotes the tri-gamma function.

The n^{th} moments of random variable X can be computed from the derivatives of its characteristic function as:

$$\mathbb{E}(\Lambda^n) = i^{-n} \varphi_\Lambda^{(n)}(0) = i^{-n} \left[\frac{d^n}{dt^n} \varphi_\Lambda(t) \right]_{t=0} \quad (\text{A.9})$$

Thus

$$\begin{aligned}\mathbb{E}(\Lambda) &= i^{-1} \left[\frac{d\varphi_\Lambda(t)}{dt} \right]_{t=0} \\ &= i^{-1} \left[\frac{i2^{it}\Gamma(L+it)}{\Gamma(L)} [\ln 2 + \psi^0(L+it)] \right]_{t=0}\end{aligned}$$

That is

$$avg(\Lambda) = \psi^0(L) + \ln(2) \quad (\text{A.10})$$

Similarly,

$$\begin{aligned} E(\Lambda^2) &= i^{-2} \left[\frac{d^2 \varphi_\Lambda(t)}{dt^2} \right]_{t=0} \\ &= \left[\frac{2^{it} \Gamma(L+it)}{\Gamma(L)} \left([\ln 2 + \psi^0(L+it)]^2 + \psi^1(L+it) \right) \right]_{t=0} \end{aligned}$$

That is:

$$E(\Lambda^2) = [\psi^0(L) + \ln(2)]^2 + \psi^1(L) \quad (\text{A.11})$$

Thus

$$var(\Lambda) = E(\Lambda^2) - E^2(\Lambda) = \psi^1(L) \quad (\text{A.12})$$

A.1 Averages and Variances of POLSAR Covariance Matrix Determinant and Log-Determinant

In this section, the expected value and variance value of these mixture of random variables is derived

$$\chi_L^d \sim \prod_{i=0}^{d-1} \chi(2L-2i) \quad (\text{A.13})$$

$$\Lambda_L^d \sim \sum_{i=0}^{d-1} \Lambda(2L-2i) \quad (\text{A.14})$$

given the averages and variances of individual components.

$$avg[\chi(2L)] = 2L \quad (\text{A.15})$$

$$var[\chi(2L)] = 4L \quad (\text{A.16})$$

$$avg[\Lambda(2L)] = \psi^0(L) + \ln 2 \quad (\text{A.17})$$

$$var[\Lambda(2L)] = \psi^1(L) \quad (\text{A.18})$$

Making use of the mutual indepent property of each component X_i , the variance and

expectation of the sumation and product of random variables can be written as:

$$\begin{aligned}
\text{avg} \left(\sum_{i=1}^n X_i \right) &= \sum_{i=1}^n \text{avg}(X_i), \\
\text{var} \left(\sum_{i=1}^n X_i \right) &= \sum_{i=1}^n \text{var}(X_i), \\
\text{avg} \left(\prod_{i=1}^n X_i \right) &= \prod_{i=1}^n \text{avg}(X_i), \\
\text{var} \left(\prod_{i=1}^n X_i \right) &= \prod_{i=1}^n [\text{avg}^2(X_i) + \text{var}(X_i)] - \prod_{i=1}^n \text{avg}^2(X_i).
\end{aligned}$$

Thus they can be computed as:

$$\begin{aligned}
\text{avg} [\chi_L^d] &= 2^d \cdot \prod_{i=0}^{d-1} (L-i), \\
\text{var} [\chi_L^d] &= \prod_{i=0}^{d-1} 4(L-i)(L-i+1) - \prod_{i=0}^{d-1} 4(L-i)^2, \\
\text{avg} [\Lambda_L^d] &= d \cdot \ln 2 + \sum_{i=0}^{d-1} \psi^0(L-i), \\
\text{var} [\Lambda_L^d] &= \sum_{i=0}^{d-1} \psi^1(L-i)
\end{aligned}$$

A.2 Deriving the Characteristic Functions for the Consistent Measures of Distance

Given that the characteristic function (CF) of the elementary log-chi square distributions can be written as:

$$CF_{\Lambda(2L)}(t) = 2^{it} \Gamma(L+it)/\Gamma(L)$$

the CF for the following random variables, which are combinations of the above elementary random variables, can be derived

$$\begin{aligned}\Lambda_L^d &\sim \sum_{i=0}^{d-1} \Lambda(2L - 2i) \\ \mathbb{L} &\sim \Lambda_L^d - d \cdot \ln(2L) \\ \mathbb{D} &\sim \mathbb{L} - d \cdot \ln L + \sum_{i=0}^{d-1} \psi^0(L - i) \\ \mathbb{C} &\sim \sum_{i=0}^{d-1} [\Lambda(2L - 2i) - \Lambda(2L - 2i)]\end{aligned}$$

Since

$$\begin{aligned}CF_{\sum X_i}(t) &= \prod CF_{X_i}(t) \\ CF_{x+k}(t) &= e^{itk} CF_x(t)\end{aligned}$$

we have:

$$CF_{\chi_L^d}(t) = \frac{2^{idt}}{\Gamma(L)^d} \prod_{j=0}^{d-1} \Gamma(L - j + it) \quad (\text{A.19})$$

$$CF_{\mathbb{L}} = \frac{1}{L^{idt} \Gamma(L)^d} \prod_{j=0}^{d-1} \Gamma(L - j + it) \quad (\text{A.20})$$

$$CF_{\mathbb{D}} = \frac{1}{\Gamma(L)^d} \prod_{j=0}^{d-1} e^{idt\psi^0(L-j)} \Gamma(L - j + it) \quad (\text{A.21})$$

Also due to

$$\begin{aligned}CF_{-\Lambda(2L)}(t) &= 2^{-it} \frac{\Gamma(L - it)}{\Gamma(L)} \\ \Delta(2L) &\sim \Lambda(2L) - \Lambda(2L) \\ \Gamma(L - it)\Gamma(L + it) &= \Gamma(2L)B(L - it, L + it) \\ CF_{\Delta(2L)}(t) &= \frac{\Gamma(2L)B(L - it, L + it)}{\Gamma^2(L)}\end{aligned}$$

we arrive at:

$$CF_C = \prod_{j=0}^{d-1} \frac{\Gamma(2L-2j)B(L-j-it, L-j+it)}{\Gamma^2(L-j)} \quad (\text{A.22})$$

with $\Gamma()$ and $B()$ denotes Gamma and Beta functions respectively.

A.3 SAR intensity as a special case of POLSAR covariance matrix determinant

In this appendix, the following results for SAR intensity I are shown to be special cases of the results given in this thesis for the determinant of POLSAR's covariance matrix $\det|C_v|$. Specifically, not only the following results from chapter 3, i.e. $d = L = 1$, is reviewed:

$$I \sim \bar{I} \cdot \text{pdf} [e^{-R}] \quad (\text{A.23})$$

$$\log_2 I \sim \log_2 \bar{I} + \text{pdf} [2^{D-2^D}] \quad (\text{A.24})$$

$$\frac{I}{\bar{I}} = \mathbb{R} \sim \text{pdf} [e^{-R}] \quad (\text{A.25})$$

$$\log_2 I - \log_2 \bar{I} = \mathbb{D} \sim \text{pdf} [2^D e^{-2^D} \ln 2] \quad (\text{A.26})$$

$$\log_2 I_1 - \log_2 I_2 = \mathbb{C} \sim \text{pdf} \left[\frac{2^c}{(1+2^c)^2} \ln 2 \right] \quad (\text{A.27})$$

$$\text{avg}(\mathbb{D}) = -\gamma / \ln 2 \quad (\text{A.28})$$

$$\text{var}(\mathbb{D}) = \frac{\pi^2}{6} \frac{1}{\ln^2 2} \quad (\text{A.29})$$

$$\text{mse}(\mathbb{D}) = \frac{1}{\ln^2 2} (\gamma^2 + \pi^2 / 6) = 4.1161 \quad (\text{A.30})$$

but also the following well-known results for multi-look SAR, i.e. $d = 1, L > 1$ is also considered:

$$I \sim \text{pdf} \left[\frac{L^L I^{L-1} e^{-LI/\bar{I}}}{\Gamma(L) \bar{I}^L} \right] \quad (\text{A.31})$$

$$N = \ln I \sim \text{pdf} \left[\frac{L^L}{\Gamma(L)} e^{L(N-\bar{N}) - L e^{N-\bar{N}}} \right] \quad (\text{A.32})$$

It will be shown that all of these results are special cases of the result derived previously and rewritten below:

$$|C_v| \sim \frac{|\Sigma_v|}{(2L)^d} \prod_{i=0}^{d-1} \chi^2(2L - 2i) \quad (\text{A.33})$$

$$\ln |C_v| \sim \ln |\Sigma_v| + \sum_{i=0}^{d-1} \Lambda(2L - 2i) - d \cdot \ln 2L \quad (\text{A.34})$$

$$\frac{|C_v|}{|\Sigma_v|} = \mathbb{R} \sim \frac{1}{(2L)^d} \prod_{i=0}^{d-1} \chi^2(2L - 2i) \quad (\text{A.35})$$

$$\ln |C_v| - \ln |\Sigma_v| = \mathbb{D} \sim \sum_{i=0}^{d-1} \Lambda(2L - 2i) - d \cdot \ln 2L \quad (\text{A.36})$$

$$\ln |C_{1v}| - \ln |C_{2v}| = \mathbb{C} \sim \sum_{i=0}^{d-1} \Delta(2L - 2i) \quad (\text{A.37})$$

$$avg(\mathbb{D}) = \sum_{i=0}^{d-1} \psi^0(L - i) - d \cdot \ln L \quad (\text{A.38})$$

$$var(\mathbb{D}) = \sum_{i=0}^{d-1} \psi^1(L - i) \quad (\text{A.39})$$

$$mse(\mathbb{D}) = \left[\sum_{i=0}^{d-1} \psi^0(L - i) - d \cdot \ln L \right]^2 + \sum_{i=0}^{d-1} \psi^1(L - i) \quad (\text{A.40})$$

This appendix also derives new results for multi-look SAR data, which can be thought of either as extensions of the corresponding single-look SAR results or as simple cases of the POLSAR results presented above. They are:

$$\frac{I}{\bar{I}} = \mathbb{R} \sim \frac{1}{2L} \chi^2(2L) \quad (\text{A.41})$$

$$\ln I - \ln \bar{I} = \mathbb{D} \sim \Lambda(2L) - \ln 2L \quad (\text{A.42})$$

$$\ln I_1 - \ln I_2 = \mathbb{C} \sim \Delta(2L) \quad (\text{A.43})$$

$$avg(\mathbb{D}) = \psi^0(L) - \ln L \quad (\text{A.44})$$

$$var(\mathbb{D}) = \psi^1(L) \quad (\text{A.45})$$

$$mse(\mathbb{D}) = [\psi^0(L) - \ln L]^2 + \psi^1(L) \quad (\text{A.46})$$

The derivation process detailed below consists of two-phases. The first phase collapses the generic multi-dimensional POLSAR results into the classical one-dimensional SAR domain. Mathematically this means setting the dimensional number in POLSAR to $d = 1$ and collapsing the POLSAR covariance matrix into the variance measure in SAR, which also equals the SAR intensity i.e. $|C_v| = I, |\Sigma_v| = \bar{I}$.

The output of the first phase, in the general case, is applicable to multi-look SAR data, where $d = 1$ but $L > 1$. The second phase simplifies the multi-look results into single-look results. Mathematically, that means setting $L = 1$ in the multi-look result and converting from natural logarithmic domain to the base-2 logarithm used in 3.

A.4 Original Domain: SAR Intensity and its ratio

Setting $d = 1$, $|C_v| = I$ and $|\Sigma_v| = \bar{I}$ into Eqns. A.33 and A.35 we have:

$$\begin{aligned} I &\sim \frac{\bar{I}}{2L} \chi^2(2L) \\ \frac{I}{\bar{I}} = \mathbb{R} &\sim \frac{1}{2L} \chi^2(2L) \end{aligned}$$

Or in PDF forms, and applying the variable change theorem we have:

$$\begin{aligned} \frac{2LI}{\bar{I}} &\sim pdf \left[\frac{x^{L-1} e^{-x/2}}{2^L \Gamma(L)} \right] \\ \frac{I}{\bar{I}} &\sim pdf \left[\frac{x^{L-1} e^{-x/2}}{2^L \Gamma(L)} \cdot dx/dt \right]_{x=2L \cdot t} \\ &\sim pdf \left[\frac{L^L t^{L-1} e^{-Lt}}{\Gamma(L)} \right] \\ I &\sim pdf \left[\frac{L^L t^{L-1} e^{-Lt}}{\Gamma(L)} \cdot dt/dx \right]_{t=x/\bar{I}} \\ &\sim pdf \left[\frac{L^L x^{L-1} e^{-Lx/\bar{I}}}{\bar{I}^L \Gamma(L)} \right] \end{aligned}$$

Thus we have the following results for multi-look SAR

$$I \sim pdf \left[\frac{L^L x^{L-1} e^{-Lx/\bar{x}}}{\bar{I}^L \Gamma(L)} \right] \quad (\text{A.47})$$

$$\frac{I}{\bar{I}} = \mathbb{R} \sim pdf \left[\frac{L^L x^{L-1} e^{-Lx}}{\Gamma(L)} \right] \quad (\text{A.48})$$

Now setting $L = 1$, these results become:

$$I \sim pdf \left[\frac{e^{x/\bar{I}}}{\bar{I}} \right] \quad (\text{A.49})$$

$$\frac{I}{\bar{I}} = \mathbb{R} \sim pdf [e^{-x}] \quad (\text{A.50})$$

which is the same as in chapter 3.

A.5 Log-transformed domain: SAR log-intensity and the log-distance

The result for multi-look SAR data written in log-transformed domain can be derived from two different approaches. The first is to follow the simplification method, where the results for log-transformed POLSAR data are simplified into a log-transformed multi-look SAR result.

The second approach is to apply log-transformation into the results derived in the previous section. In this section, it is shown that both approaches would result in identical results.

Setting $d = 1$, $|C_v| = I$ and $|\Sigma_v| = \bar{I}$ into Eqns. A.34 and A.36 we have

$$\begin{aligned} \ln I &\sim \ln \bar{I} + \Lambda(2L) - \ln 2L \\ \ln I - \ln \bar{I} = \mathbb{L} &\sim \Lambda(2L) - \ln 2L \end{aligned}$$

Or in PDF form, and applying variable change theorem we have:

$$\begin{aligned}
\ln I - \ln \bar{I} + \ln 2L &\sim pdf \left[\frac{e^{Lx-e^x/2}}{2^L \Gamma(L)} \right] \\
\ln I - \ln \bar{I} &\sim pdf \left[\frac{e^{Lx-e^x/2}}{2^L \Gamma(L)} \cdot dx/dt \right]_{x=t+\ln 2L} \\
&\sim pdf \left[\frac{L^L e^{Lt-Le^t}}{\Gamma(L)} \right] \\
\ln I &\sim pdf \left[\frac{L^L e^{Lt-Le^t}}{\Gamma(L)} \cdot dt/dx \right]_{t=x-\ln \bar{I}} \\
&\sim pdf \left[\frac{L^L e^{L(x-\bar{N})-Le^{x-\bar{N}}}}{\Gamma(L)} \right]
\end{aligned}$$

with $\bar{N} = \ln \bar{I}$.

Thus the first approach arrives at

$$\ln I = \mathbb{N} \sim pdf \left[\frac{L^L e^{L(x-\bar{N})-Le^{x-\bar{N}}}}{\Gamma(L)} \right] \quad (\text{A.51})$$

$$\ln I - \ln \bar{I} = \mathbb{L} \sim pdf \left[\frac{L^L e^{Lt-Le^t}}{\Gamma(L)} \right] \quad (\text{A.52})$$

In the second approach, log-transformation is applied on previous result for multi-look SAR intensity and its ratio in the original domain (Eqns. A.48 and A.47). This also arrives at the same results as above, the detailed working however is omitted here for brevity.

To compute summary statistics for the multi-look SAR dispersion, set $d = 1$ into the Eqns. A.40, A.38 and A.39 we have:

$$\begin{aligned}
avg(\mathbb{L}) &= \psi^0(L) - \ln L \\
var(\mathbb{L}) &= \psi^1(L) \\
mse(\mathbb{L}) &= [\psi^0(L) - \ln L]^2 + \psi^1(L)
\end{aligned}$$

This completes the first phase of the derivation process. The second phase of simpli-

fication involves setting $L = 1$ into the above results for multi-look SAR data, and converting natural logarithms into base-2 logarithms. First, setting $L = 1$ makes the above results become

$$\begin{aligned}\ln I = \mathbb{N} &\sim pdf \left[e^{(x-\bar{N})-e^{x-\bar{N}}} \right] \\ \ln I - \ln \bar{I} = \mathbb{L} &\sim pdf \left[e^{x-e^x} \right] \\ avg(\mathbb{L}) &= \psi^0(1) = -\gamma \\ var(\mathbb{L}) &= \psi^1(1) = \pi^2/6 \\ mse(\mathbb{L}) &= [\psi^0(1)]^2 + \psi^1(1) = \gamma^2 + \pi^2/6\end{aligned}$$

with γ denotes the Euler-Mascharoni constant. Then to convert to base-2 logarithm from natural logarithmic transformation, the variable change theorem is invoked. That is:

$$\begin{aligned}\log_2 I = \mathbb{N}_2 &\sim pdf \left[e^{(x-\bar{N})-e^{x-\bar{N}}} \cdot dx/dt \right]_{x=t \cdot \ln 2} \\ \mathbb{N}/\ln 2 = \mathbb{N}_2 &\sim pdf \left[e^{(t \cdot \ln 2 - \bar{N})-e^{t \cdot \ln 2 - \bar{N}}} \ln 2 \right]_{\bar{N}_2=\bar{N} \cdot \ln 2} \\ &\sim pdf \left[2^{t-\bar{N}_2} e^{2^{t-\bar{N}_2}} \ln 2 \right]\end{aligned}$$

$$\begin{aligned}\log_2 I - \log_2 \bar{I} = \mathbb{L}/\ln 2 = \mathbb{L}_2 &\sim pdf \left[e^{x-e^x} \right]_{x=t \cdot \ln 2} \\ &\sim pdf \left[2^t e^{2^t} \ln 2 \right]\end{aligned}$$

$$\begin{aligned}avg(\mathbb{L}_2) &= avg(\mathbb{L})/\ln 2 = -\gamma/\ln 2 \\ var(\mathbb{L}_2) &= var(\mathbb{L})/\ln^2 2 = \frac{\pi^2}{6} \frac{1}{\ln^2 2} \\ mse(\mathbb{L}_2) &= mse(\mathbb{L})/\ln^2 2 = \frac{1}{\ln^2 2} (\gamma^2 + \pi^2/6) = 4.1161\end{aligned}$$

A.6 Deriving the PDF for SAR dispersion and contrast

The PDF for SAR dispersion can be easily derived from the PDF for the Log-distance given above as:

$$\ln I - \text{avg}(\ln I) = \mathbb{D} \sim \text{pdf} \left[\frac{e^{L[x+\psi^0(L)]-Le^{x+\psi^0(L)-\ln L}}}{\Gamma(L)} \right] \quad (\text{A.53})$$

due to $d = 1$ and

$$\begin{aligned} \mathbb{D} &\sim \mathbb{L} - \text{avg}(\mathbb{L}) \\ \text{avg}(\mathbb{L}) &= \psi^0(L) - \ln L \\ \mathbb{L} &\sim \text{pdf} \left[\frac{L^L e^{Lt-Le^t}}{\Gamma(L)} \right] \end{aligned}$$

Setting $L = 1$ for Single-Look SAR we have

$$\mathbb{D} \sim \text{pdf} \left[e^{x-\gamma-e^{x-\gamma}} \right] \quad (\text{A.54})$$

due to: $\psi^0(1) = -\gamma$ and $\Gamma(1) = 1$ with γ being the Euler Mascheroni Constant which equals 0.5772. In base-2 logarithm, the variable change theorem is invoked

$$\begin{aligned} \mathbb{D}_2 &= \log_2 I - \text{avg}(\log_2 I) = \mathbb{D}/\ln 2 \\ \mathbb{D}_2 &\sim \text{pdf} \left[e^{x-\gamma-e^{x-\gamma}} \cdot \frac{dx}{dt} \right]_{x=t \cdot \ln 2} \end{aligned}$$

Thus we have

$$\mathbb{D}_2 \sim \text{pdf} \left[e^{-(2^x e^{-\gamma})} (2^x e^{-\gamma}) \ln 2 \right] \quad (\text{A.55})$$

which is consistent to the result in chapter 3.

Setting $d = 1$ into Eqn. for contrast result in

$$\ln I_1 - \ln I_2 = \mathbb{C} \sim \Delta(2L) \quad (\text{A.56})$$

The characteristic function would then be

$$CF_{\mathbb{C}} = \frac{\Gamma(2L)B(L-it, L+it)}{\Gamma(L)^2} \quad (\text{A.57})$$

Thus PDF can be written as

$$\mathbb{C} \sim pdf \left[\frac{\Gamma(2L)}{\Gamma(L)^2} \frac{e^{Lx}}{(1+e^x)^{2L}} \right] \quad (\text{A.58})$$

due to

$$\begin{aligned} CF_{\mathbb{C}}(x) &= \frac{\Gamma(2L)}{\Gamma(L)^2} B(1/(1+e^x), L-it, L+it) \\ &= \frac{\Gamma(2L)}{\Gamma(L)^2} \int_0^{1/(1+e^x)} z^{L-it-1} (1-z)^{L+it-1} dz \\ \frac{\partial}{\partial x} CF_{\mathbb{C}}(x) &= \frac{\partial CF_{\mathbb{C}}(x)}{\partial 1/(1+e^x)} \cdot \frac{\partial 1/(1+e^x)}{\partial x} \\ &= e^{itx} \frac{\Gamma(2L)}{\Gamma(L)^2} \frac{e^{Lx}}{(1+e^x)^{2L}} \end{aligned}$$

Setting $L = 1$ into Eqn. A.58 we have the PDF for contrast of single-look SAR:

$$\mathbb{C} \sim pdf \left[\frac{e^x}{(1+e^x)^2} \right] \quad (\text{A.59})$$

Converting to base-2 logarithm we have

$$\begin{aligned} \mathbb{C}/\ln 2 = \mathbb{C}_2 &\sim pdf \left[\frac{e^x}{(1+e^x)^2} \cdot dx/dt \right]_{x=t \cdot \ln 2} \\ &\sim pdf \left[\ln 2 \frac{2^t}{(1+2^t)^2} \right] \end{aligned}$$

which is also consistent to the result in chapter 3.

References

- [1] IAN G. CUMMING AND FRANK H. WONG. *Digital Processing of Synthetic Aperture Radar Data: Algorithms and Implementation*. Artech House, Jan. 2005. 1
- [2] E.J.M. RIGNOT AND J.J. VAN ZYL. **Change detection techniques for ERS-1 SAR data.** *IEEE Transactions on Geoscience and Remote Sensing*, **31**(4):896 –906, Jul 1993. 4, 42, 118, 123, 129
- [3] B.M. OLIVER. **Sparkling spots and random diffraction.** *Proceedings of the IEEE*, **51**(1):220 – 221, Jan 1963. 14
- [4] E.N. LEITH. **Quasi-holographic techniques in the microwave region.** *Proceedings of the IEEE*, **59**(9):1305 – 1318, Sep 1971. 14
- [5] J. W. GOODMAN. **Statistical properties of laser speckle patterns.** In *Laser Speckle and Related Phenomena*, **9**, pages 9–75. Springer Berlin / Heidelberg, 1975. 14
- [6] J. W. GOODMAN. **Some fundamental properties of speckle.** *Journal of the Optical Society of America*, **66**(11):1145–1150, 1976. 14, 87
- [7] JONG-SEN LEE AND ERIC POTTIER. *Polarimetric Radar Imaging: From Basics to Applications*. CRC Press, 2009. 14, 37, 38
- [8] G. SINCLAIR. **The Transmission and Reception of Elliptically Polarized Waves.** *Proceedings of the IRE*, **38**(2):148 – 151, Feb. 1950. 20, 22
- [9] S.V. NGHIEM, S.H. YUEH, R. KWOK, AND F.K LI. **Symmetry properties in polarimetric remote sensing.** *Radio Sci.*, **27**(5):693–711, Oct. 1992. 20

- [10] A. GUISARD. **Mueller and Kennaugh matrices in radar polarimetry.** *Geoscience and Remote Sensing, IEEE Transactions on*, **32**(3):590 –597, May 1994. [21](#)
- [11] H.A. ZEBKER AND J.J. VAN ZYL. **Imaging radar polarimetry: a review.** *Proceedings of the IEEE*, **79**(11):1583 –1606, Nov. 1991. [22](#)
- [12] J.C. SOUYRIS, P. IMBO, R. FJORTOFT, SANDRA MINGOT, AND JONG-SEN LEE. **Compact polarimetry based on symmetry properties of geophysical media: the pi/4 mode.** *Geoscience and Remote Sensing, IEEE Transactions on*, **43**(3):634 – 646, Mar. 2005. [22](#), [23](#), [25](#)
- [13] R. RANEY. **Hybrid-Polarity SAR Architecture.** In *Geoscience and Remote Sensing Symposium, 2006. IGARSS 2006. IEEE International Conference on*, pages 3846 –3848, July 2006. [22](#), [23](#)
- [14] R.K. RANEY. **Comments on hybrid-polarity SAR architecture.** In *Geoscience and Remote Sensing Symposium, 2007. IGARSS 2007. IEEE International*, pages 2229 –2231, 23-28 2007. [24](#)
- [15] R.K RANEY. **Hybrid-polarity SAR architecture.** *IEEE Transactions on Geoscience and Remote Sensing*, **45**(11):3397–3404, 2007. [24](#)
- [16] C.A LARDEUX, P.-L.A FRISON, C.B TISON, D.D DELEFLIE, J. C. SOUYRIS, J.P RUDANT, AND B.C STOLL. **Comparison of compact polarimetric with full polarimetric radar data for land use discrimination based on SVM classification.** Number SP-644, Frascati, 2007. [24](#)
- [17] R.K. RANEY. **DESDynI adopts hybrid polarity SAR architecture.** In *Radar Conference, 2009 IEEE*, pages 1 –4, May 2009. [24](#)
- [18] M.E NORD, T.L AINSWORTH, J.S LEE, AND J.S STACY. **Comparison of compact polarimetric synthetic aperture radar mode.** *IEEE Trans. Geosci. Remote Sens.*, **47**(1):634–646, Jan. 2009. [25](#)
- [19] T.L. AINSWORTH, J.P. KELLY, AND J.-S. LEE. **Classification comparisons between dual-pol, compact polarimetric and quad-pol SAR imagery.** *ISPRS Journal of Photogrammetry and Remote Sensing*, **64**(5):464 – 471, 2009. [25](#)

- [20] W.-M. BOERNER, W.-L. YAN, A.-Q. XI, AND Y. YAMAGUCHI. **On the basic principles of radar polarimetry: the target characteristic polarization state theory of Kennaugh, Huynen's polarization fork concept, and its extension to the partially polarized case.** *Proceedings of the IEEE*, **79**(10):1538 –1550, October 1991. [26](#)
- [21] ERIC POTTIER AND LAURENT FERRO-FAMIL. **SAR Polarimetry: Basics, Processing Techniques and Applications.** In *Geoscience and Remote Sensing Symposium, 2008. IGARSS 2008. IEEE International*, **3**, 2008. [26](#)
- [22] V. ALBERGA, G. SATALINO, AND D. K. STAYKOVA. **Comparison of polarimetric SAR observables in terms of classification performance.** *International Journal of Remote Sensing*, **29**(14):4129–4150, 2008. [27](#)
- [23] RICHARD BARAKAT. **The Statistical Properties of Partially Polarized Light.** *Optica Acta: International Journal of Optics*, **32**(3):295–312, 1985. [29](#)
- [24] D. ELIYAHU. **Vector statistics of correlated Gaussian fields.** *Phys. Rev. E*, **47**:2881–2892, Apr 1993. [29](#)
- [25] CHRISTIAN BROSSEAU. **Statistics of the normalized Stokes parameters for a Gaussian stochastic plane wave field.** *Applied Optics*, **34**(22):4788–4793, Aug 1995. [29](#)
- [26] I.R. JOUGHIN, D.P. WINEBRENNER, AND D.B. PERCIVAL. **Probability density functions for multilook polarimetric signatures.** *Geoscience and Remote Sensing, IEEE Transactions on*, **32**(3):562 –574, may 1994. [29](#)
- [27] JONG-SEN LEE, K.W. HOPPEL, S.A. MANGO, AND A.R. MILLER. **Intensity and phase statistics of multilook polarimetric and interferometric SAR imagery.** *IEEE Transactions on Geoscience and Remote Sensing*, **32**(5):1017 – 1028, Sep 1994. [29, 71](#)
- [28] R. TOUZI AND A. LOPES. **Statistics of the Stokes parameters and of the complex coherence parameters in one-look and multilook speckle fields.** *Geoscience and Remote Sensing, IEEE Transactions on*, **34**(2):519 –531, mar 1996. [29](#)
- [29] C. LOPEZ-MARTINEZ AND X. FABREGAS. **Polarimetric SAR speckle noise model.** *Geoscience and Remote Sensing, IEEE Transactions on*, **41**(10):2232–2242, 2003. [30](#)

- [30] E. ERTEM. **The performance analysis based on SAR sample covariance matrix.** *Sensors (Basel)*, **12**(3):2766–2786, 2012. [30](#)
- [31] JONG-SEN LEE, M.R. GRUNES, AND G. DE GRANDI. **Polarimetric SAR speckle filtering and its implication for classification.** *IEEE Transactions on Geoscience and Remote Sensing*, **37**(5):2363 –2373, Sep 1999. [30, 36, 133](#)
- [32] J. S. LEE, M. R. GRUNES, AND R. KWOK. **Classification of multi-look polarimetric SAR imagery based on complex Wishart distribution.** *International Journal of Remote Sensing*, **15**(11):2299–2311, 1994. [30](#)
- [33] STIAN NORMANN ANFINSEN, ROBERT JENSSEN, AND TORBJORN ELTOFT. **Spectral Clustering of Polarimetric SAR Data With Wishart-Derived Distance Measures.** In *3rd International Workshop on Science and Applications of SAR Polarimetry and Polarimetric Interferometry*, **3**, Jan 2007. [30](#)
- [34] P.R. KERSTEN, JONG SEN LEE, AND T.L. AINSWORTH. **Unsupervised classification of polarimetric synthetic aperture Radar images using fuzzy clustering and EM clustering.** *IEEE Transactions on Geoscience and Remote Sensing*, **43**(3):519 – 527, Mar 2005. [31](#)
- [35] KEN YOONG LEE AND T.R. BRETSCHNEIDER. **Derivation of separability measures based on central complex Gaussian and Wishart distributions.** In *IEEE Internationaal Geoscience and Remote Sensing Symposium (IGARSS)*, 2011, pages 3740 –3743, Jul 2011. [31](#)
- [36] FANG CAO, WEN HONG, YIRONG WU, AND E. POTTIER. **An Unsupervised Segmentation With an Adaptive Number of Clusters Using the SPAN/H/ α /A Space and the Complex Wishart Clustering for Fully Polarimetric SAR Data Analysis.** *IEEE Transactions on Geoscience and Remote Sensing*, **45**(11):3454 –3467, Nov 2007. [31](#)
- [37] K. CONRADSEN, A.A. NIELSEN, J. SCHOU, AND H. SKRIVER. **A test statistic in the complex Wishart distribution and its application to change detection in polarimetric SAR data.** *IEEE Transactions on Geoscience and Remote Sensing*, **41**(1):4 – 19, Jan 2003. [31, 32, 132, 133](#)
- [38] J.-S. LEE. **Digital image enhancement and noise filtering by use of local statistics.** *IEEE Transactions on Pattern Analysis and Machine Intelligence*, **2**:165–168, Mar 1980. [32, 45, 46](#)

- [39] DARWIN T. KUAN, ALEXANDER A. SAWCHUK, TIMOTHY C. STRAND, AND PIERRE CHAVEL. **Adaptive Noise Smoothing Filter for Images with Signal-Dependent Noise.** *IEEE Transactions on Pattern Analysis and Machine Intelligence*, **PAMI-7**(2):165 –177, Mar 1985. [32](#), [46](#)
- [40] VICTOR S. FROST, JOSEPHINE ABBOTT STILES, K. S. SHANMUGAN, AND JULIAN C. HOLTZMAN. **A Model for Radar Images and Its Application to Adaptive Digital Filtering of Multiplicative Noise.** *IEEE Transactions on Pattern Analysis and Machine Intelligence*, **PAMI-4**(2):157 –166, Mar 1982. [33](#), [41](#), [46](#)
- [41] M. AMIRMAZLAGHANI, H. AMINDAVAR, AND A. MOGHADDAMJOO. **Speckle Suppression in SAR Images Using the 2-D GARCH Model.** *Image Processing, IEEE Transactions on*, **18**(2):250 –259, 2009. [33](#)
- [42] JOHN W. WOODS AND JAN BIEMOND. **Comments on “A Model for Radar Images and Its Application to Adaptive Digital Filtering of Multiplicative Noise”.** *Pattern Analysis and Machine Intelligence, IEEE Transactions on*, **PAMI-6**(5):658 –659, sept. 1984. [33](#)
- [43] F. N S MEDEIROS, N. MASCARENHAS, AND L. DA F.COSTA. **Combined use of MAP estimation and K-means classifier for speckle noise filtering in SAR images.** In *Image Analysis and Interpretation, 1998 IEEE Southwest Symposium on*, pages 250 –255, April 1998. [34](#)
- [44] A. LOPES, E. NEZRY, R. TOUZI, AND H. LAUR. **Maximum A Posteriori Speckle Filtering And First Order Texture Models In Sar Images.** In *Geoscience and Remote Sensing Symposium, 1990. IGARSS '90. 'Remote Sensing Science for the Nineties'., 10th Annual International*, pages 2409 –2412, May 1990. [34](#)
- [45] F.N.S MEDEIROS, N.D.A MASCARENHAS, AND L.F COSTA. **Evaluation of speckle noise MAP filtering algorithms applied to SAR images.** *International Journal of Remote Sensing*, **24**(24):5197–5218, Dec 2003. [35](#), [39](#), [40](#), [41](#), [123](#)
- [46] Z. SUN AND C. HAN. **MAP filtering for SAR images based on heavy-tailed Rayleigh modeling of speckle.** In *Vehicular Electronics and Safety 2006, IEEE International Conference on*, pages 323–328, 2006. [35](#)

- [47] E. NEZRY, A. LOPES, AND F. YAKAM-SIMEN. **Prior scene knowledge for the Bayesian restoration of mono- and multi-channel SAR images.** In *Geoscience and Remote Sensing, 1997. IGARSS '97. Remote Sensing - A Scientific Vision for Sustainable Development., 1997 IEEE International*, **2**, pages 758 –760 vol.2, 3-8 1997. [35](#)
- [48] D. LEWINSKI. **Nonstationary probabilistic target and clutter scattering models.** *Antennas and Propagation, IEEE Transactions on*, **31**(3):490 – 498, may 1983. [35](#)
- [49] M. WALESSA AND M. DATCU. **Model-based despeckling and information extraction from SAR images.** *Geoscience and Remote Sensing, IEEE Transactions on*, **38**(5):2258 –2269, sep 2000. [35](#)
- [50] L GAGNON AND A JOUAN. **Speckle filtering of SAR images - A comparative study between complex-wavelet-based and standard filters.** In *Proceedings of The Society of Photo-optical Instrumentation Engineers (SPIE)*, **3169**, pages 80–91, 1997. [35, 39, 40, 41](#)
- [51] A. VIDAL-PANTALEONI AND D. MARTI. **Comparison of different speckle-reduction techniques in SAR images using wavelet transform.** *International Journal of Remote Sensing*, **25**(22):4915–4932, 2004. [35](#)
- [52] PIERRE MOULIN. **A wavelet regularization method for diffuse radar-target imaging and speckle-noise reduction.** *Journal of Mathematical Imaging and Vision*, **3**(1):123–134, March 1993. [35](#)
- [53] E. HERVET, R. FJORTOFT, P. MARTHON, AND A. LOPES. **Comparison of wavelet-based and statistical speckle filters.** In F. POSA, editor, *Society of Photo-Optical Instrumentation Engineers (SPIE) Conference Series*, **3497** of *Presented at the Society of Photo-Optical Instrumentation Engineers (SPIE) Conference*, pages 43–54, November 1998. [35](#)
- [54] M. HEBAR, D. GLEICH, AND Z. CUCEJ. **Autobinomial Model for SAR Image Despeckling and Information Extraction.** *Geoscience and Remote Sensing, IEEE Transactions on*, **47**(8):2818 –2835, Aug. 2009. [35](#)
- [55] G. CHEN, XINGZHAO LIU, AND ZHIXIN ZHOU. **Despeckling SAR images in the undecimated wavelet domain based on scale correlation and GMRF**

- model.** In *Radar Systems, 2007 IET International Conference on*, pages 1 –5, 15-18 2007. [35](#)
- [56] T. BIANCHI, F. ARGENTI, AND L. ALPARONE. **Segmentation-Based MAP Despeckling of SAR Images in the Undecimated Wavelet Domain.** *Geoscience and Remote Sensing, IEEE Transactions on*, **46**(9):2728 –2742, Sept. 2008. [35](#)
- [57] F. ARGENTI, T. BIANCHI, AND L. ALPARONE. **Multiresolution MAP despeckling of SAR images based on locally adaptive generalized Gaussian pdf modeling.** *IEEE Transactions on Image Processing*, **15**(11):3385–3399, 2006. [35](#)
- [58] HONG-QIAO WANG, FU-CHUN SUN, YAN-NING CAI, AND ZONG-TAO ZHAO. **Edge-enhanced speckle suppression using curvelet transform with an optimal soft thresholding.** In *Wavelet Analysis and Pattern Recognition, 2007. ICWAPR '07. International Conference on*, **1**, pages 204 –209, 2-4 2007. [35](#)
- [59] B.B. SAEVARSSON, J.R. SVEINSSON, AND J.A. BENEDIKTSSON. **Speckle reduction of SAR images using adaptive curvelet domain.** In *Geoscience and Remote Sensing Symposium, 2003. IGARSS '03. Proceedings. 2003 IEEE International*, **6**, pages 4083 – 4085 vol.6, 21-25 2003. [35](#)
- [60] Y.A GUO AND Z.A B BAI. **A new denoising method of SAR images in curvelet domain.** In *2008 10th International Conference on Control, Automation, Robotics and Vision, ICARCV 2008*, pages 1909–1913, Hanoi, 2008. [35](#)
- [61] S.A FOUCHER, G.B FARAGE, AND G.B.B BNI. **SAR image filtering based on the stationary contourlet transform.** In *International Geoscience and Remote Sensing Symposium (IGARSS)*, pages 4021–4024, Denver, CO, 2006. [35](#)
- [62] B.B. SAEVARSSON, J.R. SVEINSSON, AND J.A. BENEDIKTSSON. **Combined wavelet and curvelet denoising of SAR images.** In *International Geoscience and Remote Sensing Symposium (IGARSS)*, **6**, pages 4235–4238, Anchorage, AK, 2004. [35](#)
- [63] HUA CHENG AND JINWEN TIAN. **Speckle Reduction of Synthetic Aperture Radar Images Based on Fuzzy Logic.** *Education Technology and Computer Science, 2009. ETCS '09. First International Workshop on*, **1**:933 –937, March 2009. [35](#)

- [64] O. D'HONDT, L. FERRO-FAMIL, AND E. POTTIER. **Nonstationary Spatial Texture Estimation Applied to Adaptive Speckle Reduction of SAR Data.** *Geoscience and Remote Sensing Letters, IEEE*, **3**(4):476 –480, Oct. 2006. 35
- [65] M. AMIRMAZLAGHANI, H. AMINDAVAR, M. AMIRMAZLAGHANI, AND H. AMINDAVAR. **A novel statistical approach for speckle filtering of SAR images.** *2009 IEEE 13th Digital Signal Processing Workshop and 5th IEEE Signal Processing Education Workshop, DSP/SPE 2009, Proceedings*, pages 457–462, Jan. 2009. 35
- [66] C J OLIVER. **Information from SAR images.** *Journal of Physics D: Applied Physics*, **24**(9):1493, 1991. 36
- [67] S.P. LUTTRELL AND C.J. OLIVER. **Prior knowledge in synthetic-aperture radar processing.** *Journal of Physics D: Applied Physics*, **19**(3):333–356, 1986. 36
- [68] A.N. NYOUNGUI, E. TONYE, AND A. AKONO. **Evaluation of speckle filtering and texture analysis methods for land cover classification from SAR images.** *International Journal of Remote Sensing*, **23**(9):1895–1925, 2002. 36, 91
- [69] LESLIE M. NOVAK AND MICHAEL C. BURL. **Optimal speckle reduction in polarimetric SAR imagery.** *IEEE Transactions on Aerospace and Electronic Systems*, **26**(2):293–305, 1990. 36
- [70] JONG-SEN LEE, T.L. AINSWORTH, J.P. KELLY, AND C. LOPEZ-MARTINEZ. **Evaluation and Bias Removal of Multilook Effect on Entropy/Alpha/Anisotropy in Polarimetric SAR Decomposition.** *Geoscience and Remote Sensing, IEEE Transactions on*, **46**(10):3039 –3052, oct. 2008. 36
- [71] JONG-SEN LEE, MITCHELL R. GRUNES, AND STEPHEN A. MANGO. **Speckle reduction in multipolarization, multifrequency SAR imagery.** *IEEE Transactions on Geoscience and Remote Sensing*, **29**(4):535–544, 1991. 36
- [72] R. TOUZI AND A. LOPES. **Principle of speckle filtering in polarimetric SAR imagery.** *IEEE Transactions on Geoscience and Remote Sensing*, **32**(5):1110–1114, 1994. 36

- [73] C. LOPEZ-MARTINEZ AND X. FABREGAS. **Model-Based Polarimetric SAR Speckle Filter.** *Geoscience and Remote Sensing, IEEE Transactions on*, **46**(11):3894 –3907, Nov. 2008. [37](#)
- [74] G. VASILE, E. TROUVE, JONG-SEN LEE, AND V. BUZULOIU. **Intensity-driven adaptive-neighborhood technique for polarimetric and interferometric SAR parameters estimation.** *Geoscience and Remote Sensing, IEEE Transactions on*, **44**(6):1609 – 1621, June 2006. [38](#)
- [75] J.-S. LEE, M.R. GRUNES, D.L. SCHULER, E. POTTIER, AND L. FERRO-FAMIL. **Scattering-model-based speckle filtering of polarimetric SAR data.** *IEEE Transactions on Geoscience and Remote Sensing*, **44**(1):176–187, 2006. [38](#)
- [76] G. VASILE, J.-P. OVARLEZ, F. PASCAL, AND C. TISON. **Coherency Matrix Estimation of Heterogeneous Clutter in High-Resolution Polarimetric SAR Images.** *Geoscience and Remote Sensing, IEEE Transactions on*, **48**(4):1809 –1826, April 2010. [38](#)
- [77] N.V. RODIONOVA. **Phase difference application in fully polsar images.** In *European Space Agency, (Special Publication) ESA SP*, **668** SP, Frascati, 2009. [38](#)
- [78] CHRIS OLIVER AND SHAUN QUEGAN. *Understanding Synthetic Aperture Radar Images*. SciTech Publishing, 2004. [39](#)
- [79] X. WANG AND H. SUN. **An evaluation for speckle filters of SAR images.** In *Society of Photo-Optical Instrumentation Engineers (SPIE) Conference Series*, **6043**, pages 761–766, Nov 2005. [39](#), [40](#)
- [80] JONG-SEN LEE. **Speckle analysis and smoothing of synthetic aperture radar images.** *Computer Graphics and Image Processing*, **17**(1):24 – 32, 1981. [39](#)
- [81] E JAKEMAN. **On the statistics of K-distributed noise.** *Journal of Physics A: Mathematical and General*, **13**(1):31, 1980. [44](#)
- [82] JONG-SEN LEE, KARL HOPPEL, AND STEPHEN A. MANGO. **Unsupervised estimation of speckle noise in radar images.** *International Journal of Imaging Systems and Technology*, **4**(4):298–305, 1992. [44](#)

- [83] R. TOUZI. **A review of speckle filtering in the context of estimation theory.** *IEEE Transactions on Geoscience and Remote Sensing*, **40**(11):2392 – 2404, Nov 2002. [45](#), [99](#)
- [84] JONG-SEN LEE, JEN-HUNG WEN, T.L. AINSWORTH, KUN-SHAN CHEN, AND A.J. CHEN. **Improved Sigma Filter for Speckle Filtering of SAR Imagery.** *IEEE Transactions on Geoscience and Remote Sensing*, **47**(1):202 –213, Jan 2009. [45](#), [52](#)
- [85] A.C. AITKEN. **On least squares and linear combination of observations.** *Proceedings of the Royal Society of Edinburgh*, **55**:42–48, 1934. [46](#)
- [86] A. LOPES, R. TOUZI, AND E. NEZRY. **Adaptive speckle filters and scene heterogeneity.** *IEEE Transactions on Geoscience and Remote Sensing*, **28**(6):992 –1000, Nov 1990. [46](#), [105](#)
- [87] H. H. ARSENAULT AND G. APRIL. **Properties of speckle integrated with a finite aperture and logarithmically transformed.** *Journal of the Optical Society of America*, **66**(11):1160–1163, 1976. [48](#), [118](#), [133](#)
- [88] T. H. LE, I. V. McLOUGHLIN, K. Y. LEE, AND T. BRESTCHNEIDER. **SLC SAR speckle filtering using homoskedastic features of logarithmic transformation.** In *Proceedings of the 31st Asian Conference on Remote Sensing (ACRS)*, Hanoi, Vietnam, Nov 2010. [54](#), [86](#), [87](#), [130](#), [133](#)
- [89] N. R. GOODMAN. **The Distribution of the Determinant of a Complex Wishart Distributed Matrix.** *Annals of Mathematical Statistics*, **34**(1):178–180, 1963. [57](#)
- [90] R.K. RANEY AND G.J. WESSELS. **Spatial considerations in SAR speckle consideration.** *IEEE Transactions on Geoscience and Remote Sensing*, **26**(5):666 –672, Sep 1988. [71](#)
- [91] S.N. ANFINSEN, A.P. DOULGERIS, AND T. ELTOFT. **Estimation of the Equivalent Number of Looks in Polarimetric Synthetic Aperture Radar Imagery.** *IEEE Transactions on Geoscience and Remote Sensing*, **47**(11):3795 –3809, Nov 2009. [71](#), [72](#)
- [92] NASA/JPL. **AIRsar Implementation**, 1996. [<http://airsar.jpl.nasa.gov/documents/genairsar/chapter3.pdf> Accessed Feb 2013]. [71](#)

- [93] MDA. **RadarSat-2 Product Description**, 2009.
[\[http://gs.mdaeorporation.com/products/sensor/radarsat2/
 RS2_Product_Description.pdf Accessed Feb 2013\]. 71](http://gs.mdaeorporation.com/products/sensor/radarsat2/RS2_Product_Description.pdf)
- [94] D.H. HOEKMAN. **Speckle ensemble statistics of logarithmically scaled data.** *IEEE Transactions on Geoscience and Remote Sensing*, **29**(1):180 –182, Jan 1991. 94, 103
- [95] HUA XIE, L.E. PIERCE, AND F.T. ULABY. **Statistical properties of logarithmically transformed speckle.** *Geoscience and Remote Sensing, IEEE Transactions on*, **40**(3):721–727, Mar. 94
- [96] MACIEJ A. MAZUROWSKI AND GEORGIA D. TOURASSI. **Evaluating Classifiers: Relation Between Area Under the Receiver Operator Characteristic Curve and Overall Accuracy.** In *IEEE International Joint Conference on Neural Networks (IJCNN), Vols 1- 6, Atlanta, GA, JUN 14-19, 2009*, pages 1196–1200, 2009. 94
- [97] Y.-L. YOU AND M. KAVEH. **Fourth-order partial differential equations for noise removal.** *IEEE Transactions on Image Processing*, **9**(10):1723 –1730, Oct 2000. 101, 118
- [98] H. XIE, L.E PIERCE, AND F.T. ULABY. **Statistical Properties of Logarithmically Transformed Speckle.** *IEEE Transactions on Geoscience and Remote Sensing*, **40**(3):721–727, Mar 2002. 103
- [99] S SOLBO AND T ELTOFT. **Homomorphic wavelet-based statistical de-speckling of SAR images.** *IEEE Transactions on Geoscience and Remote Sensing*, **42**(4):711–721, Apr 2004. 105
- [100] THANH-HAI LE, I. MCLOUGHLIN, KEN YOONG LEE, AND T. BRETSCHNEIDER. **Neural network-assisted reconstruction of full polarimetric SAR information.** In *Communications, Control and Signal Processing (ISCCSP), 2010 4th International Symposium on*, pages 1–5, 2010. 130
- [101] T. H. LE AND I. V. MCLOUGHLIN. **SAR Fuzzy-MLE Speckle Filter using the Distance Consistency Property in Homoskedastic Log-Transformed Domain.** In *Proceedings of the 32nd Asian Conference on Remote Sensing (ACRS)*, Taipei, Taiwan, Nov 2011. 130, 133

- [102] A. FREEMAN AND S.L. DURDEN. **A three-component scattering model for polarimetric SAR data.** *IEEE Transactions on Geoscience and Remote Sensing*, **36**(3):963 –973, May 1998. [131](#)
- [103] S.R. CLOUDE AND E. POTTIER. **An entropy based classification scheme for land applications of polarimetric SAR.** *IEEE Transactions on Geoscience and Remote Sensing*, **35**(1):68 –78, Jan 1997. [131](#)
- [104] J. SCHOU, H. SKRIVER, A.A. NIELSEN, AND K. CONRADSEN. **CFAR edge detector for polarimetric SAR images.** *IEEE Transactions on Geoscience and Remote Sensing*, **41**(1):20 – 32, Jan 2003. [133](#)
- [105] W.H. RICHARDSON. **Bayesian-Based Iterative Method of Image Restoration.** *Journal of the Optical Society of America*, **62**(1):55–59, 1972. [135](#)
- [106] L. B. LUCY. **An iterative technique for the rectification of observed distributions.** *The Astronomical Journal*, **79**:745, June 1974. [135](#)